Università degli Studi di Pisa

Dipartimento di Fisica

Corso di Dottorato in Fisica Applicata
(XVIII Ciclo)

Tesi di Dottorato

Nonlinear collisionless plasma dynamics

Laura Galeotti

January 2006

Relatore:

Dr. Francesco Califano

Table of Contents

Introduction

In high temperature laboratory and rarefied space plasmas, many situations arise where the observed dynamics is characterized by non collisionality. This is due to the fact that, in such plasmas, the collision frequency can be orders of magnitude smaller than the typical frequencies of the plasma dynamics (as the plasma frequency), corresponding to a mean free path of the particles much longer than all other plasma characteristic length scales. From a theoretical point of view, the dynamics of these plasmas can be considered as Hamiltonian.

The study of such non collisional systems represents one of the widest fields of investigation of plasma physics. The capability of generating, during the time evolution, smaller and smaller scales in the velocity space is a characteristic of the majority of the processes developing in such plasmas. Thanks to this feature, it is possible to observe fascinating phenomena, like the Landau damping, in which the passage of energy through macroscopic to microscopic scales can produce the exponential damping of macroscopic oscillating quantities as the electric field and the charge density. In this process the initial energy associated to these macroscopic quantities is not dissipated, since the system is collisionless, but, it is stored in the distribution function as velocity-space fluctuations that oscillate indefinitely in time on increasingly finer velocity scales (the so-called ballistic term). This interplay between macroscopic and microscopic processes is very elegantly exemplified by the plasma wave echoes [1, 2]. Echoes are, in fact, one of the most direct proofs and one of the more significant demonstration of microscopic reversibility in collisionless plasmas since, as a matter of fact, they are capable to bringing back on macroscopic scales the memory of the initial perturbation Landau damped away in time.

Like in the Landau damping and in the echo phenomenon, the dynamics of a collisionless system, especially in the long time, non linear evolution, is often driven by kinetic effects. Therefore, to describe theoretically its evolution, a kinetic approach is

necessary. This kinetic theory is a mean field theory, in which Coulomb interactions between particles are replaced by a common mean electromagnetic field. In other words, each particle feels the averaged field of the collective system, while single particle interactions are neglected. The equation which governs the evolution of such systems is known as the Vlasov equation.

This equation, self-consistently coupled with Maxwell ones, describes the plasma dynamics for times shorter than the binary collision time in terms of the distribution function of particles $f(x, v, t)$. The distribution function represents the number of particles per unit volume, at the time t, in the point (x, v) of the phase space. One of the fundamental characteristics of the Vlasov equation is that different curves of level of the distribution function in the phase space can wind round themselves in very complicate ways but cannot reconnect. Furthermore this equation is characterized by the fact that any function $G(f)$ is a constant of motion, i.e. $dG/dt = 0$, as, in particular, the n-order invariants $I_n = \int f^n dxdv$. Through Vlasov and Maxwell equations, the distribution function time evolution is calculated self-consistently with the electromagnetic fields produced by the plasma particles. However, the Vlasov-Maxwell system is a non linear system of equations, and hence to solve it analytically, even in simplified problems, results usually very difficult and in general even impossible. For this reason, when one wants to study the non linear dynamics of a plasma, numerical simulations are one of the most effective tools of investigation. However, the necessity of the numerical approach to discretize the equations on a numerical mesh introduces a strong limit. In fact, in Vlasov simulations, when a process develops scales so small to be comparable with the size of the numerical mesh, the algorithm becomes necessarily unable to describe correctly the plasma dynamics, with the consequent effect of introducing in the system numerical dissipation and dispersion. The role of these numerical dissipative effects on the study of collisionless plasma dynamics is a complex question still open and can be considered as one of the outstanding problems of plasma physics. One of the main problems to understand is how much the feedback of small scales on large ones is relevant for the macroscopic dynamics, even if the mesh length scale, that is comparable to the dissipative one, is much shorter than any physical length scale.

We tried to face this question by considering several specific cases of one dimensional electrostatic collisionless dynamics and, we made numerical simulations of the

non linear long time evolution of several non collisional plasma systems by varying the mesh size and/or the algorithm used to solve the Vlasov equation.

The first phenomenon investigated is the long time evolution of the Landau damping phenomenon which can be summarized as a resonant interaction between a plasma wave and particles moving at nearly its phase velocity. The effect of this interaction is an exchange of energy between these particles and the wave. In the case in which the initial distribution function is Maxwellian and the wave has a positive phase velocity, the net transfer of energy is from the wave to the particles, producing the damping of the wave in time. However, during the non-collisional damping process, other mechanisms can come into play changing the evolution of the phenomenon. When the amplitude of the initial wave is "sufficiently" large, one of these mechanisms is represented by the particles trapping in the potential well of the wave. This process has a characteristic time τ_p, called the trapping time, that is the time necessary for a particle to go across the potential well and bounce back. Hence, the long time dynamics of the plasma can change in conformity with the relations between the characteristic times scales of the system (Landau damping time τ_L, trapping time τ_p and the wave oscillation period $\tau_0 = 1/\omega$). When $\tau_p \gg \tau_L \gg \tau_0$ (Landau regime) the plasma oscillation for large times is exponentially damped to zero [3], while when $\tau_L \gg \tau_p \gg \tau_0$ particles are rapidly trapped before the wave is damped and, at t about τ_p, the linear Landau theory breaks down. The result is that, at large times, the wave amplitude reaches a constant nonzero value (O'Neil regime) [4]. If instead τ_p is about τ_L, the behaviour of the system is intermediate [5]. In the case when particle trapping is relevant in the system dynamics, phase space vortices, representing particle oscillations in the potential wells, are generated. We are interested in the regime in which vortices are created because it represents one of the most important and typical examples of the violation of the Vlasov equation.

Our numerical study of the long time evolution of Landau damping has been made in the regime in which $\tau_L \simeq \tau_p$ with the initial perturbation amplitude such that a phase space vortex is generated around the resonant velocity. In our model we take the protons as a fixed neutralizing background since the dynamics under study evolves on the electron time scale. We compared the results obtained with different meshes and three different numerical schemes, corresponding to different values of artificial numerical dissipation. Through the measure of macroscopic quantities (the

distribution and number of trapped particles, invariants, electric field, etc...), we found that, at large times, the same initial plasma system reaches different final macroscopic states depending on the grid size and/or the numerical scheme. These final states are a superposition of 'averaged' Bernstein-Greene-Kruskal (BGK) states [6, 7], i.e. a superposition of exact solutions of Vlasov-Poisson equations, stationary in the reference frame moving at the phase velocity of the wave, obtained averaging the particle distribution function of these states over the energy curves.

Differences among final macroscopic states of the Vlasov Poisson system are even more evident in the results of the two stream instability evolution, an instability which develops thanks to the initial anisotropy in velocity of the particle distribution function given by two counter streaming beams carrying no net total current in the system. The study of its linear and non-linear behaviour [8] has acquired new interest in the last ten years with the discovery of bipolar electric field pulses in space plasmas (Earth's ionosphere [9, 10], magnetosphere [11] and foreshock region [12]). We are interested in this process because it produces a vortex that involves the bulk of the distribution function and not only a small portion as in the non linear Landau damping. We investigated the evolution of this instability for a one dimensional unmagnetized collisionless plasma with an initial equilibrium configuration where the electrons are distributed in two beams with equal but opposite mean velocities, while (as a first step) protons are considered of infinite mass. When the system is perturbed, the amplitude of the electric perturbation increases to the disadvantage of electrons kinetic energy, until it becomes large enough to trap electrons starting from less energetic ones. At this point the instability begins to saturate and a new stable state is reached. In the phase space, the oscillations of the trapped electrons in the potential well are represented by vortices. The number of vortices which can be generated by this system depends on the spatial dimension L_x of the phase space.

If more vortices are generated in the system, they interact together [13, 14]. This interaction process of merging (inverse cascade) is forbidden in the Vlasov collisionless theory and is driven by the artificial dissipation introduced by the numerical approach. We observed that varying the length scale of the numerical grid, corresponding so to vary the artificial dissipative effects, changes both the way in which the vortices interact together to develop a final unique vortex and the characteristic time in which this merging process is completed.

The cause of the differences among final states of the Vlasov-Poisson system is hence due to the fact that simulations made with different algorithms or with the same algorithm but with different resolution grids, brings in the system different quantities of artificial effects which are relevant also for the macroscopic dynamics, even if the dissipative length scale is much shorter than any physical length scale. Therefore, when artificial dissipation comes into play, even if we are formally dealing with a collisionless plasma, the final effect will be very similar to inserting in the system a collisional operator.

Since the echo phenomenon, for which a non linear solution is available, is one of the most sensitive process to "collisions", capable of distinguish between collisional or non-collisional damping effects, we have decided to employ it for the study of numerical schemes to investigate the dissipative effects problem. But how the echo manage to realize the differences between a collisionless and a collisional system? Let's now give a brief explanation. A wave echo arises when two plasma waves are excited in the plasma with a time delay and, long after they have been Landau damped away, a macroscopic electric field reappears because of the nonlinear constructive interference between the ballistic terms of the two waves. In absence of dissipation, the memory of the two plasma waves, after they are Landau damped away exponentially, is stored in the ballistic terms. Instead, if collisions are present in the system, they can destroy the phase informations stored in these ballistic terms before the echo appears. A detailed analytical study of this phenomenon was developed by O'Neil [15] and showed how Coulomb collisions and microturbulence can affect the final amplitude and shape of the echo. This very fine sensibility of the echoes to dissipative effects, permits us to use this phenomenon to investigate the dissipative properties of a numerical code [16]. We tested, with the echo phenomenon, all the algorithms we used at different numerical resolutions. We found that code accuracy affects the final amplitude and shape of the echo in agreement with theoretical analysis. In the limit of very high resolution, no grids dissipative effects are introduced in the system at least for $t < t_{echo}$. The echo test results more discriminating than those based on the conservation of (a finite set of) Casimir invariants (see Ref. [17]). In fact, in all runs where there is a decrease of the echo's amplitude (up to complete disappearance) with respect to the expected value, due to any kind of (numerical) dissipative effect, the set of Casimir invariants of the Vlasov - Poisson system (here up to third order, $m = 1, 2, 3$) are

"perfectly" conserved (i.e. no variations are observed all along the simulation). Indeed such invariants, often considered as the relevant test for a Vlasov code, may provide misleading informations since they are global quantities unable to capture small-scale features of non-Vlasov local effects.

Considering all these results, one question arises: up to what point can a system, studied through numerical simulations, be considered as really non-collisional? As seen before, in fact, even if the plasma under study is formally collisionless, when the numerical scheme becomes unable to describe the system small scales, collisional effects come into play. A way to understand how and when the plasma looses its non collisionality is given by the study of particle correlations. As already mentioned, in a collisionless system, and therefore for the Vlasov theory, the correlations, as for example binary interactions, are negligible with respect to the averaged field produced by all the particles of the plasma. However, when strong spatial and velocity gradients are generated by the system during the dynamical evolution, correlations become more and more important at least in local large gradient regions. For this reason, we studied the generation of binary correlations in numerical simulations of two different kind of collisionless plasma systems: a one dimensional electrostatic two stream instability and a system where the field produced by the plasma particles is neglected and an external sinusoidal fixed electric field is imposed. In both problems a phase space vortex is formed. To investigate the correlations, we used passive tracers, whose time evolution is determined only by the electric field present in the system. In the two stream instability case, the electric field that make move the tracers is given by the self-consistent averaged electric field computed through Vlasov and Poisson equations. We found that in the two stream instability process correlations are negligible until the scales produced by the system are large enough to be correctly solved by the numerical mesh. When the plasma fluctuations characteristic lengths become comparable to the numerical grid step, the Vlasov theory is violated and both short range and long range correlations appear and their strength begins to increase in time, up to reach asymptotic constant values. Furthermore, in the regions in which correlations appear, the dynamics of the passive tracers becomes chaotic. In the second system, instead, for all times nor correlations neither chaotic dynamics have been found. The presence of correlations in the two stream instability case is due to the presence of the self-consistent field, i.e. the field calculated, for every time steps, through

the distribution function. In fact, when the fluctuations length scales generated by the distribution function become smaller than the mesh grid step, the algorithm is forced to approximate the distribution function on the discrete mesh, reconnecting the distribution isolines. This effect allows the tracers, constrained to follow the isolines of the distribution function, to go from an isoline to another, meaning, for particles with kinetic energies of the order of the potential energy, the possibility of passing from a closed orbit to a free motion, i.e. the generation of chaotic trajectories. At the same time, the approximation of the distribution function on the numerical mesh produce also deviations on the averaged electric field that make appear the correlations between particles. In the second system, correlation are not generated because numerical effects cannot affect the electric field since it is fixed.

A different subject with respect to the study of the influence of artificial dissipation on long time numerical simulation, has been investigated in this work: the evolution of electromagnetic and electrostatic waves injected from the boundary in a magnetized plasma. The study of these processes through a numerical kinetic approach permits to investigate the evolution of waves, as Bernstein ones, that don't exist in the fluid theory but are of great importance in phenomena as, for example, the mode conversion [18, 19]. This phenomenon is one of the most important when one investigates the evolution of injected waves in inhomogeneous plasmas when the upper hybrid resonance is encountered and represents a relevant process in tokamak systems [20, 21, 22, 23, 58]. We hence decided to study the evolution of injected electromagnetic wave in an 1D-2V inhomogeneous magnetized plasma in which the Harris pinch magnetic configuration, which is a full Vlasov-Maxwell equilibrium, has been used as the supporting medium for wave propagation. We investigated the interaction of the injected waves with the upper hybrid resonance and/or with the cut off, discussing the induced excitation of electric and magnetic fluctuations and the competition between electromagnetic and electrostatic effects. Furthermore we studied the formation and evolution of Bernstein waves, through the external excitation of electromagnetic waves or electrostatic perturbations, in homogeneous collisionless magnetized plasma.

The work is organized as follows: in Chapter 1 there is a brief review of the theory of the basic plasma processes at play in our system (linear and non-linear regimes of Landau damping and two stream instability, plasma wave echo phenomenon and

correlations); a description of the numerical schemes used will be provided in Chapter 2; in Chapter 3 we will present the results of the numerical simulations made. The theory and the numerical results of the study of the evolution of electrostatic and electromagnetic waves injected by the boundary in a magnetized plasma are shown instead in Appendix C and D respectively, since this is a very preliminary work.

Chapter 1

Collisionless plasma phenomena

The dynamics of many plasma phenomena are governed by kinetic effects. For this reason the fluid theory is often inadequate to describe such phenomena and a kinetic approach is hence necessary. Echoes, Landau damping, particle trapping, propagation of Bernstein waves in a hot magnetized plasma and the long time behaviour of the two stream instability are examples of phenomena that can be properly described only by the kinetic theory. In this chapter we will make a brief review of the linear and non linear theory of these systems.

1.1 Kinetic theory of small amplitude plasma waves in a field free collisionless plasma

The dynamics of a field free collisionless plasma can be studied using the Vlasov and Poisson equations, that provide the evolution of the particles distribution function $f(x, v, t)$ in time. Since the Vlasov-Poisson system of equations is nonlinear, it becomes really difficult to calculate $f(x, v, t)$ in the majority of the cases. One of the limits for which it is possible to solve analytically the equations is when the distribution function, in its evolution, is only slightly perturbed from the initial condition. In this regime, also called the linear regime, Vlasov and Poisson equations can be linearized assuming that the electron distribution function and the fields can be expressed as an equilibrium part plus a small perturbation. In this section we are interested to show how to derive this equations and their solutions.

We limit here to the fast electron dynamics. Let's consider a one dimensional field free collisionless plasma composed by mobile electrons and a fixed background of neutralizing ions. Hence, Vlasov and Poisson equations can be write as:

$$\frac{\partial f_e}{\partial t} + v\,\frac{\partial f_e}{\partial x} + \frac{e}{m_e}\frac{\partial \phi}{\partial x}\,\frac{\partial f_e}{\partial v} = 0; \tag{1.1.1}$$

$$\frac{\partial^2 \phi}{\partial x^2} = 4\pi e\left(\int f_e\,dv - n_0\right); \quad E = -\frac{\partial \phi}{\partial x}; \tag{1.1.2}$$

where n_0, f_e and ϕ represent the protons density, the electron distribution function and the electrostatic potential, respectively. To linearize the equations, we consider the electron distribution function and the electrostatic potential expressed as an equilibrium part plus a perturbation as

$$f_e(x,v,t) = f_{e0}(v) + \epsilon f_{e1}(x,v,t) \tag{1.1.3}$$

$$\phi(x,t) = \phi_0 + \epsilon\phi_1(x,t) \tag{1.1.4}$$

where $\phi_0 = constant$ and $\int dv f_{e0} = n_0$. In this problem, the electron distribution function $f_{e0}(v)$ and ϕ_0 represent the stationary plasma state, while the distribution function $f_{e1}(x,v,t)$ and ϕ_1 represent the development of an initial perturbation. To satisfy the condition, for the distribution function, of small departures from the initial configuration, the perturbation f_{e1} is assumed not only to be small, $\mid f_{e1} \mid << f_{e0}$, but also to satisfy the condition

$$\mid \frac{\partial f_{e1}(x,v,t)}{\partial v} \mid << \mid \frac{\partial f_{e0}(v)}{\partial v} \mid \tag{1.1.5}$$

Substituting these expressions in Vlasov and Poisson equations and retaining only the first order terms, we obtain:

$$(\frac{\partial}{\partial t} + v\,\frac{\partial}{\partial x})f_{e1} = -\frac{e}{m_e}\frac{\partial \phi_1}{\partial x}\,\frac{\partial f_{e0}}{\partial v}; \tag{1.1.6}$$

$$\frac{\partial^2 \phi_1}{\partial x^2} = 4\pi e\int f_{e1}\,dv\ . \tag{1.1.7}$$

In order to solve the linearized equations 1.1.6, 1.1.7, we apply them the Fourier transform with respect to the spatial variables and we take the Laplace transform in time as made by Landau [3]. As usual Fourier and Laplace transforms are defined as:

$$f_{ek}(v,t) = \frac{1}{2\pi}\int f_{e1}(x,v,t)exp(-ikx)dx \tag{1.1.8}$$

$$\phi_k(t) = \frac{1}{2\pi}\int \phi_1(x,t)exp(-ikx)dx \tag{1.1.9}$$

$$\tilde{f}_{ek}(v,p) = \int_0^\infty f_{ek}(v,t)e^{-pt}dt \quad Re(p) \geq p_0 \tag{1.1.10}$$

$$\widetilde{\phi}_k(p) = \frac{1}{2\pi}\int_0^\infty \phi_k(t)exp(-pt)dt \quad \Re(p) > p_0 \tag{1.1.11}$$

where p_0 is chosen large enough that the integral so $\int_0^\infty f_{ek}(v,t)e^{-pt}dt$ converges.

Since f_{e0} is not a function of x or t, equations 1.1.6, 1.1.7 become:

$$(p+ikv)\tilde{f}_{ek}(v,p) = f_{ek}(v,t=0) - \frac{e}{m_e}\frac{ik\partial f_{e0}}{\partial v}\tilde{\phi}_k \tag{1.1.12}$$

$$k^2\tilde{\phi}_k = 4\pi e\int \tilde{f}_{ek}(v,p)dv \tag{1.1.13}$$

Combining equations 1.1.12 and 1.1.13 together we obtain:

$$k^2\tilde{\phi}_k = \frac{4\pi e\int \tilde{f}_{ek}(v,t=0)dv/(p+ikv)}{1-4\pi\frac{e^2}{m_e k^2}\int \frac{ik\partial f_{e0}}{\partial v}dv/(kv-ip)} \tag{1.1.14}$$

To obtain the space and time dependence of the potential for a given initial distribution function, it is now necessary to take the inverse Laplace and Fourier transforms. However, the inversion integrals can be analytically carried out only for few simple initial distribution functions (for example in the case of an equilibrium distribution $f_{e0} = \delta(v)$ and an initial perturbation $f_{e1} = f_{e0}sinkx$ or for $f_{e0} = A\delta(v)/v^2$ and $f_{e1} = f_{e0}sinkx$). To achieve analytical solutions for a wide class of initial distribution functions is hence necessary an approximation by searching long-time solutions.

These asymptotic solutions are the normal modes of oscillations of the plasma and are represented by all those wavelike disturbances, induced by an initial perturbation, that persist long after the transient period in which all other disturbances died out. Details of the computation of Laplace inverse transforms on equation 1.1.14 can be found in reference [3] and [25]. However, before showing the result, it's important to underline that the prime contribution to the Laplace contour integral comes, for $t \to \infty$, from the poles of $\tilde{\phi}_k$, which are the zeros of the denominator of equation 1.1.14, i.e. the zeros of the dielectric function:

$$D(k, ip) = 1 - 4\pi \frac{e^2}{m_e k^2} \frac{\int \frac{ik\partial f_{e0}}{\partial v} dv}{kv - ip}. \tag{1.1.15}$$

The time-asymptotic solution of the linearized Vlasov-Poisson equations for the perturbed potential results:

$$\phi_k(t \to \infty) = \sum_j R_j e^{p_j(k)t} \tag{1.1.16}$$

where R_j are the residues

$$R_j = \lim_{p \to p_j} (p - p_j)\tilde{\phi}_k(p). \tag{1.1.17}$$

In terms of the frequency $\omega = ip$, the asymptotic potential becomes:

$$\phi_k(t \to \infty) = \sum_j R_j e^{-i\omega_j t} \tag{1.1.18}$$

where ω_j is the complex quantity $\omega_j = \omega_r + i\omega_i$ and satisfies

$$D(k, \omega) = 1 - \frac{\omega_{pe}^2}{k} \int \frac{\partial f_{e0}/\partial v}{kv - \omega} dv = 0 \ . \tag{1.1.19}$$

In last equation, ω_{pe}, called the electron plasma frequency, defined as $\omega_{pe} = \sqrt{(4\pi n_0 e^2/m_e)}$, represents the characteristic frequency of the collective oscillations exhibited by plasma

electrons as the response to an unbalance of charge, in order to maintain the quasi-neutrality of the system.

1.2 Landau damping

In this section we will present the theory of the Landau damping of an electron plasma wave in a collisionless plasma. We will first make a brief review of the linear theory (see reference [3], [25]). Then, we will show O'Neil and Lancellotti and Dorning analytical theories, and their field of applicability, that have been developed in order to describe the phenomenon when linear theory breaks down and effects, as particles trapping, come into play.

1.2.1 Linear regime

The system we want to describe is a one dimensional unmagnetized collisionless plasma. Since Landau damping is a high frequency phenomenon governed by the electron dynamics, we can consider protons at rest (i.e. of infinite mass), just as a fixed neutralizing background, without loosing generality. In order to study the linear regime of Landau damping, we have to take the Vlasov and Poisson equations, linearized them and compute the dispersion relation. From $D(k,\omega)$ we will derive the frequencies of the waves supported by the plasma. Since the system considered here is the same for which the linear theory has been developed in section 1.1, we can directly take the dispersion relation 1.1.18:

$$D(k,\omega) = 1 - \frac{\omega_{pe}^2}{k} \int \frac{\partial f_{e0}/\partial v}{kv - \omega} dv = 0 \ . \tag{1.2.1}$$

To obtain the dispersion relation, we need to find solutions of $D(k,\omega) = 0$ which give us the frequencies $\omega = \omega_r + i\omega_i$ of these waves as function of the wave number k. We limit here to solutions for which the plasma is stable, by taking into account only for frequencies with a negative imaginary part. It is important to recall that we are searching, as in section 1.1, long-time solutions, i.e. the normal modes of oscillation of the system. Therefore, we will consider only the solutions of $D(k,\omega) = 0$ having eigenfrequency ω purely real or, at least, with a very small imaginary part,

i.e. $\omega_i << \omega_r$. In fact, all waves for which ω has a large value of the imaginary part are damped very fast and so they cannot be considered as normal modes. The most interesting feature of equation 1.2.1 is the presence in the dispersion relation of a pole at $v = \omega/k$. It is therefore necessary to solve the integral contained in $D(k,\omega)$ by choosing a proper integration contour in the complex plane. This contour, as indicated in Landau prescription, has to pass under the pole (see for example [25] pg.375). Then, choosing from 1.2.1 only those solution for which $\omega = \omega_r + i\gamma$ with $|\gamma| << \omega_r$, we can simplify the computation of $D(k,\omega)$ roots by expanding it in Taylor series around $\gamma = 0$

$$\begin{aligned} D(k,\omega) &= D(k,\omega_r) + i\gamma \frac{\partial D(k,\omega)}{\partial \omega}|_{\omega=\omega_r} = \\ &= 1 - \frac{\omega_{pe}^2}{k}\left[\lim_{\epsilon\to 0^+}\int_{-\infty}^{+\infty}\frac{\partial f_{e0}/\partial v}{kv-\omega_r-i\epsilon}dv + i\gamma\frac{\partial}{\partial\omega_r}\left(\lim_{\epsilon\to 0^+}\int_{-\infty}^{+\infty}\frac{\partial f_{e0}/\partial v}{kv-\omega_r-i\epsilon}dv\right)\right] \end{aligned} \tag{1.2.2}$$

It's important to note that, for $\omega = \omega_r$, the integral is evaluated along the Landau contour by writing $\omega = \omega_r + i\epsilon$, i.e. in a pole just above the v axis, and then taking the limit for $\epsilon \to 0^+$.

We can use the relation (see reference [26] p.481):

$$\lim_{\epsilon\to 0^+}\int_{-\infty}^{+\infty}\frac{G(v)}{v-\omega_r/k-i\epsilon}dv = P\int\frac{G(v)}{v-\omega_r/k}dv + \pi i G(v=\frac{\omega_r}{|k|}) \tag{1.2.3}$$

obtaining

$$1 - \frac{\omega_{pe}^2}{k^2}\left(1 + i\gamma\frac{\partial}{\partial\omega_r}\right)\left[P\int\frac{\partial f_{e0}/\partial v}{v-\omega_r/k}dv + \pi i\left[\frac{\partial f_{e0}}{\partial v}\right]_{v=\omega_r/k}\right] = 0 \tag{1.2.4}$$

where P is the Cauchy principal value. The above relation can be also written as

$$D(k,\omega) = D_r(k,\omega) + iD_i(k,\omega) + i\gamma\frac{\partial(D_r(k,\omega)+iD_i(k,\omega))}{\partial\omega_r} \tag{1.2.5}$$

where

$$D_r(k,\omega) = 1 + \frac{1}{k} P \int \frac{\partial f_{e0}/\partial v}{\omega - kv} dv \tag{1.2.6}$$

$$D_i(k,\omega) = -\frac{\pi}{k^2} \frac{\partial f_{e0}(v)}{\partial v}|_{v=v_{ph}} \ . \tag{1.2.7}$$

If we consider the case for which the phase velocity of the wave is much larger than the thermal velocity, $v_{ph} >> v_{th}$ (i.e. in long-wavelength limit $k\lambda_D << 1$), the principal value integral in equation 1.2.4 can be evaluated by an expansion in v. In order to calculate ω_r, we search the zeros of the real part of the dielectric function by putting $D_r(k,\omega_r) = 0$. Hence using a Maxwellian equilibrium electron distribution function

$$f_{e0}(v) = \left(\frac{m_e}{2\pi\kappa T_e}\right)^{1/2} exp\left(-\frac{m_e v^2}{2\kappa T_e}\right) \tag{1.2.8}$$

and evaluating the principal value integral by an expansion in v, we obtain:

$$D_r(k,\omega_r) \simeq 1 + \frac{\omega_{pe}^2}{\omega^2}\left[1 + \frac{3\omega_{pe}^2}{\omega^2}(k\lambda_D)^2\right] = 0 \ . \tag{1.2.9}$$

where λ_D, the Debye length, is a measure of the radius of the characteristic sphere of influence of a test charge in a plasma, defined as $\lambda_D = \sqrt{(\kappa T/(4\pi n_0 e^2))} = v_{th,e}/\omega_{pe}$ (where T represents the plasma temperature and κ the Boltzmann constant). Solving equation 1.2.8 we obtain:

$$\omega_r = \omega_{pe}\left[1 + \frac{3}{2}k^2\lambda_D^2\right] \ . \tag{1.2.10}$$

The frequency already found is associated to a wave called Langmuir wave. In the limit of a cold plasma, i.e. $\lambda << \lambda_D$ or equivalently $k\lambda_D << 1$ or also $\omega/k = v_{th}$, this wave will have a real part of the frequency $\omega_r \simeq \omega_{pe}$, i.e. not depending on the wave number k, and no imaginary part. The expression for the frequency γ can be found equating the real and imaginary part of equation 1.2.5, obtaining:

$$\gamma = -D_i(k, \omega_r) / \frac{\partial D_r(k, \omega_r)}{\partial \omega_r} \quad . \tag{1.2.11}$$

An important result of equations 1.2.7 and 1.2.11, is that the damping rate γ of the wave is proportional to the first derivative of the equilibrium electron distribution function with respect to velocity, calculated at the phase velocity $v_{ph} = \omega/k$ of the wave. Hence the sign of $\partial f_{e0}(v)/\partial v|_{v=v_{ph}}$ determines if the wave is damped or the growing.

Inserting 1.2.6 and 1.2.7 in equation 1.2.11 and using the Maxwellian defined in 1.2.8, the imaginary part of the frequency results:

$$\gamma \equiv \gamma_L = -\sqrt{\frac{\pi}{8}} \frac{\omega_{pe}}{|k^3 \lambda_D^3|} exp\left[-\left(\frac{1}{2k^2\lambda_D^2} + \frac{3}{2} \right) \right] \tag{1.2.12}$$

The presence of an imaginary part of the frequency tells us that even if we're in a collisionless system, the electrostatic waves undergo to a damping, called the Landau damping. Since we are in the long-wavelength limit, the damping time scale, $\tau_d = 1/|\gamma_L|$, results much loner than the time scale of plasma oscillation $\tau_0 = 1/\omega_{pe}$ (in fact in the long-wavelength limit $\gamma_L << \omega_r \simeq \omega_{pe}$ because $k\lambda_D << 1$).

But what is the physical explanation for the development of a damping phenomenon ia a collisionless system? As can be seen also in the dispersion relation from the presence of the singularity at $v = v_{ph}$, if in the plasma there are electrons that travel with almost the same velocity of the wave (i.e. resonant particles), that therefore see a "quasi static" electric field $E \simeq const$, they will interact with the wave absorbing energy from it or giving energy to it depending on their velocities. Particles that move slightly slower than the wave absorb energy from the wave, while those that move faster give energy to the wave. In our case, where the equilibrium distribution function is a maxwellian, for a positive phase velocity of the wave, there will be more resonant particles that travel slightly slower than the phase velocity of the wave than particles that move slightly faster. This produces a net effect of a transfer of energy from the wave to the electrons, damping the wave in time. However, as the system is non collisional, this energy of the wave must be "hidden" somewhere else. As we will seen in the next section, the energy lost by the wave is transferred to small

scales fluctuation of the electron distribution function. Since the distribution function becomes, with the growing of time, more and more highly oscillating function, $\int f dv$ will phase mix to zero and hence the electric field, that is proportional to this quantity, becomes zero. However it i possible to retrieve such energy, as later times, in the form of a plasma wave echo.

1.2.2 Electron trapping and O'Neil regime

Let's consider an electron that moves in a plasma where an electrostatic wave is present. If the electron moves with nearly the same velocity of the electrostatic wave and the amplitude of the electric field is large enough, i.e. $mv^2 \leq e\phi$, it will be trapped in the wave potential well. If, for example, the electrostatic wave is of the form $E(x,t) = E_k(t)sin(kx - \omega t)$, these electrons will oscillate in the well with a period:

$$T = \frac{1}{2\pi}\sqrt{\frac{m_e}{eE_k k}} \equiv \frac{\tau_p}{2\pi}\,. \tag{1.2.13}$$

where τ_p is called the trapping time and T is obtained solving the equation $m_e\ddot{x} = -eE_k sinkx \approx -eE_k kx$ (in the limit of small oscillations) and represents the time taken by a trapped electron to go across the potential well and bounce back.

In the previous section we described the Landau damping phenomenon in the framework of a linear theory. However, if the damping time τ_L is shorter than this trapping time τ_p, the linear theory breaks down since, as will be shown in the following, if $\tau_p < \tau_L$, the assumption $|\ \frac{\partial f_{e1}(x,v,t)}{\partial v}\ | << |\ \frac{\partial f_{e0}(v)}{\partial v}\ |$, on which the linear theory is based, ceases to be valid when $t \geq \tau_p$.

Let us consider the linearized Vlasov-Poisson system of equations

$$\left(\frac{\partial}{\partial t} + v\frac{\partial}{\partial x}\right) f_1(x,v,t) = \frac{e}{m_e}E_1(x,t)\frac{\partial f_0(v)}{\partial v} \tag{1.2.14}$$

$$\frac{\partial E_1(x,t)}{\partial x} = -4\pi\int_{-\infty}^{\infty} f_1(x,v,t)dv\,. \tag{1.2.15}$$

The initial electric perturbation chosen is:

$$E_1(x,t) = E_k(t)sin(kx - \omega_r t)\,; \quad k\lambda_D << 1 \tag{1.2.16}$$

where $E_k(t) = E_k(0)exp(\gamma_L t)$ and γ_L and ω_r given by equations 1.2.10 and 1.2.12, that corresponds to an initial perturbation of the electron distribution function of:

$$f_1(x,v,0) = f_1(v,0)cos(kx)\,. \tag{1.2.17}$$

In order to solve the Vlasov-Poisson system of equations we define the particle trajectories in absence of electric field $x_0(\tau)$ and $v_0(\tau)$ and then we integrate the equations along these orbits. This procedure of integration is called the method of characteristics. Therefore, observing that the term of Vlasov equation 1.2.14:

$$\left(\frac{\partial}{\partial t} + v\frac{\partial}{\partial x}\right) f_1 = \frac{df_1}{d\tau} \tag{1.2.18}$$

represents the temporal derivative of f_1 evaluated along an unperturbed particle trajectory in absence of electric field, we can rewrite the Vlasov linearized equation as:

$$\frac{df_1[x_0(\tau), v_0(\tau), \tau]}{d\tau} = \frac{e}{m_e} E_1[x_0(\tau), \tau]\left[\frac{\partial}{\partial v'} f_0(v')\right] \tag{1.2.19}$$

where the unperturbed particle orbits x_0 and v_0 are given by:

$$x_0(\tau) = x + v(\tau - t) \quad v_0(\tau) = v \tag{1.2.20}$$

such that $x_0(\tau = t) = x$ and $v_0(\tau = t) = v$. Integrating equation 1.2.19 along the characteristics 1.2.20 from $\tau = 0$ to $\tau = t$, one obtains:

$$f_1(x,v,t) = f_1(x - vt, v, t) + \frac{e}{m_e}\frac{\partial}{\partial v} f_0(v) \int_0^t E_1[x + v(\tau - t), \tau]\,. \tag{1.2.21}$$

Inserting in equation 1.2.21 the expressions 3.1.3 and 3.1.4, and considering that for $t << \tau_L$ the amplitude of the electric field $E_k(t) = \widehat{E}$ can be taken as constant, equation 1.2.21 becomes:

$$f_1(x,v,t) = f_1(v,0)cos(kx - kvt) + \frac{e}{m_e}\frac{\partial}{\partial v}f_0(v)\widehat{E}\left[\frac{cos(kx-\omega_r t) - cos(kx - kvt)}{\omega_r - kv}\right]. \tag{1.2.22}$$

Expanding the numerator of the second term of the right hand side of equation 1.2.22 around v_{ph}, taking the velocity integral and retaining only the dominant contribution for large time, we obtain:

$$\frac{\partial}{\partial v}f_1(x,v,t)|_{v=v_{ph}} = -\frac{\partial}{\partial v}f_0(v)|_{v=v_{ph}}\frac{ek\widehat{E}}{m_e}\frac{t^2}{2}cos(kx-\omega_r t)\,. \tag{1.2.23}$$

We see from equation 1.2.23 that for $t \geq t_p = \sqrt{ek\widehat{E}/m_e}$ the condition of validity of the linear analysis $|\ \frac{\partial f_{e1}(x,v,t)}{\partial v}\ |<<|\ \frac{\partial f_{e0}(v)}{\partial v}\ |$ breaks down for the resonant electrons. Furthermore, from equation 1.2.23, at $t = t_p$ it can be observed that the electron distribution function begins to develop a plateau in the resonant velocity, i.e. $\frac{\partial}{\partial v}f(x,v,t)|_{v=v_{ph}} = \frac{\partial}{\partial v}f_0(v)|_{v=v_{ph}} + \frac{\partial}{\partial v}f_1(x,v,t)|_{v=v_{ph}} \simeq 0$. Hence the linear Landau analysis is valid only on times much smaller with respect to the trapping time, i.e. $t << \tau_p$. Then, if $\tau_L << \tau_p$, the electric field will be "completely" damped to zero before non linear effects, that can significantly distort particles trajectories, like the particles trapping, take place. In the opposite limit, $\tau_p << \tau_L$, the long time theory was developed by O'Neil [4] in 1965. He solved the Vlasov-Poisson system of equations using the method of characteristics taking into account the oscillation motion of resonant particles in the potential well. He used two mainly assumptions. The first is to choose the electric field as a monochromatic sinusoidal wave and the second, is that the amplitude of the electric field can be considered constant in time on time scales of the order of τ_p, based on the condition $\tau_p << \tau_L$. Takin into account the slow time variations of this electric field through the total energy expression (kinetic energy plus electric field energy), O'Neil obtained the law for the time variation of the electric field energy density ε as:

$$\varepsilon(t) = \varepsilon(0) exp\left[2\int_0^t \gamma(t)dt\right] \tag{1.2.24}$$

where

$$\gamma(t) = \gamma_L \sum_{n=0}^{\infty} \frac{64}{\pi} \int_0^1 dy \left\{ \frac{2n\pi^2 sin(\pi nt/y\tau_p F)}{y^5 F^2 (1+q^{2n})(1+q^{-2n})} + \frac{(2n+1)\pi^2 y sin[(2n+1)\pi t/(2\tau_p F)]}{F^2(1+q^{2n+1})(1+q^{-2n-1})} \right\} . \tag{1.2.25}$$

In the above equation γ_L is the linear Landau damping rate, F is the elliptic integral defined as:

$$F(\beta, z) \equiv \int_0^z \frac{dz'}{(1-\beta^2 sinz'^2)^{1/2}} \tag{1.2.26}$$

and

$$q \equiv exp(\pi F'/F); \quad F \equiv F(y, \pi/2); \quad F' \equiv F((1-y^2)^{1/2}, \pi/2)\,. \tag{1.2.27}$$

O'Neil also showed that in Eq. 1.2.25, the contribution of untrapped electrons is represented by the first term of the right-hand side while the contribution of the trapped particles is given by the second term. In the limit $t' \ll \tau_p$ the major contribution to $\gamma(t)$, 1.2.25, comes from the first term in the curly brackets for $n = 1$. In this limit $\gamma(t) \simeq \gamma_L$. On the other hand, when $t' \gg \tau_p$, the integration over y of the fast oscillating quantities of both terms in the right-hand side of equation 1.2.25, as $sin[(2n+1)\pi t'/2y\tau_r F]$ or $sin[(n\pi t'/y\tau_r F]$, phase mix to zero leading $\gamma(t) \simeq 0$. Hence, the behaviour of the electric field energy computed by O'Neil in the case $\tau_p \ll \tau_L$ can be summarized in this way: until $t < \tau_p$ the electric field energy damps exponentially according with the linear Landau theory; when $t \simeq \tau_p$ non linear effects come into play and the electric field energy, while is damped, begins to oscillate with a period of the order of τ_p; when $t \to \infty$, as $\gamma(t) \to 0$, the amplitude of the oscillations decreases and the electric energy field density tends to a constant value.

1.2.3 Long time evolution of Landau damping

In the previous sections we've seen that the relations between the characteristic times scales of the system, Landau damping time τ_L, trapping time τ_p and the wave oscillation period $\tau_0 = 1/\omega$, determine the way in which the system develops. Until now we have described two cases: 1) when $\tau_p >> \tau_L >> \tau_0$, where the linear Landau's theory remains valid because the electrostatic wave is completely damped before particles can be trapped in the potential wells; 2) when $\tau_L >> \tau_p >> \tau_0$, for which particles are rapidly trapped before the wave starts to be damped, for which, at t about τ_p, the Landau theory is no longer valid [4]. The result of this last case is that the wave amplitude, at large times, reaches a constant nonzero value. This regime is called O'Neil regime. In this section we want to discuss the intermediate regime when $\tau_p \sim \tau_L >> \tau_0$. The theory has been developed by Lancellotti and Dorning [5] in 1998. They found that there is a threshold for the initial perturbation amplitude: when initial amplitude is down the threshold there will be Landau's regime while if it is above the threshold we will have O'Neil regime. Also in this case, due to the mathematical difficulties to solve the nonlinear Vlasov-Poisson system of equations, it has been necessary make use of some approximations to solve the problem analytically. The Lancellotti and Dorning theory is based on the assumption that the electric field can be decomposed in a transient part $\bar{T}$ and in a time-asymptotic part $\bar{A}$ such that $E(x,t) = \bar{A}(x,t) + \bar{T}(x,t)$. The decomposition allows to obtain an approximate solution through the linearization of the Vlasov and Poisson equations for the transient part of the electric field $\bar{T}$. The Vlasov equation written in terms of $\bar{A} + \bar{T}$ is given by:

$$\frac{\partial f}{\partial t} + v\,\frac{\partial f}{\partial x} - \frac{e}{m_e}\bar{A}\frac{\partial f}{\partial v} = \frac{e}{m_e}\bar{T}\frac{\partial f_0}{\partial v} \tag{1.2.28}$$

where f_0 is the initial distribution function. The 'transient linearization' allows the equations to remain uniformly valid even when $t \to \infty$ because $\bar{T}$ decays fast enough before the distribution function deviates too much from the equilibrium one, while, the non linear part remains stored in the A term. Instead, as already discussed, in the Landau linearization the approximation of $\partial f/\partial v$ with $\partial f_0(v)/\partial v$ ceases to be valid at $t \simeq \tau_p$.

The transient linearization theory used in the regime $\tau_p \simeq \tau_d$, allowed to Lancellotti

and Dorning to compute analytically the existence of a threshold ϵ_c for the initial perturbation amplitude a that leads to the linear Landau damping regime ($\bar{A} = 0$) if $a < \epsilon_c$, or to the O'Neil regime ($\bar{A} \neq 0$) if $a > \epsilon_c$. This result justifies why in large scale numerical simulations in some cases the electric field is damped to zero while in some others nonzero travelling waves are present. Furthermore they found that, if the amplitude of the wave is just above the threshold ($a > \epsilon_c$), the electron distribution function evolves in time to reach a superposition of Bernstein-Greene-Kruskel (BGK) [**?**, 7] states in a 'coarse graining sense', i.e. averaging the particle distribution function over the invariant curves discovered by Buchanan and Dorning [27] (as explained in Appendix A). The BGK states are exact undamped periodic wave solutions of the Vlasov-Poisson system which are stationary in the frame of reference moving at their phase velocity. They are Vlasov equilibria and therefore they are computed trough Vlasov and Poisson system of equations by setting $\partial f/\partial t = 0$ (see Appendix A). Brunetti et al. [28] numerically studied this problem and verified the Lancellotti and Dorning theory [**?**] in the case of small amplitudes initial perturbations. They showed with the help of numerical simulations that the Vlasov-Poisson system reaches asymptotically in time a BGK state also in the case of large perturbation amplitudes, where Lancellotti and Dorning theory cannot be used, and studied the non linear stability of the system (side band instability).

1.3 Plasma wave echoes

In the study of Landau damping phenomenon an interesting paradox comes out: where does the energy associated to the electric wave goes when the wave is damped? At first sight, we could think that the energy has been converted into particles temperature. However this explanation is in conflict with fact that since the plasma is collisionless, the system conserves the entropy. The solution of the paradox can be found by calculating what happens to the distribution function when the damping takes place. It can be seen, in fact, that the excitation of an electric wave with wave number k_1 modulates the electron distribution function leaving, in addition to terms proportional to the electric field that damps away in time, a perturbation of the form $f_1(v)exp(-ik_1x + ik_1vt)$. This last term, called the ballistic term, conserves the memory of the initial perturbation but it produces no electric field since it oscillates more

and more rapidly as time goes on: $\int f_1(v)exp(ik_1vt) \rightarrow 0$ when t increases. The informations contained in the initial perturbation remain therefore hidden on the small scales fluctuations of the distribution function.

The experimental proof of this result is given by the echo phenomenon [2]. This phenomenon is, as a matter of fact, capable to bring back to the macroscopic scales part of the initial perturbation Landau damped away in time. In fact, if a second plasma wave is excited in the plasma after the first wave is Landau damped, an electric field reappears in the plasma many Landau damping periods after the application of the second pulse. The generation of this new wave, called the echo, is due to the nonlinear constructive interference between the ballistic terms of the two waves distribution functions. But how is generated this interference? Let's take a collisionless plasma and excite an electric field of spatial dependence e^{-ik_1x}. When time goes on, the electric field is Landau damped away and, as seen previously, it modulates the distribution function leaving a perturbation term of the form

$$\delta f_1^{(1)}(x, v, t) = f_1(v)exp(-ik_1x + ik_1vt) \ . \tag{1.3.1}$$

If at time τ we excite a second electric field with spatial dependence e^{ik_2x}, it will damp away in time, leaving a new perturbation in the electron distribution function. This second wave will modulate the unperturbed part of the distribution, as made by the first wave, producing a first order term of the form $f_2(v)exp(ik_2x - ik_2vt)$. Furthermore it will modulated also the first order perturbation $\delta f_1(x, v, t)$ producing a second order distribution function perturbation of the form

$$\delta f^{(2)}(x, v, t) = f_1(v)f_2(v)exp(i(k_2 - k_1)x + ik_2v\tau - i(k_2 - k_1)vt) \ . \tag{1.3.2}$$

Both the first order perturbations give no contribution to the electric field, because the velocity integral over them for large t will phase mix to zero. Instead, the second order one, provides a contribution to the electric field, but only when time t reaches the value $\tau' = \tau k_2/(k_2 - k_1)$. In fact, when $t < \tau'$, also the second order perturbation is a highly oscillatory function as the first order perturbations, and hence its velocity integral tend to zero when t increases. However, when t approaches the time τ',

the second order perturbation stops to be a highly oscillatory function because the exponent $i(k_2 - k_1)x + ik_2v\tau - i(k_2 - k_1)vt$ vanishes at $t = \tau'$. So, at this time, the velocity integral over this term will no more phase mix to zero, leading to the appearance again of an electric field, i.e. the echo. Then, after a certain time interval, the second order perturbation term comes back to be again an highly oscillatory function since its velocity integral will again phase mix to zero.

The first analytical study of the temporal echo phenomenon is due to Gould, O'Neil and Malmberg in 1967 [1, 2]. Using the Vlasov and Poisson equations, they derived the electric potential of a second order echo. Making a brief review of this theory we will show how to get the echo potential. The theory assumes the plasma to be collisionless, one dimensional and that ions are at rest forming a neutralizing background. The electron distribution function is expanded in terms of an equilibrium homogeneous distribution, $f_e(x, v, t = 0) = f_0(v)$ plus a perturbation term $f_1(x, v, t)$. The total potential ϕ includes the potential due to the plasma charge distribution $\rho = e \int f dv$ and an externally produced potential ϕ_{ext} containing the two external pulse we want to perturb the system with. The external potential, composed by one pulse of wave number k_1 excited at $t = 0$ and a second one with wave number k_2 applied after τ times from the first, takes the form:

$$\phi_{ext} = \phi_{k_1} cos(k_1 x)\delta(\omega_{pe} t) + \phi_{k_2} cos(k_2 x)\delta[\omega_{pe}(t - \tau)] \tag{1.3.3}$$

where δ is the Dirac function.

The 1D-1V Vlasov - Poisson system, with fixed neutralizing protons, becomes:

$$\frac{\partial f}{\partial t} + v\frac{\partial f}{\partial x} + \frac{e}{m_e}\frac{\partial \phi}{\partial x}\frac{\partial f}{\partial v} = 0 \tag{1.3.4}$$

$$\frac{\partial^2 \phi}{\partial x^2} = \frac{\partial^2 \phi_{ext}}{\partial x^2} + 4\pi e \left(\int f \, dv \, - \, n_0 \right). \tag{1.3.5}$$

By taking the Fourier and Laplace transforms of Vlasov and Poisson equations, substituting $\tilde{f}_k(v, p)$ calculated from Vlasov equation in Poisson one and expanding the total potential $\tilde{\phi}_k$ in terms of the external applied potentials ϕ_{k_1} and ϕ_{k_2}, we can

compute the second order potential (for the detailed computation see Appendix B) for the wave number $k_3 = k_2 - k_1$ (the one associated to the echo), obtaining:

$$\phi_{k_3}(2)(t) = \phi_{k_1}\frac{\omega_{pe}e\lambda_D}{T}\tau\frac{\phi_{k_2}k_1^4k_2}{Tk_3(k_1+k_3)^2}\times$$

$$\times\frac{-(k_3/k_1)\gamma(k_1)e^{\gamma(k_1)k_3/k_1(\tau'-t)}cos[\omega(k_1)(k_3/k_1)(\tau'-t)+\delta}{\{[\omega_{pe}^2(k_3-k_1)/(k_3+k_1)]^2+\gamma(k_1)^2\}\{1/2\}}\ for\ \ t<\tau'$$

$$\times\frac{\gamma(k_3)e^{\gamma(k_3)(t-\tau')}cos[\omega(k_3)(t-\tau')+\delta'}{\{[\omega_{pe}^2(k_3-k_1)/(k_3+k_1)]^2+\gamma(k_3)^2\}\{1/2\}}\ for\ \ t>\tau' \tag{1.3.6}$$

where

$$\begin{aligned}\tan(\delta) &= \gamma(k_1)(k_3-k_1)/[\omega_{pe}(k_3+k_1)]\\ \tan(\delta') &= \gamma(k_3)(k_1-k_3)/[\omega_{pe}(k_3+k_1)].\end{aligned} \tag{1.3.7}$$

We observe that the echo is symmetric in time only when k_1 is exactly equal to k_3, otherwise it grows up at the rate $exp[\gamma(k_1)k_3/k_1(\tau'-t)]$ and damps at the rate $exp[\gamma(k_3)(t-\tau')]$.

This theory is based on the collisionless Vlasov equation, and looses its validity when collisional effects are enough "rapid" to destroy the phase informations stored in the ballistic terms before the echo can appear. In order to investigate the importance of collisions in the long time dynamics of a weakly collisional plasma, it is possible to add a collisional operator to the Vlasov equation. O'Neil developed an analytical weakly collisional theory [**?**] for two small angle collisional processes: Coulomb collisions and microturbulence. These collisional processes result particularly effective at smoothing the distribution function ballistic term (large velocity gradients of the distribution function) and therefore, at destroying the plasma wave echo. With this theory, O'Neil computed how the presence of Coulomb collisions and microturbulence

affect the echo, as we will show in the rest of this section. Even in this case, the theory is developed in the limit of a one dimensional unmagnetized plasma. The part of the theory that we discuss here refers to the case of second order temporal echoes in presence of Coulomb collisions. A Fokker-Plank operator [29, 30, 31] of the form

$$FP(f) = -\frac{\partial}{\partial v}[D_1 f] + \frac{\partial^2}{\partial v^2}[D_2 f] \tag{1.3.8}$$

has been chosen by O'Neil to represent small-angle collisions. When this operator is applied to a free streaming perturbation as $f_1(x, v, t) = exp(ikx - ikvt)$, the leading term of the operator at large times is the second velocity derivative. Therefore, at large times the Fokker-Plank operator acting on $f_1(x, v, t)$ can be approximate as:

$$FP(exp(ixk - ikvt)) \simeq -D_2 k^2 t^2 exp(ikx - ikvt) \tag{1.3.9}$$

where the coefficient of $exp(ikx - ikvt)$ can be interpreted as the effective collision frequency $\nu_{eff}(k, t) = D_2 k^2 t^2$.

Before presenting the analytical steps for obtaining the echo potential expression, some assumptions have to be made. These assumption are useful to make easier the calculation. The first, coming from the choice of considering a weakly collisional plasma, is that, during the Landau damping phase, collisional damping must be negligible, i.e. $\gamma_L^{-1}\nu_{eff} << 1$. This assumption means that the theory is valid only for regimes in which the coefficient D_2 is sufficiently small so that, while Landau damping is acting, collisions practically produce no effect. Second, the time τ' between the application of the first pulse and the appearance of the echo must be much longer than the Landau damping time, i.e. $\tau'\gamma_L >> 1$. This last assumption is necessary to ensure that collisions have a relevant effect on the echo. In fact, since D_2 is small the effect of collisions can be felt only when the time t is large enough to overcome the smallness of D_2. Hence, if τ' is too small (i.e. ν_{eff} is small), collisions have no time to affect the ballistic terms before the echo is formed.

With these assumption, O'Neil first used collisionless theory to obtain the initial form of the electron distribution function perturbation resulting from the application of the two pulses and then used the Fokker-Plank equation without electric field

driving terms to determine the collisional damping affecting the perturbations during the free streaming.

If we excite in the plasma a first pulse of the form $\phi_{k_1} cos(k_1 x)\delta(\omega_{pe} t)$, collisionless theory predicts that the form of the first order electron distribution function streaming perturbation will be:

$$f_k^{(1)}(v,t) = \frac{e}{m_e} \frac{\phi_{k_1}[\delta(k-k_1)+\delta(k+k_1)]ik}{2\omega_{pe}\epsilon(k,-ikv)} \frac{\partial f_0}{\partial v} e^{-ikvt} \tag{1.3.10}$$

where, as above, $f_0(v)$ is the initial Maxwellian distribution function and $\epsilon(k,-ikvt)$ is the dielectric function. Using equation C.0.21 as the initial condition, the electron distribution function streaming perturbation evolves according to the homogeneous Fokker-Plank equation

$$\frac{\partial f_k}{\partial t} + ivkf_k - FP(f_k) = 0 \tag{1.3.11}$$

until the excitation of the second pulse. Substituting equation C.0.21 in C.0.22 one obtains:

$$f_k^{(1)}(v,t) = \frac{e}{m_e} \frac{\phi_{k_1}[\delta(k-k_1)+\delta(k+k_1)]ik}{2\omega_{pe}\epsilon(k,-ikv)} \frac{\partial f_0}{\partial v} exp\left(-ikvt - \int_0^t \nu_{eff}(k,t')dt'\right) \tag{1.3.12}$$

where $\nu_{eff}(k,t) = D_2 k^2 t^2$. The collisional damping factor that appears in the previous equation was already determined by Karpman [32] and Su and Oberman [33] for a streaming perturbation damped by Coulomb collisions and by Dupree [31] for the microturbulence case.

When also the second pulse, of the form $\phi_{k_2} cos(k_2 x)\delta[\omega_{pe}(t-\tau)]$ is excited in the plasma, it will generate a first order streaming perturbation of the same type of equation C.0.21 but with k_2 instead of k_1 and $t-\tau$ instead of t, and a second order one derived from the modulation of the perturbation already left by the first pulse. This second order term is produced only for wave numbers k_1+k_2 and k_2-k_1 but, as already mentioned before, the one for which the echo is generated will be only $k_3 = k_2 - k_1$. Hence the second order streaming perturbation of interest is:

$$f_{k_3}^{(2)}(v,t) = \left(\frac{e}{m_e}\right)^2 k_1 k_2 \phi_{k_1}\phi_{k_2} i k_1 \tau \frac{\partial f_0}{\partial v} \frac{exp\left(-ik_3 v(t-\tau) + ik_1 v\tau - \int_0^\tau \nu_{eff}(k_1,t')dt'\right)}{4\omega_{pe}^2 \epsilon(k_2,-ik_2 v)\epsilon(-k_1,ik_1 v)}. \tag{1.3.13}$$

Substituting equation C.0.24 as initial condition in the homogeneous Fokker-Plank, equation C.0.22, one obtains:

$$\begin{aligned} f_{k_3}^{(2)}(v,t) = \left(\frac{e}{m_e}\right)^2 k_1 k_2 \phi_{k_1}\phi_{k_2} i k_1 \tau \frac{\partial f_0}{\partial v} exp(-ik_3 v(t-\tau) + ik_1 v\tau)\times \\ \times \frac{exp\left(-\int_0^\tau \nu_{eff}(k_1,t')dt' - \int_\tau^t \nu_{eff}(k_1,k_2,\tau,t')dt'\right)}{4\omega_{pe}^2 \epsilon(k_2,-ik_2 v)\epsilon(-k_1,ik_1 v)} \end{aligned} \tag{1.3.14}$$

where $\nu_{eff}(k_1,k_2,\tau,t') = D_2[-k_3(t'-\tau)+k_1\tau]^2$ is the effective collision frequency that one obtains when the Fokker-Plank operator acts on the second order ballistic term $exp[-ik_3 v(t-\tau)+ik_1 v\tau]$. To determine the echo potential we divide equation C.0.25 by $\epsilon(k_3,-ik_3 v)$ (to account for the self-consistent field associated to the echo itself), and inserting it in Poisson equation. The potential calculated at time τ' at which the echo occurs, results:

$$\begin{aligned} \phi_{k_3} = \frac{e k_1^2 k_2 \phi_{k_1}\phi_{k_2} i\tau}{4mk_3^2} \int_{-\infty}^{+\infty} dv \frac{\partial f_0}{\partial v} exp[ik_3 v(\tau'-t)]\times \\ \times \frac{exp\left(-\int_0^\tau \nu_{eff}(k_1,t)dt - \int_\tau^{\tau'} \nu_{eff}(k_1,k_2,\tau,t)dt\right)}{\epsilon(k_2,-ik_2 v)\epsilon(-k_1,ik_1 v)\epsilon(k_3,-ik_3 v)}. \end{aligned} \tag{1.3.15}$$

If the diffusion coefficient D_2 is independent of time, as occurs for Coulomb collisions, the exponential term containing the collisional damping rate can be easily evaluate obtaining:

$$exp\left(-\int_0^\tau \nu_{eff}(k_1,t)dt - \int_\tau^{\tau'} \nu_{eff}(k_1,k_2,\tau,t)dt\right) = exp\left(-D_2(v)\frac{k_1^2 k_2 \tau^3}{3k_3}\right). \tag{1.3.16}$$

In the case where D_2 is also independent of velocity, the collisional damping factor can be extracted integral sign. In this way, the shape of the echo results the same as the one obtained in the collisionless case but the amplitude is reduced by a factor

$$exp\left(-D_2\frac{k_1^2 k_2 \tau^3}{3k_3}\right). \tag{1.3.17}$$

When instead D_2 is a function of velocity, the amplitude as well as the shape of the echo will result different from the collisionless ones. O'Neil found that in this case the collisional damping reduces the wings of the echo more that the peak of the echo.

The existence of plasma echoes was proved experimentally by Gould, O'Neil and Malmberg in 1967 [2]. In this work they also verified some of the echo properties predicted by the theory, even for echoes of higher orders. Many other studies are made on the echo phenomenon, as theoretical as experimental (see for example [34, 35, 36, 38, 39, 40]).

1.4 Two stream instability

The two stream instability is a velocity-space instability driven by electron momentum anisotropy. To generate a two stream instability in a collisionless plasma we take, as the initial anisotropic equilibrium, two electron streams of density n_a and n_b drifting with uniform velocities V_a and V_b in opposite direction on a background of neutralizing protons, such that the initial total current in the plasma is zero. Because of the initial anisotropy of the electron distribution function, if we perturb longitudinally the system with a small amplitude electrostatic wave, the amplitude of the perturbation begins to increase, corresponding to the development of the two stream instability. We will see, however, that only a limited range of wavelengths are unstable. This increase in the electric field energy is obtained to the disadvantage of electrons kinetic energy. During the development of the instability, in fact, the electrons of the two streams begin to be accelerated and decelerated by the wave field. When the amplitude of the electric field becomes large enough to trap less energetic electrons (i.e. when $e\Phi$ is about $mv_e^2/2$, where v_e is the velocity of an electron), the instability starts to saturate and the system reaches a new equilibrium situation. This non-linear dynamic of

electron trapping, driven by kinetic effects, necessitate of a kinetic approach, while the initial development of the instability (linear regime) can be described also by a fluid theory if we're dealing with a cold plasma. In the following of this section we compute the dispersion relation by using the linearized kinetic equations. If the direction of propagation of the electrostatic perturbation is chosen to lie along the same direction of the two electron streams, the system can be easily described in a one dimensional space using the Vlasov and Poisson equations. Considering the neutralizing ions to be of infinite mass, we can neglect their motion. In this way, the analysis is restricted only to high frequency effects. We take the Vlasov Poisson system of equations 1.1.1, 1.1.2 where n_0, f_e and ϕ represent the protons density, the electron distribution function and the electrostatic potential, respectively. The linearized equations can be obtained expressing the distribution function f_e and the electric potential ϕ as $f_e(x,v,t) = f_{e0}(x,v,t) + \epsilon f_{e1}(x,v,t)$ and $\phi(x,t) = \phi_0(x,t) + \epsilon\phi_1(x,t)$ and taking the Fourier transform with respect to the spatial variables and the Laplace transform in time. The resulting equations are:

$$(p + ikv)\widetilde{f_{ek}} = f_{ek}(k,v,t=0) + ik\frac{e}{m_e}\frac{\partial f_{e0}}{\partial v}\widetilde{\phi_k} = 0 \tag{1.4.1}$$

$$k^2\widetilde{\phi_k} = 4\pi e\int \widetilde{f_{ek}}\,dv \tag{1.4.2}$$

where

$$f_{ek}(v,t) = \frac{1}{2\pi}\int f_{e1}(x,v,t)exp(-ikx)dx \tag{1.4.3}$$

$$\widetilde{f}_{ek}(v,p) = \frac{1}{2\pi}\int_0^\infty f_{ek}(v,t)exp(-pt)dt \quad \Re(p) > p_0 \tag{1.4.4}$$

$$\phi_k(t) = \frac{1}{2\pi}\int \phi_1(x,t)exp(-ikx)dx \tag{1.4.5}$$

$$\widetilde{\phi}_k(p) = \frac{1}{2\pi}\int_0^\infty \phi_k(t)exp(-pt)dt \quad \Re(p) > p_0 \tag{1.4.6}$$

Choosing the initial electron distribution function as

$$f_{e0}(v) = \delta(v - V_{a0}) + \delta(v + V_{b0}) \tag{1.4.7}$$

and assuming, for simplicity, that the two electron streams have equal density ($n_{a0} = n_{b0} = 1/2$) and equal but opposite velocities ($V_{a0} = -V_{b0} = V_0/2$), the dispersion relation resulting from equations 1.4.1, 1.4.2 is:

$$1 = \frac{\omega_{pe}^2}{2(\omega - kV_0/2)^2} + \frac{\omega_{pe}^2}{2(\omega + kV_0/2)^2} + \frac{\omega_{pi}^2}{\omega^2} \tag{1.4.8}$$

where the last term can be neglected since $\omega^2 >> \omega_{pi}^2$. The roots of equation 1.4.8 are:

$$\omega^2 = \frac{\omega_{pe}^2}{2} + \frac{k^2V_0^2}{4} \pm \sqrt{(\frac{\omega_{pe}^2}{2} + \frac{k^2V_0^2}{4})^2 + \frac{k^2V_0^2}{4}(\omega_{pe}^2 - \frac{k^2V_0^2}{4})} \tag{1.4.9}$$

To generate the instability it is necessary that equation 1.4.9 admits almost one positive complex root. This can be obtained if:

$$|kV_0| < 2\omega_{pe} \tag{1.4.10}$$

This condition says that unstable modes will correspond to wavelengths in the range $0 < \lambda < \pi V_0/\omega_{pe}$ with $k = 2\pi/\lambda$. When $V_0 \to 0$ the grow rate vanishes, as expected and we retrieve plasma oscillations at $\omega = \omega_{pe}$ since we neglected thermal effects. The maximum grow rate is achieved for $kV_0 = 3\omega_{pe}/\sqrt{2}$ and is equal to

$$\omega_{i,max} = \frac{\omega_{pe}}{\sqrt{8}} \ . \tag{1.4.11}$$

As in Landau damping phenomenon, when the wave is large enough to trap the particles, the linear theory breaks down. In fact, the linear Vlasov theory (see section 1.1) is based on the assumption that the orbits of plasma particles are only slightly perturbed by the wave field. On the other hand, when trapping comes into play, the trajectories are strongly deformed: the free streaming motion is converted in quasi-periodic orbits. This process corresponds, in phase space, to the development in the distribution function of coherent structures called vortices corresponding, in

the particle density, to phase space holes [41]. Such coherent structures are associated to BGK states for which the density of trapped particles is lower than the density of free and reflected particles [42]. We can distinguish two kinds of vortices: those generated in the electron distribution function called electron holes, and those of ion distribution function called ion holes. Electron holes are associated to a positive potential perturbation while ion holes to a negative potential one. In our case, where ion are fixed, obviously only electron vortices can be developed. We note that the generation of an hole is formally forbidden by the Vlasov theory and, therefore, it needs of dissipative effects.

The two stream instability can generate more than one vortex. The number of these coherent structures depends on the spatial dimension of the plasma model. All vortices are generated with the same velocity and develop close enough to each other to interact. Berk et al. have shown, in 1970, that phase space holes attract each other [43]. The basic idea of this demonstration is the following. Looking at the particle density, one can represent the holes of the phase space as assemblies of particles with charge $-q$ and mass $-m$ on a stable band of particles of mass m and charge q. The particles that represent the holes will interact electrostatically. The electrostatic interaction between particles of the same charge and negative mass is attractive. Hence each phase space hole, since it is considered as to be "composed" by such particles, will tend to remain a coherent structure. Furthermore, since every phase space holes in the particle density will be made of the same kind of particles with negative charge and negative mass, they will attract each other. This attraction process will lead to collisions among holes which, if in the system some dissipation comes into play, generate a merging process. Bertrand et al. [13] demonstrated through numerical and analytical studies of the two stream instability in the case of a collisionless 1D umagnetized plasma, where ions are considered as a neutralizing fixed backgrund, that BGK states composed by a number of vortex $N \geq 2$ are always unstable. They observed from numerical simulations, that this fact induced a coalescence process leading to the formation of a final stable single vortex.

1.4.1 Ion-acoustic waves

Let's consider the same one dimensional unmagnetized collisionless plasma system described previously but, this time, assuming also the ions free to move. In this

conditions the Vlasov and Poisson equations become:

$$\frac{\partial f_\alpha}{\partial t} + v\,\frac{\partial f_\alpha}{\partial x} - \frac{q_\alpha}{m_\alpha}\frac{\partial \phi}{\partial x}\frac{\partial f_\alpha}{\partial v} = 0 \quad \alpha = e, i \tag{1.4.12}$$

$$\frac{\partial^2 \phi}{\partial x^2} = -4\pi e\left(\int f_e\, dv - \int f_i dv\right); \quad E = -\frac{\partial \phi}{\partial x}\,. \tag{1.4.13}$$

The dispersion relation of the system can be obtained using the same Fourier-Laplace transform procedure of the case with fixed ions:

$$D(k,\omega) = 1 - \sum_\alpha \frac{\omega_{p\alpha}^2}{k}\int \frac{\partial f_{\alpha 0}/\partial v}{kv - \omega} dv = 0\ . \tag{1.4.14}$$

From the solution of this dispersion relation, farther to Langmuir oscillations, shifted in frequency by a small amount for the presence of ions, another kind of electrostatic waves is found in the lower frequencies if electrons are warm ($T_e \gg T_i$). For these waves, called ion-acoustic waves, ions do play a major role. The range of phase velocities in which these waves exist is: $\sqrt{\kappa T_i/m_i} < v_{ph} < \sqrt{\kappa T_e/m_e}$. To obtain the main properties of ion-acoustic waves we compute the zeros of $D(k,\omega)$ in this velocity range. We hence evaluate the velocity integrals of 1.4.14 and we use the result to calculate the real and imaginary parts of the dielectric function $D(k,\omega)$. The procedure is the same as for Langmuir wave previously described in details in section 2.1. In this section we will limit to show only the results of these calculations. Thus, by choosing maxwellian equilibrium distribution functions, we obtain a real and imaginary part of $D(k,\omega)$ of the form:

$$\begin{aligned} D_r &= 1 + \frac{1}{k^2\lambda_D^2} - \frac{\omega_{pi}^2}{\omega_r^2}\left(1 + \frac{3k^2 T_i}{m_i \omega_r}\right) \\ D_i &= \pi \sum_\alpha \frac{\omega_{p\alpha}^2}{k^2}\left(\frac{m_\alpha}{2\pi\kappa T_\alpha}\right)^{1/2}\frac{m_\alpha}{T_\alpha}\frac{\omega_r}{k} exp\left(-\frac{\omega^2 m_\alpha}{2k^2\kappa T_\alpha}\right) \end{aligned} \tag{1.4.15}$$

where we recall that ω_r is the real part of the frequency ω and $\alpha = i, e$. Setting $D_r = 0$ we find the expression for ω_r:

$$\omega_r^2 = \frac{k^2 \kappa T_e}{2m_i(1+k^2\lambda_D^2)} \left[1 + \sqrt{1 + \frac{12T_i}{T_e}(1+k^2\lambda_D^2)}\right] . \tag{1.4.16}$$

In the limit of warm electrons, i.e. $T_e >> T_i$, equation 1.4.16 becomes:

$$\omega_r^2 \simeq \frac{k^2 C_s^2}{1+k^2\lambda_D^2} \tag{1.4.17}$$

where C_s is called the ion-acoustic, or ion-sound, speed and is given by $C_s = \sqrt{\kappa T_e/m_i}$. In the large wavelength limit $k^2\lambda_D^2 \ll 1$ the above expression reduces to:

$$\omega_r^2 \simeq k^2 C_s^2 . \tag{1.4.18}$$

The damping rate, as previously explained in section 1.2, can be obtained using the expression $\gamma = -D_i/\partial D_r/\partial\omega_r$, for ω_r of equation 1.4.17, which gives :

$$\gamma = -\frac{|\omega_r|\sqrt{\pi/8}}{(1+k^2\lambda_D^2)^{3/2}} \left[\left(\frac{T_e}{T_i}\right)^{3/2} exp\left(-\frac{T_e/T_i}{2(1+k^2\lambda_D^2)}\right) + \sqrt{\frac{m_e}{m_i}}\right] . \tag{1.4.19}$$

These waves are called ion-acoustic waves because in the large wavelength limit, see equation 1.4.18, all wavelength propagate at the same speed that is about the ion-sound speed C_s.

1.5 Correlations

A plasma is composed by a very large number of charged particles, each producing an electric potential with a characteristic length of influence of a Debye length λ_D, much greater than the distance between particles $1/n_0^{1/3}$. Therefore plasma particles interact at all times, but the average interaction energy $< W_{i,j} >$ between two of them is very weak with respect to the interactions with the collective system. This allows to express the thermodynamics functions of the plasma by a virial expansion similar to the case of an ideal gas, although for a gas $\omega/\nu_{coll} \ll 1$, while for a plasma

$\omega/\nu_{coll} \ll 1$, using $< W_{i,j} > /\kappa T$ as the expansion parameter. However, interactions, even if weak in average, produce correlations among particles, i.e. particles of the same sign charges tend to stay less time possible near to each other while particles with different sign charges tend to cluster, thus affecting the equation of state of the system. For a plasma, the parameter that describes the deviation of the system from an "ideal gas" is:

$$g = \left(\frac{8\pi e^2}{\kappa T}\right)^{3/2} n_0^{1/2} = \frac{1}{n_0 \lambda_D^3} \tag{1.5.1}$$

defined as the ratio between the mean distance of closest approach and the average spacing between particles, and where n_0 is the density of particles and λ_D is the Debye length. Eq. 1.5.1 tells us that if there are many particles in the Debye sphere, the average potential energy becomes much less than the kinetic one and hence the interaction energy can be neglected. In this condition, g becomes very small and the thermodynamic functions of the plasma can be expressed through ideal gas thermodynamic functions expanded in terms of this small parameter g. As we will now see, the parameter g measures the departure of the thermodynamic function of the plasma from those of an ideal gas.

Let's consider a plasma composed of N particles, half ions and half electrons, at a fixed temperature T. The probability of finding the N particles at locations $(x_1, x_2, ..., x_N)$ is given by the Gibbs distribution:

$$D(x_1, x_2, ..., x_N) = \frac{1}{Z} exp\left(-\frac{\sum_k \sum_{i>k} W_{ik}}{\kappa T}\right) \tag{1.5.2}$$

where

$$Z = \int exp\left(-\frac{\sum_k \sum_{i>k} W_{ik}}{\kappa T}\right) dx_1 dx_2 ... dx_N \tag{1.5.3}$$

is the partition function and

$$W_{ik} = \frac{q_k q_i}{|x_i - x_k|} + \phi_{ext} \tag{1.5.4}$$

is the potential and ϕ_{ext} is an external potential that takes into account any potential energy due to external sources. The probability of finding a particle labelled 1 in the location x_1 is:

$$F_1(x_1) = \int Ddx_2dx_3...dx_N \tag{1.5.5}$$

and if there are no external force acting on particles, the probability F_1 becomes constant because there are no preferred locations for the particles. Hence F_1 can be expressed as $F_1 = 1/V$, where V is the volume of the system. The probability density to have simultaneously particle 1 in the position x_1 and particle 2 in the position x_2 is:

$$F_2(x_1, x_2) = \int Ddx_3dx_4...dx_N\,. \tag{1.5.6}$$

Similarly, the s particle distribution will be given by the expression:

$$F_s(x_1, x_2, ..., x_s) = \int Ddx_{s+1}dx_{s+2}...dx_N\,. \tag{1.5.7}$$

This probability density $F_{s>1}$ contains the effects of the interactions among particles. If we consider the case in which the interaction potential can be neglected, then the probability of having a particle at a certain location will not affect the probability of finding other particles in another location and the probability density F_s can be written as:

$$F_s = F_1(x_1)F_1(x_2)...F_1(x_s) = V^{-s}\,. \tag{1.5.8}$$

When instead the interaction potential among particles is present, the probability densities F_i can be written trough the Mayer cluster expansion [46] obtaining:

$$
\begin{aligned}
F_2(x_1, x_2) &= (1 + P_{12}(x_1, x_2))\, F_1(x_1) F_1(x_2) \\
F_3(x_1, x_2, x_3) &= (1 + P_{12}(x_1, x_2) + P_{12}(x_2, x_3) + P_{12}(x_1, x_3) + T_{123})\, F_1(x_1) F_1(x_2) F_1(x_3) \\
&\quad etc....
\end{aligned}
\tag{1.5.9}
$$

where P_{12} is the two particle correlation function and T_{123} is the three particle one. The particles correlation function takes into account the fact that repelling particles have a lower probability to be near neighbors while attracting particles have an higher one. In our case, in which the force that produce the correlations is the Coulomb force, the dependence of the two particle correlation function can be expressed as:

$$
P_{12}(x_1, x_2) = P(|x_1 - x_2|)\,. \tag{1.5.10}
$$

Since the plasma interactions are weak, one can use the approximation $T_{123} \ll P_{12} \ll 1$.

Indeed the complete Gibbs distribution take into account also of the velocity of particles and can be write as:

$$
\hat{D}(x_1, x_2, ..., x_N, v_1, v_2, ..., v_N) = \frac{1}{\hat{Z}} exp\left(-\frac{\sum_i \frac{1}{2} m_i v_i^2}{\kappa T}\right) exp\left(-\frac{\sum_k \sum_{i>k} W_{ik}}{\kappa T}\right) \tag{1.5.11}
$$

The distribution function is separable in the velocity coordinates of the N particles:

$$
\hat{D} = \frac{\prod_i exp(-m_i v_i^2 / 2\kappa T)}{[\int dv_1 exp(-m_i v_i^2 / 2\kappa T)]^N} D(x_1, x_2, ..., x_N) \tag{1.5.12}
$$

implying that no velocity space correlations are present and therefore that the probability densities can ba written as:

$$\begin{aligned} \hat{F}_1(x_1, v_2) &= f_1(v_1)F_1(x_1) \\ \hat{F}_2(x_1, x_2) &= f_1(v_1)f_1(v_2)F_2(x_1, x_2) \end{aligned} \tag{1.5.13}$$

where

$$f_1(v_1) = \left(\frac{m}{2\pi\kappa T}\right)^{3/2} exp\left(-\frac{m_i v_i^2}{2\kappa T}\right) . \tag{1.5.14}$$

The two correlation function P_{12} can be computed analytically, as made in reference [25] in the case for which $T_{123} \ll P_{12} \ll 1$ and when only Coulomb interactions are considered, obtaining:

$$P_{12} = -\frac{q_1 q_2}{e^2}\frac{g}{8\pi}\frac{exp(-|\vec{R}|/\lambda_D)}{|\vec{R}|/\lambda_D} \tag{1.5.15}$$

where $\vec{R} = \vec{x}_1 - \vec{x}_2$ and g is the plasma parameter of equation 1.5.1. The first property to note of equation 1.5.15, is that if the parameter g is small, the correlation between particles becomes weak. The equation also shows that P_{12} is proportional to the signs of the coupling between correlated particles, hence taking into account if particles are like of oppositely charged.

Until now, we have used the fundamental hypothesis of being at the thermodynamic equilibrium, assumption which become questionable in the case of strongly non linear dynamics. This approach allows to derive the Vlasov equation, i.e. the mean field theory in which each particle interacts principally with the average field generated by all plasma particles while the interactions between single particles are neglected. The Vlasov equation is, in fact, obtained integrating the Liouville equation for the n-particles Gibbs equation $F(x_1, ..., x_n, v_1, ..., v_n)$ at the thermodynamic equilibrium:

$$\int \frac{\partial F}{\partial t} dx_1 \cdots dx_n dv_1 \cdots dv_n +$$
$$+ \sum_i \left(\int v_i \frac{\partial F}{\partial x_i} dx_1 \cdots dx_n dv_1 \cdots dv_n + \int a_i^T \frac{\partial F}{\partial v_i} dx_1 \cdots dx_n dv_1 \cdots dv_n \right) = 0 \tag{1.5.16}$$

over the coordinates and velocities of all but one particles and where a_i^T is the total acceleration of particle i due to external and interparticle forces. In this way, if we neglect the interparticle forces, we obtain a Liouville equation for a one particle distribution function (i.e. the Vlasov equation) with the fundamental constraint that the isolines of this distribution function can be transported in phase space, but never reconnected.

Chapter 2

Numerical schemes

The numerical simulations that we show in this thesis are made using numerical schemes based on the solution of the Hamiltonian Vlasov-Poisson system of equations (or of the Vlasov-Maxwell system if the plasma is magnetized). These numerical codes integrate the Vlasov equation by using a splitting scheme (see for example Cheng and Knorr, 1976, [47]) which is accurate to second order in Δt, and based on symplectic integration approach. Indeed one of the most critical aspect of Vlasov numerical schemes is the fact that the equations must be solved on a discretized phase space and time. As we will show in the following section, in fact, while the time discretization, obtained in this case using the splitting scheme, results a symplectic integration (i.e. it ensures the conservation of the volume element in phase space during time evolution), this is no longer valid when one performs also the dicretization in the (x, v) space.

2.1 The splitting scheme

Even in the simplest case of a one dimensional plasma interacting with an electrostatic field, the Vlasov equation is an advection equation that depends on two independent variables (x, v). This equation has the important property that the particles trajectories

$$\frac{dx}{dt} = v \quad \frac{dv}{dt} = -E \tag{2.1.1}$$

describe a Hamiltonian flow $\mathcal{T}^t$ in the phase space (see Mangeney et al. [50]). This flow determines the evolution of a point $z_0 = (x_0, v_0)$ of the phase space in time:

$$z = \mathcal{T}^t z_0 \tag{2.1.2}$$

This flow is reversible

$$z_0 = \mathcal{T}^{-t} z \quad \mathcal{T}^{-t}\dot{\mathcal{T}}^t = identity\,. \tag{2.1.3}$$

and conserves the volume element in the phase space, i.e. it is a symplectic transformation. In term of this flow the solution of the Vlasov equation can be written as

$$f(z,t) = f(z_0, t=0) = f(\mathcal{T}^{-t}z, t=0) = T^t f(z, t=0) \tag{2.1.4}$$

where T^t is the evolution operator for the distribution function. Assuming T^t as known, the next step is to obtain the formulation of this operator on the discrete x and v grid. As shown in reference [50], the space and velocity approximation of this operator on the discrete grid is no more reversible, implying that the phase space flow is no longer Hamiltonian and the resulting scheme is dissipative, even if the time advancing is of symplectic form. Since usually the flow $\mathcal{T}^t$ (or equivalently T^t) is not known explicitly, the advection equation must be solved using little time steps δt that allows to solve it approximately. In the case of the splitting scheme the numerical scheme solves the advection equation to the second order in δt.

Let's now describe how works this method in a one dimensional electrostatic system.

The Vlasov equation can be written as:

$$\frac{\partial f}{\partial t} = \mathcal{L}[f] \equiv \mathcal{L}_x[f] + \mathcal{L}_v[f] \tag{2.1.5}$$

where the displacement operators $\mathcal{L}_x$ and $\mathcal{L}_v$ are defined as:

$$\begin{aligned} \mathcal{L}_x &= -v\frac{\partial}{\partial x} \\ \mathcal{L}_v &= E\frac{\partial}{\partial v}\,. \end{aligned} \tag{2.1.6}$$

Since the Vlasov equation can be also written as:

$$\frac{\partial f}{\partial t} = -[H, f] \tag{2.1.7}$$

where $H = v^2/2 + \Phi(x)$ is the Hamiltonian of the system and [] are the Poisson brackets. The above operation corresponds to split the Hamiltonian in the sum two parts, the first $H_1 = v^2/2$ depending only by v and the second $H_2 = \Phi(x)$ depending only by x.

If the coupling between the distribution function f and the electric field E is not considered, the operators 2.1.6 can be considered as linear. Therefore, if $f(x, v, t)$ at the time t is known, after a time interval Δt the distribution function can be written as:

$$f(x, v, t + \Delta t) = e^{\int_t^{t+\Delta t} d\tau \mathcal{L}(\tau)} f(x, v, t) = \left[e^{(\Delta t/2)\mathcal{L}_x} e^{(\Delta t)\mathcal{L}_v} e^{(\Delta t/2)\mathcal{L}_x}\right] f(x, v, t) + O(\Delta t^2)\,. \tag{2.1.8}$$

called the splitting scheme.

Note that the operators $T_x^{\Delta t} = e^{(\Delta t)\mathcal{L}_x}$ and $T_v^{\Delta t} = e^{(\Delta t)\mathcal{L}_v}$ of the previous equation correspond respectively to a spatial translation and a translation along the v axis:

$$\begin{aligned} T_x^{\Delta t} f(x, v) &= f(x - v\Delta t, v) \\ T_v^{\Delta t} f(x, v) &= f(x, v + E\Delta t)\,. \end{aligned} \tag{2.1.9}$$

Hence, the integration made by the splitting scheme, to obtain for example the solution f^{n+1} at the time $t_{n+1} = t_n + \Delta t$ knowing the distribution function f^n at the time $t_n = n\Delta t$

$$f^{n+1}(x, v) = \mathcal{T}_x^{\Delta t}(\Delta t/2)\mathcal{T}_v^{\Delta t}(\Delta t)\mathcal{T}_x^{\Delta t}(\Delta t/2) f^n(x, v) \tag{2.1.10}$$

can be seen as a sequence of shifting along the x axis or v axis:

$$f^*(x,v) = f^n(x - v\Delta t/2, v) \tag{2.1.11}$$

$$f^{**}(x,v) = f^*(x, v + E\Delta t) \tag{2.1.12}$$

$$f^{n+1}(x,v) = f^{**}(x - v\Delta t/2, v) \tag{2.1.13}$$

In terms of the phase space points and of the flow $\mathcal{T}^{\Delta t}$ we instead obtain:

$$\begin{aligned} x_{\Delta t} = \mathcal{T}_x^{\Delta t} x = x + v\Delta t + \frac{\Delta t^2}{2} E\left(x + v\Delta t/2\right) \\ v_{\Delta t} = \mathcal{T}_v^{\Delta t} v = v + E\Delta t\left(x + v\Delta t/2\right) . \end{aligned} \tag{2.1.14}$$

These equations are the Verlet equations for a second order particle advance. Also these equations have the property of conserving in time a volume of the phase space. As a consequence, the approximate Hamiltonian characteristic of the particle motion described by these equations:

$$\hat{H} = H + \frac{v\Delta t}{2} E + \frac{\Delta t^2}{12}\left(E^2 + v^2 \frac{\partial E}{\partial x}\right) \tag{2.1.15}$$

is exactly conserved during the evolution.

In summary, the integration of the Vlasov equation through the splitting scheme reduces to three shifts: the first along the x axis by an amount $v\Delta t/2$, corresponding to half a time step, the second along the v axis by an amount $E(x), \Delta t$, and finally another shift along on the x axis by a half time step. The electric field E is computed after the first shift from the function f^* through the Poisson equation. Our code integrate the Poisson equation in the Fourier space, with a standard fast Fourier transform algorithm. Since the phase space points obtained with the shifts very often do not coincide with the mesh points, the value of the distribution function after the shift must be usually derived by using an interpolation method.

In our codes we use two kind of interpolation algorithms: the second order and third order Van Leer schemes (defined as VL2 and VL3) and the third order Spline scheme (SPL).

2.2 Van Leer interpolation scheme

In this section we will give a brief description of the second (VL2) and third order (VL3) Van Leer interpolation algorithms. These interpolation methods (see [48, 49, 50]) are based on the enforcing of the mass conservation between the cells of the numerical phase space. As in our simulations, we consider a phase space given by $0 \leqslant x < L$ and $-v_{max} \leqslant v \leqslant v_{max}$ discretized on a numerical grid (x_i, v_j) where $x_i = i\Delta x$ with $i = 1, ..., N_x$ and $\Delta x = L/N_x$ and where $v_j = -v_{max} + j\Delta v$ with $j = 0, ..., 2N_v$ and $\Delta v = v_{max}/N_v$. The time is discretized as $t_n = n\Delta t$ and the numerical solution of the distribution function on the mesh points at the time t_n is defined as $F^n_{i,j} = f(x_i, v_j, t^n)$ and satisfy the following boundary conditions $F^n_{i,0} = F^n_{i,2N_v} = 0$ and periodic spatial boundary conditions $F^n_{N_x,j} = F^n_{0,j}$. To obtain a second order accurate solution, the electron distribution function profile on each cell of surface $\Delta x \Delta v$ centered on the point (x_i, v_j) can be approximate with a plan function:

$$\mathcal{F}^n_{i,j}(x, v) = F^n_{i,j} + A(x - x_i) + B(v - v_j) \tag{2.2.1}$$

where A and B are the finite difference expressions for the first order derivative in x and v respectively, defined as:

$$\begin{aligned} A &= (F^n_{i+1,j} - F^n_{i-1,j})/(2\Delta x) \\ B &= (F^n_{i,j+1} - F^n_{i,j-1})/(2\Delta v) \end{aligned} \tag{2.2.2}$$

Let us now consider the first step of the splitting scheme, Eq.2.1.11, where it is made a shift along the x axis by the amount $v_j \delta t/2$. If the total mass contained inside the cell (x_i, v_j) at the time t^n is defined as:

$$\mathcal{M}^n_{i,j} = \int_{x_i - \Delta x/2}^{x_i + \Delta x/2} dx \int_{v_i - \Delta v/2}^{v_i + \Delta v/2} dv \mathcal{F}^n_{i,j}(x, v) = F^n_{i,j} \Delta x \Delta v \tag{2.2.3}$$

after this shift along the spatial direction, for $v_j > 0$, the cell looses a portion $\delta\mathcal{M}_{i,j}$ of its mass, given by:

$$\delta\mathcal{M}_{i,j} = \int_{x_i+\Delta x/2}^{x_i+\Delta x/2-\delta x_j} dx \int_{v_i-\Delta v/2}^{v_i+\Delta v/2} dv \mathcal{F}^n_{i,j}(x,v) = \\ \delta x \Delta v \left[F^n_{i,j} + \frac{1}{4}\left(1 - \frac{\delta x}{\Delta x}\right)(F^n_{i+1,j} - F^n_{i-1,j}) \right] \tag{2.2.4}$$

and receives the mass $\delta\mathcal{M}_{i-1,j}$ from the cell (x_{i-1}, v_j). From the balance between the mass lost and gained by the cell (x_i, v_j), we can obtain the final expression for the interpolation value F^* of the distribution function

$$\begin{aligned} F^*_{i,j} &= F^n_{i,j} + \frac{1}{\Delta x \Delta v}(\delta\mathcal{M}_{i-1,j} - \delta\mathcal{M}_{i,j}) \\ &= -\alpha_j(1-\alpha_j)F^n_{i-2,j}/4 + \alpha_j[1 + (1-\alpha_j)/4]F^n_{i-1,j} \\ &+ (1-\alpha_j)(1+\alpha_j/4)F^n_{i,j} - \alpha_j(1-\alpha_j)F^n_{i+1,j}/4 \end{aligned} \tag{2.2.5}$$

where $\alpha_j = \delta x_j/\Delta x = v_j \Delta t/(2\Delta x)$.

In the case where $v_j < 0$, the same procedures gives:

$$\delta\mathcal{M}_{i,j} = -\delta x \Delta v \left[F^n_{i,j} - \frac{1}{4}\left(1 + \frac{\delta x}{\Delta x}\right)(F^n_{i+1,j} - F^n_{i-1,j}) \right] \tag{2.2.6}$$

and

$$\begin{aligned} F^*_{i,j}(x,v) &= \alpha_j(1+\alpha_j)F^n_{i-2,j}/4 - \alpha_j[1 + (1+\alpha_j)/4]F^n_{i-1,j} \\ &+ (1+\alpha_j)(1-\alpha_j/4)F^n_{i,j} + \alpha_j(1+\alpha_j)F^n_{i+1,j}/4 \end{aligned} \tag{2.2.7}$$

In the second step of the splitting scheme, Eq.2.1.12, the distribution function, after the calculation of the electric field through the Poisson equation, is shifted along the v axis by an amount of $\delta v_i = E(x_i)\Delta t$. To compute the distribution function $F^{**}_{i,j}(x,v)$ the same procedure described above can be used, obtaining two equations for $\delta v_i > 0$ and $v_i < 0$ analogue to equations 2.2.5 and 2.2.7. Finally, the third step of the splitting scheme is equal to the first.

The third order interpolation scheme is obtained in the same way of the second order one, already shown, apart for the definition of the distribution density profile. In fact, in this case, $\mathcal{F}^n_{i,j}$ contains also the second order derivative and both the derivatives are computed with the five points finite differences expressions:

$$\mathcal{F}^n_{i,j}(x,v) = F^n_{i,j} + A(x-x_i) + B(v-v_j) + C(x-x_i)^2 + D(v-v_j)^2 \tag{2.2.8}$$

where

$$\begin{aligned} A &= (F^n_{i-2,j} - 8F^n_{i-1,j} + 8F^n_{i+1,j} - F^n_{i+2,j})/(12\Delta x) \\ B &= (F^n_{i,j-2} - 8F^n_{i,j-1} + 8F^n_{i,j+1} - F^n_{i,j+2})/(12\Delta v) \\ C &= (-F^n_{i-2,j} + 16F^n_{i-1,j} - 30F^n_{i,j} + 16F^n_{i+1,j} - F^n_{i+2,j})/(24\Delta x^2) \\ D &= (-F^n_{i,j-2} + 16F^n_{i,j-1} - 30F^n_{i,j} + 16F^n_{i,j+1} - F^n_{i,j+2})/(24\Delta v^2)\,. \end{aligned} \tag{2.2.9}$$

For example, for the first splitting scheme step, we obtain, for $v_j > 0$:

$$\begin{aligned} F^*_{i,j}(x,v) = {} & \frac{\alpha_j(1-\alpha_j)}{24}\left(1 - \frac{1}{6}(1-2\alpha_j)\right) F^n_{i-3,j} \\ & - \frac{\alpha_j(1-\alpha_j)}{4}\left(1 + \frac{1}{2}\left[1 - \frac{17}{18}(1-2\alpha_j)\right]\right) F^n_{i-2,j} \\ & + \left(\alpha_j + \frac{\alpha_j(1-\alpha_j)}{4} + \frac{\alpha_j(1-\alpha_j)}{12}\left[1 - \frac{23}{6}(1-2\alpha_j)\right]\right) F^n_{i-1,j} \\ & + (1+\alpha_j)\left(1 + \frac{\alpha_j}{4} + \frac{\alpha_j}{12}\left[1 + \frac{23}{6}(1-2\alpha_j)\right]\right) F^n_{i,j} \\ & - \frac{\alpha_j(1-\alpha_j)}{4}\left(1 + \frac{1}{2}\left[1 + \frac{17}{18}(1-2\alpha_j)\right]\right) F^n_{i+1,j} \\ & + \frac{\alpha_j(1-\alpha_j)}{24}\left(1 + \frac{1}{6}(1-2\alpha_j)\right) F^n_{i+2,j} \end{aligned} \tag{2.2.10}$$

2.3 Spline interpolation scheme

The Spline interpolation method is based on a third order interpolation formula that is smooth in the first derivative, and continuous in the second derivative, both within an interval and at its boundaries [**?**, 50].

We consider the same phase space defined in the previous section and we suppose that the values of the distribution function $F^n_{i,j} = f(x_i, v_j, t^n)$ on the mesh points (x_i, v_j) at the time t^n are known. For each cell the interpolation formula for the distribution function is given by a cubic polynomial that depends on the values of the distribution function on the grid points and on their second order derivative:

$$\begin{aligned} F^n_{i,j}(x,v) = {} & A_x F^n_{i,j} + A_v F^n_{i,j} + B_x F^n_{i+1,j} + B_v F^n_{i,j+1} \\ & + C_x \frac{\partial^2 F^n_{i,j}}{\partial x^2} + C_v \frac{\partial^2 F^n_{i,j}}{\partial v^2} + D_x \frac{\partial^2 F^n_{i+1,j}}{\partial x^2} + D_v \frac{\partial^2 F^n_{i,j+1}}{\partial v^2} \end{aligned} \tag{2.3.1}$$

where

$$\begin{aligned} A_x &= \frac{x_{i+1} - x}{x_{i+1} - x_i} \\ A_v &= \frac{v_{j+1} - v}{v_{j+1} - v_j} \\ B_x &= \frac{x - x_i}{x_{i+1} - x_i} \\ B_v &= \frac{v - v_j}{v_{j+1} - v_j} \\ C_x &= \frac{1}{6}(A_x^3 - A_x)(x_{i+1} - x_i)^2 \\ C_v &= \frac{1}{6}(A_v^3 - A_v)(v_{j+1} - v_j)^2 \\ D_x &= \frac{1}{6}(B_x^3 - B_x)(x_{i+1} - x_i)^2 \\ D_v &= \frac{1}{6}(B_v^3 - B_v)(v_{j+1} - v_j)^2 \end{aligned} \tag{2.3.2}$$

Let us consider the first step of the splitting scheme. To obtain the shifted distribution function using the spline cubic formula 2.3.1 it is necessary to compute the second order derivatives $\partial^2 F^n_{i,j}/\partial x^2$ and $\partial^2 F^n_{i+1,j}/\partial x^2$. To obtain these functions it

is used the condition of continuity between the first derivatives of the interpolation functions of two near cells in the boundary point in common among the two intervals (x_{i-1}, x_i) and (x_i, x_{i+1}) in which them are defined. The resulting equation is:

$$\begin{aligned} &\frac{x_i - x_{i-1}}{6}\partial^2 F^n_{i-1,j}/\partial x^2 + \frac{x_{i+1} - x_{i-1}}{3}\partial^2 F^n_{i,j}/\partial x^2 + \frac{x_{i+1} - x_i}{6}\partial^2 F^n_{i+1,j}/\partial x^2 \\ &= \frac{F^n_{i+1,j} - F^n_{i,j}}{x_{i+1} - x_i} - \frac{F^n_{i,j} - F^n_{i-1,j}}{x_i - x_{i-1}}\,. \end{aligned} \tag{2.3.3}$$

If we impose this condition between all the N_x spatial cells of the phase space, we will obtain $(2N_v+1)(N_x-2)$ linear equation in the $(2N_v+1)N_x$ unknown $\partial^2 F^n_{i,j}/\partial x^2$. The other $2(2N_v+1)$ equations necessaries to make this computation are given by imposing the periodic boundary conditions. Since each $\partial^2 F^n_{i,j}/\partial x^2$ is coupled only to its nearest neighbors at $i \pm 1$, the set of equations 2.3.3 is represented by a tridiagonal matrix, that is solved using a tridiagonal scheme. The second order derivatives obtained from this computation are then used to calculate the function $F^*_{i,j}(x, v)$ using the spline equation 2.3.1.

The other two steps of the splitting schemes are obtain in an analogous way.

Chapter 3

Numerical results

In this chapter we will present the first part of the results of our work. Through the numerical simulations we performed on the non-linear evolution of 1D electrostatic collisionless plasmas (using the kinetic numerical schemes presented in Chapter 2), we will show how much the numerical dissipation introduced by a numerical scheme, when scales smaller than the finite dimension of the numerical grid are generated by the system, can have important uncontrolled and, at times, intriguing consequences on the macroscopic evolution, even if the dissipative length scale is much smaller than all other physical characteristic length scales. We will point out that the reaching of a certain final macroscopic state depends on the algorithm and the numerical accuracy chosen for the simulation, since they determine the amount of artificial dissipation inserted in the system. The plasma dynamics chosen for this investigation are the long time evolution of the Landau damping and of the two stream instability.

Seen the evidence of the importance of these dissipative effects, we developed a test for numerical schemes based on the echo phenomenon, in order to understand how much a numerical scheme dissipates.

Finally we will present a discussion of these results showing also that when numerical effects come into play in a collisionless plasma, they are capable to create correlations between particles, not taken into account by the Vlasov collisionless theory.

3.1 Asymptotic evolution of non-linear Landau damping

In this section we present numerical investigations on the standard problem of "nonlinear Landau damping" (NLD) in the regime where the trapping time τ_p is comparable to the Landau time τ_L. This phenomenon can be simulated in the 1D - 1V limit considering ions as a neutralizing fixed background by integrating the Vlasov - Poisson system of equations

$$\frac{\partial f_e}{\partial t} + v\,\frac{\partial f_e}{\partial x} - E\frac{\partial f_e}{\partial v} = 0; \tag{3.1.1}$$

$$\frac{\partial^2 \phi}{\partial x^2} = \int f_e\, dv\, - 1; \quad E = -\frac{\partial \phi}{\partial x} \tag{3.1.2}$$

normalized to electron characteristic quantities (the electron charge and mass e and m_e, the plasma frequency ω_{pe}, the electron thermal velocity $v_{th,e}$, the Debye length $\lambda_{_D}$, a characteristic density $\bar{n}$ and electric field $\bar{E} = m_e v_{th,e}\omega_{pe}/e$), with the following initial conditions:

$$f_e(x, v, 0) = \frac{1}{\sqrt{\pi}}\, e^{-(v^2)}\ [1 + \epsilon cos(kx)], \tag{3.1.3}$$

with $\epsilon = 0.05$, $k = 0.4$, $-5 \leq v \leq 5$ and $L_x = 5\pi$. Periodic boundary conditions are used.

It's important to recall that for the Vlasov equation any function $G(f)$ that depends on the distribution function, is a constant of motion, i.e. $dG/dt = 0$. In particular, the n-order invariants I_n, as well as the "entropy" $\mathcal{S}$,

$$I_n = \int f^n dxdv, \quad i \geq 1\,; \quad \mathcal{S} = -\int f\, ln(f) dxdv \tag{3.1.4}$$

are conserved. Furthermore, the Vlasov-Poisson system conserves the total (kinetic + electric) energy. In the following we will make use of the third order invariant and the entropy the "non dissipative" aspect of a simulation.

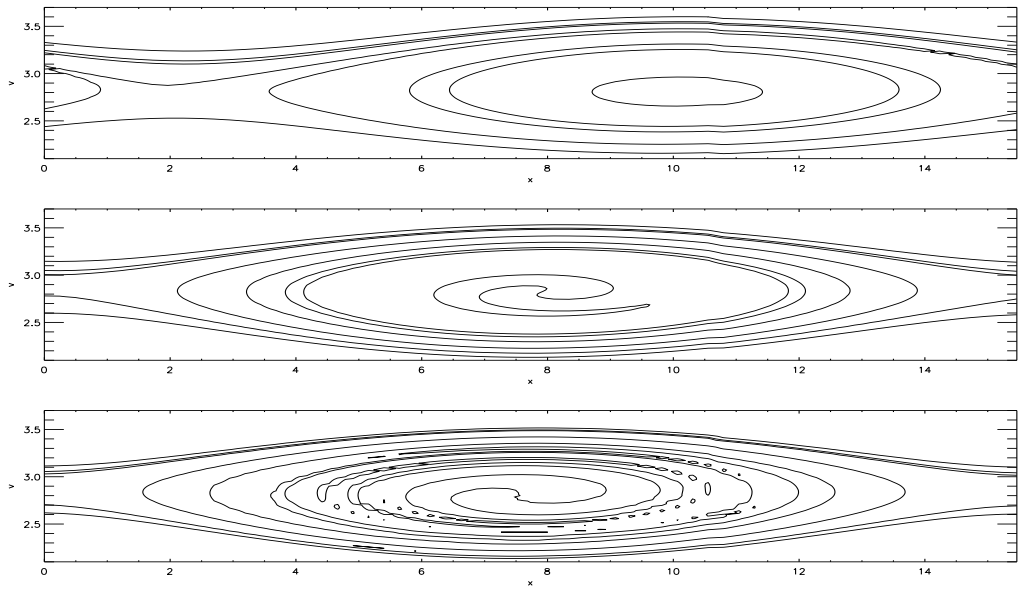

Figure 3.1: Electron distribution functions in phase space at time t=1000: VL2 run is represented in the first row, VL3 run in the second row, SPLINE run in the third row.

In the first part of this section we present Landau damping runs for the three simulation algorithms (VL2, VL3 and SPL) all starting with the same initial conditions parameters and numerical meshes. For all runs we used $N_x = 128$, $N_v = 701$ mesh points corresponding to $dx = 0.12$ and $dv = 0.014$. Since VL2 algorithm is a second order scheme, we expect it to be more diffusive than VL3 and Spline. First of all we show one of the two identical distribution function vortices generated in the phase space when resonant particles are trapped in the potential well of the perturbation wave. The figure is taken at t=1000. We observe that all vortices are centered around the resonant velocity but, along the x directions, VL2 vortex results shifted respect to VL3 and Spline one. Furthermore, each vortex present a different internal configuration of the distribution function isocontour level lines: the vortex has lesser ripples going from SPL run to VL3 run and from VL3 run to VL2 one. It's important to note the presence of closed distribution function isolines in the vortex. This is due to the introduction in the system of the numerical dissipation that, when the numerical mesh becomes inappropriate to describe the small length scales dynamics as those generated during the vortex formation, forced the system to close or also to

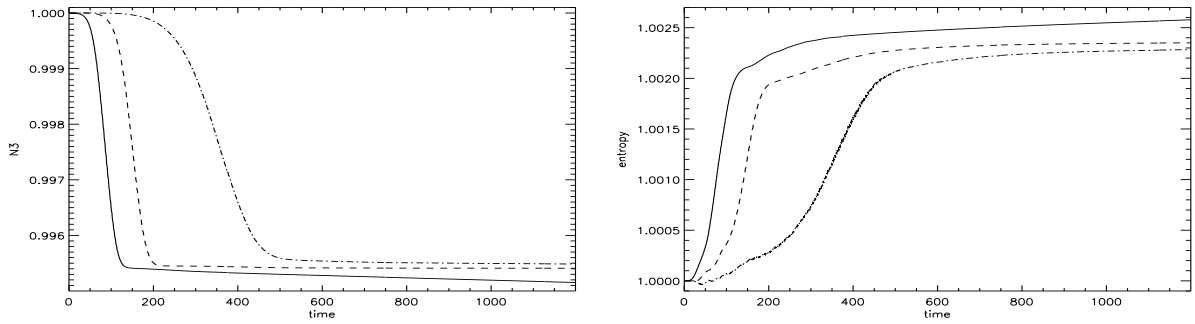

Figure 3.2: The time evolution of the third order invariant I_3 and of the entropy $\mathcal{S}$, first and second frame, respectively. Continuous, dashed and point - dashed line correspond to VL2, VL3 and SPL run, respectively.

reconnect one to each other the distribution function isolines, thing prohibited by the Vlasov collisionless theory.

Differences among the results obtained with the three algorithms are evident also in the behaviour of the third invariant $I_3 = \int f^3 dxdv$ and of the entropy $\mathcal{S} = -\int f\, ln(f) dxdv$ (see Fig. 3.2). In all cases, when numerical dissipation comes into play, i.e. in correspondence of the "closed" vortices formation, both $\mathcal{S}$ and I_3 present sudden jumps. For I_3, it can be observed that, even at parity of resolution grid, this decrease in correspondence of the vortex formation, happens at different times: first for VL2, then for VL3 and finally for SPL. In the same order in time the invariants of the three methods begin to stabilize to a constant value, even if, for VL2, the stabilization is not complete: the VL2 third invariant continues slowly to decrease.

Instead VL3 and SPL methods reach stable asymptotic constant values, even if these values are different. In fact SPL I_3 presents a less deep dissipation jump respect to VL3 one. The same kind of behaviour is showed also by entropies: the jump happens first for VL2, then for VL3 and finally for SPL. Also for the entropy, VL3 and Spline reach asymptotic constant values while VL2 entropy continues to increase slowly. Other signs of the important feedback on the final macroscopic state due to the different amounts of numerical dissipation introduced by the three algorithms, are well visible in the evolution of the electric field Fourier component for $k = 0.4$ (i.e. for the wave number of the initial perturbation wave). As predicted from the theory, the mean amplitude of electric field decreases until a constant non zero value while

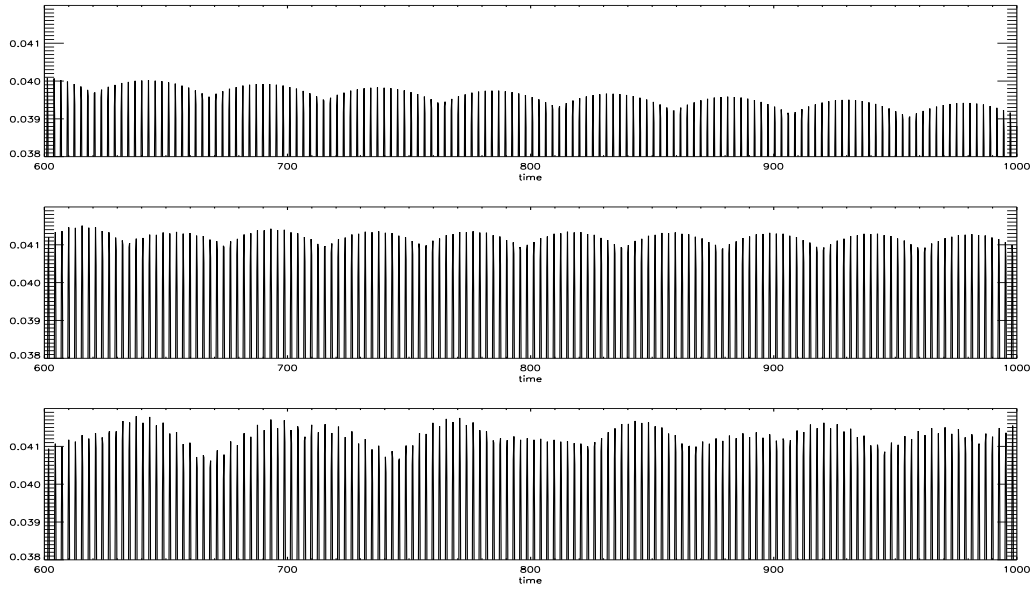

Figure 3.3: Electron distribution functions in phase space at time t=1000: VL2 run is represented in the first row, VL3 run in the second row, SPLINE run in the third row.

electric field continues to oscillate, but the period of these oscillations is different for the three methods as can be seen in Fig. 3.3. Furthermore, by considering all runs, we observe that also the min/max values of the electric field amplitude are different for different numerical schemes.

In order to show that the final structures, obtained with the three numerical algorithms, are really distinct macroscopic configurations, we have computed the total number of trapped particles contained in the phase space vortex (see for example Ref. [52] on the importance of trapped particles), for each run, at $t = 650$. We define the separatrix as the largest closed contour level around the vortex. Then, inside the separatrix, we integrate the distribution function and normalize it to the total number of trapped particles of SPL run. The maximum numerical error is estimated of the order of $\sim 2\%$. We found: $n_{SPL}^{vort} = 1$, $n_{VL_3}^{vort} = 0.83$, $n_{VL_2}^{vort} = 0.69$.

We've already seen how the use of different numerical schemes can modify the final macroscopic state of the non linear regime of Landau damping. Now, on the same system, we will present another investigation to understand the role of the dissipative numerical effects on macroscopic scales when different resolution meshes are used.

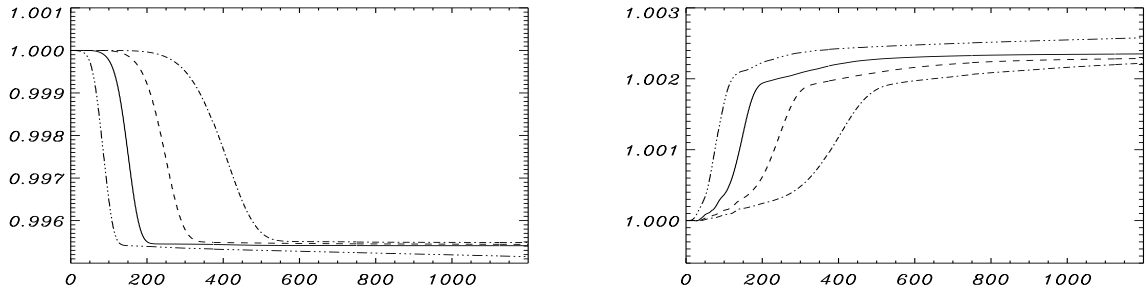

Figure 3.4: First frame: the time evolution of the third invariant I_3. The three dot-dashed, continuous, dashed and dot-dashed lines correspond to run VL2, A, B and C, respectively. Second frame: the time evolution of the entropy (same style).

These simulations are made using VL3 algorithm with the same initial conditions and parameters of the previous Landau runs apart for the number of points of the resolution grid. In the following, we present three VL3 runs (A, B, C), all starting with the same initial conditions, but from B to E with decreasing numerical diffusion, i.e. with denser numerical grid. We used $N_x = 128$, $N_v = 701$ mesh points in run A, $N_x = 256$, $N_v = 1401$ in run D, $N_x = 512$, $N_v = 2801$ in run C. Roughly speaking, the numerical diffusive length scales are of the order of the mesh size, $0.03 \leq dx \leq 0.12$, $0.0035 \leq dv \leq 0.014$. To summarize, run A is the most dissipative, run C is the less dissipative.

In Fig. 3.4 the third invariants I_3 and the entropy $\mathcal{S}$ are reported. In all runs, both the quantities present a deep jump in correspondence to the formation of the vortex.

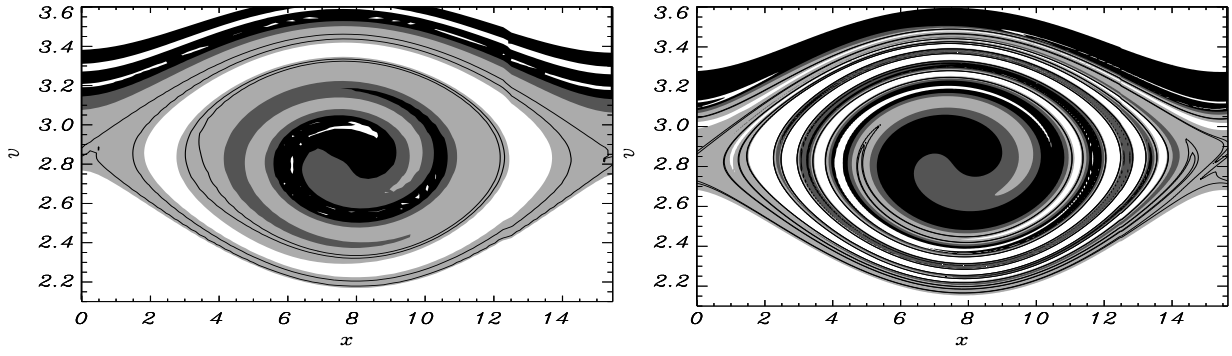

Figure 3.5: The shaded isocontour of the d.f. of runs A and C in a strip of the phase space centered around $v_{res} \simeq 2.9$.

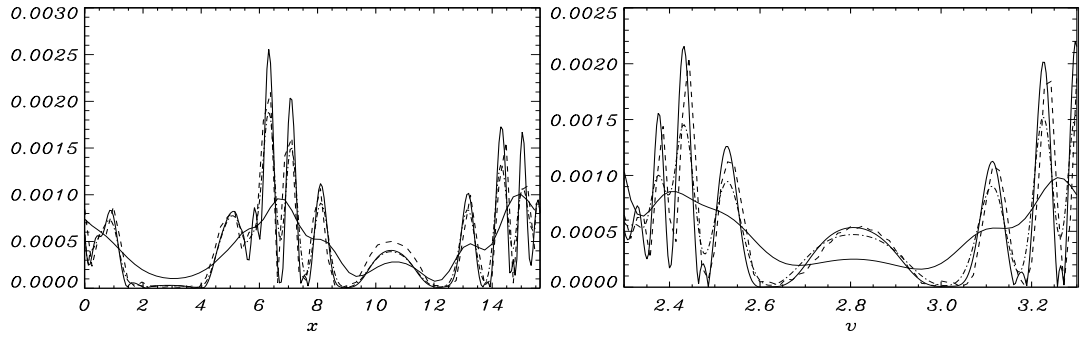

Figure 3.6: The d.f. ($t = 650$) at $v = 3.14$ vs. x, first frame, and at $x = 7.85$ vs. v, second frame, for run A (continuous thick line), run C (continuous line), run C smoothed with Fourier and with finite differences, dashed and dot-dashed line, respectively.

More dissipative is the run, before I_3 begins to decrease and deeper is the jump. The entropy shows the same behaviour apart from the fact that the jumps correspond to an increase of $\mathcal{S}$ instead, as for I_3, to a decrease. Important differences among the final states of the three runs are present also in the distribution function. In Fig. 3.5 we show the phase space vortices for run A and C, realized with the same contour levels. The more evident difference among the vortices is the presence of finer and finer ripples as diffusion is reduced. These different structures of the vortices really correspond to significant different distributions of trapped particles, as can be seen in Fig.3.6.

In the two frame we show two plots of the distribution function at $t = 650$ in the resonant region at $v = 3.14$ vs. x and at $x = 7.85$ vs. v. The thicker continuous line and the continuous line refer to run A and C, respectively. The dashed and dashed dot line are obtained after smoothing (with a Fourier or with a finite differences technique) the run C vortex on a phase space cell size $dx \times dv$ comparable to that of run A. We see that, even after the smoothing, the distribution function of run C is still very different from that of run A. Therefore run A vortex cannot be considered as a coarse graining view of run C one. Again on the phase space vortices of the three runs, we also computed the number of particles trapped, as we made previously in the three different algorithms case. Normalizing to one the total number of trapped particles of run E, $n_C^{vort} = 1$, we obtained: $n_B^{vort} = 0.87$, $n_A^{vort} = 0.83$. The maximum numerical error due to different grid resolution is estimated of the order of $\sim 1\%$.

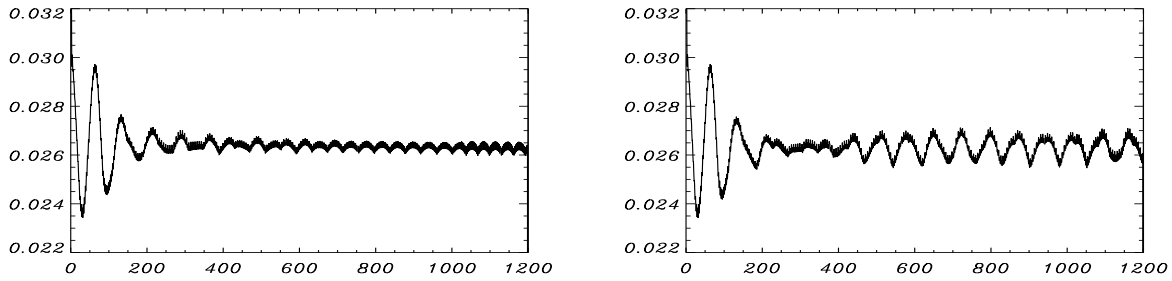

Figure 3.7: The low frequency time evolution of the electric field amplitude, run A and C.

The last important signature of the differences between the asymptotic states of the three runs that we show, concerns the electric field amplitude evolution. Fig. 3.7 has been obtained eliminating the high frequency oscillations. First of all the periods of asymptotic oscillations for the three runs are very different. We found: $\tau_A^{lf} \simeq 40$, $\tau_B^{lf} \simeq 67$, $\tau_C^{lf} \simeq 75$. Then great differences are evident also in the min/max values of the electric field amplitude.

3.2 Non linear regime of two stream instability

In the previous section we gave evidence of the importance of dissipative effects on the macroscopic evolution of the Vlasov-Poisson system in the case of the long time (non linear) evolution of Landau damping even if the dissipative length scale, of the order of the mesh size, is much shorter than all other physical characteristic length scales. However, dissipative numerical feedback on the macroscopic structures of a Hamiltonian system can be much more dramatic when the system evolution is characterized by inverse cascade processes, as for example in the case of phase space vortex merging during the evolution of the two stream instability, in the case of two-dimensional hydrodynamic turbulence, etc., since the merging process must necessarily pass through diffusive small scale reconnection effects. In this section we will present several simulations of the non linear regime of the two stream instability in a electrostatic collisionless plasma where protons are considered of infinite mass. This phenomenon can be described in the 1D-1V phase space through the Vlasov and Poisson equation 3.1.1, 3.1.2, assuming ions as a neutral fixed background and using the following initial condition:

$$f_e\left(x,v\right)=\frac{1}{\sqrt{\pi}}\left(\frac{1}{2}e^{-(v_e-v_0)^2}+\frac{1}{2}e^{-(v_e+v_0)^2}\right)\left[1+\epsilon\sum_{k=1}^{N_k}cos\left(kx+\phi_k\right)\right], \qquad (3.2.1)$$

where all quantities has been normalized, as in the previous section, to electron characteristic quantities. The first investigation we present is the study of the evolution of the instability using the three numerical scheme VL2, VL3 and SPL on identical initial systems. The parameters of the chosen system are: $v_0 = 2$, $L_x = 100$, $v_{max} = 7$, $dx = 0.1$, $dv = 0.1$, and $dt = 3 \cdot 10^{-4}$. The amplitude of the initial random perturbations is $\epsilon = 10^{-4}$ and the total simulation time is $t_f = 1200$. We chose the length of the spatial domain L_x in the way that five vortices can develop during the instability. All along the linear regime and up to the initial phase of instability saturation, when the vortices start to form and eventually to interact, the three run give the same results as can be seen in the first column of Fig.3.8. When the vortices start to merge, instead, differences among the three runs appear.

In this non linear phase of the instability, the modality and the time in which the five vortices interact to merge first into two vortices and finally in a single vortex

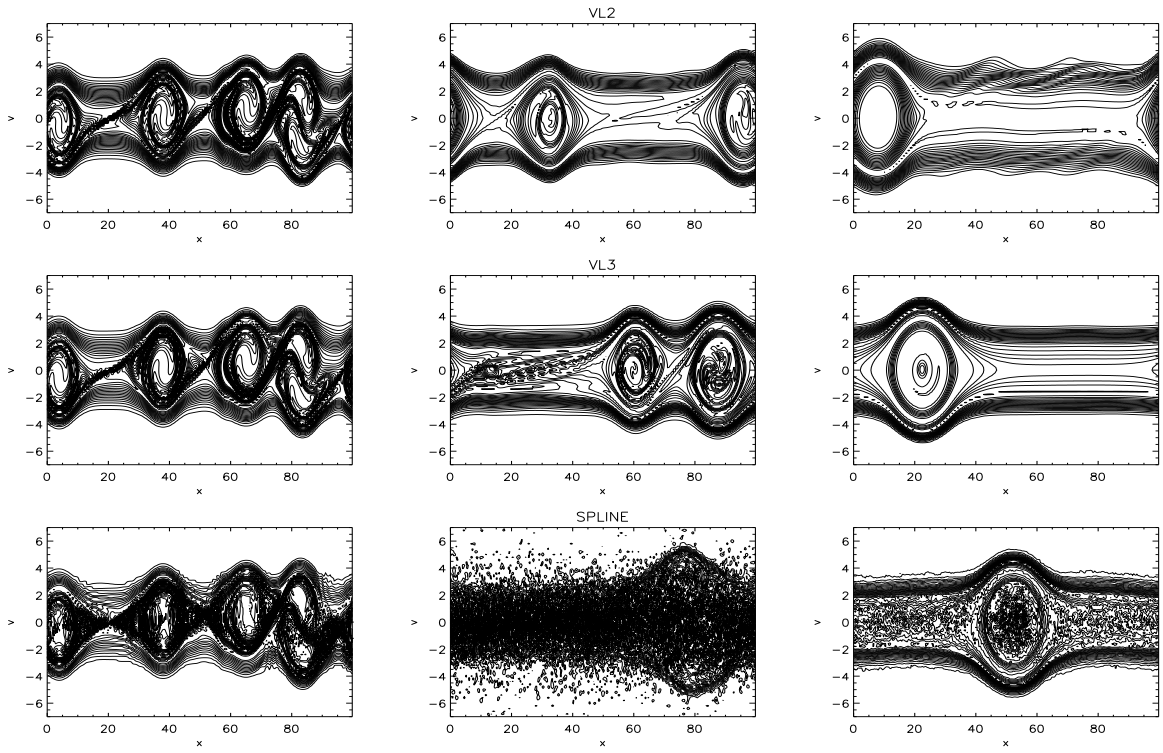

Figure 3.8: The d.f. in phase space at t=50 (left column), t=200 (central column) and t=1200 (right column). The results obtained with the VL2, VL3 and SPL algorithm are shown in the first, second and third row, respectively.

change Fig.3.8. At $t = 350$ the single vortex has been formed for all runs. Since the processes of merging depend on the numerical scheme used, the final position of this vortex in the phase space is not the same for the three runs(see third column of Fig.3.8. This is not surprising since the merging process, which violate the Hamiltonian character of the Vlasov Poisson equations, must necessarily pass through dissipative (numerical) finite grid effects which depend on the accuracy of the algorithm (as well as on the grid spacing). Such dissipative effects are particularly important during the delicate process of vortex merging (inverse cascade). In Fig.3.9, we observe also that the distribution function of VL2 run presents long wavelength oscillations in the velocity ranges $-5 < v < -2$ and $2 < v < 5$, that do not appear in the distribution functions of the other two runs. In order to show that the final macroscopic states reached in the three runs are different, we have calculated also the number of particles trapped in the final vortex. The computation has been done as in non linear

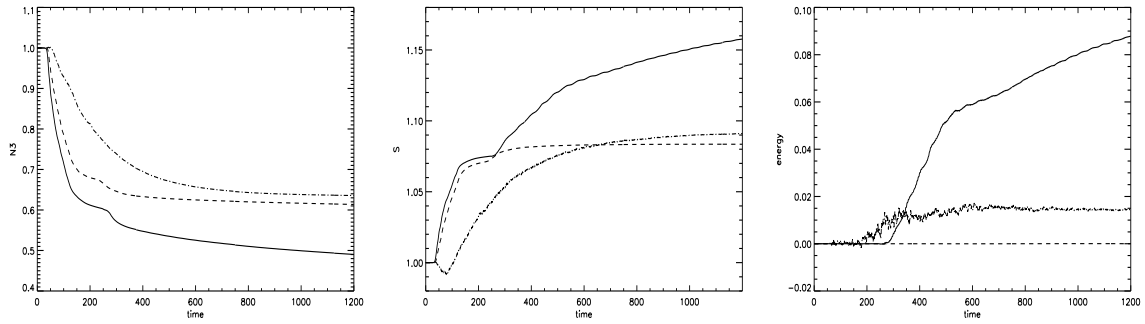

Figure 3.9: The time evolution of the third order invariant I_3, of the entropy $\mathcal{S}$ and of the energy fluctuations δE, first, second and third frame, respectively. Continuous, dashed and point - dashed line correspond to VL2, VL3 and SPL run, respectively.

Landau damping case. Normalizing to the total number of particles trapped in VL2 vortex we obtained: $N^{vort}_{VL2} = 1$, $N^{vort}_{VL3} = 0.41$ and $N^{vort}_{SPL} = 0.48$.

The important effects of numerical dissipation are also clear looking at the time evolution of the third invariant I_3 showed in the first frame of Fig.3.9. In fact after the first jump of the invariant in correspondence to the formation of the five vortices (that happens at the same time for all methods even if with a different deepness), another jump, corresponding to the merging of the two vortices in one vortex, is visible for all the runs (more evident in VL2 and VL3 but present even for SPLINE) but it appears at different times: first for SPLINE run, then for VL3 run and finally for VL2 run.

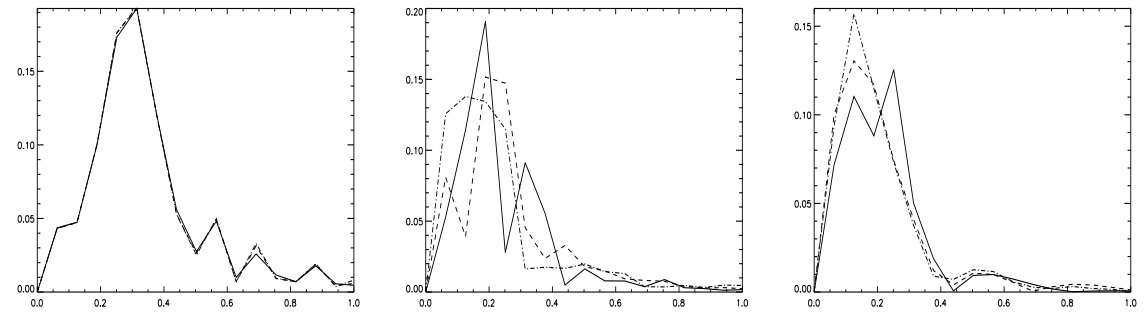

Figure 3.10: The electric field spectrum $\hat{E}(k)$ at t=50, t=200 and t=1200. The VL2, VL3 and SPL schemes are represented by the continuous, dashed and dash - dotted lines.

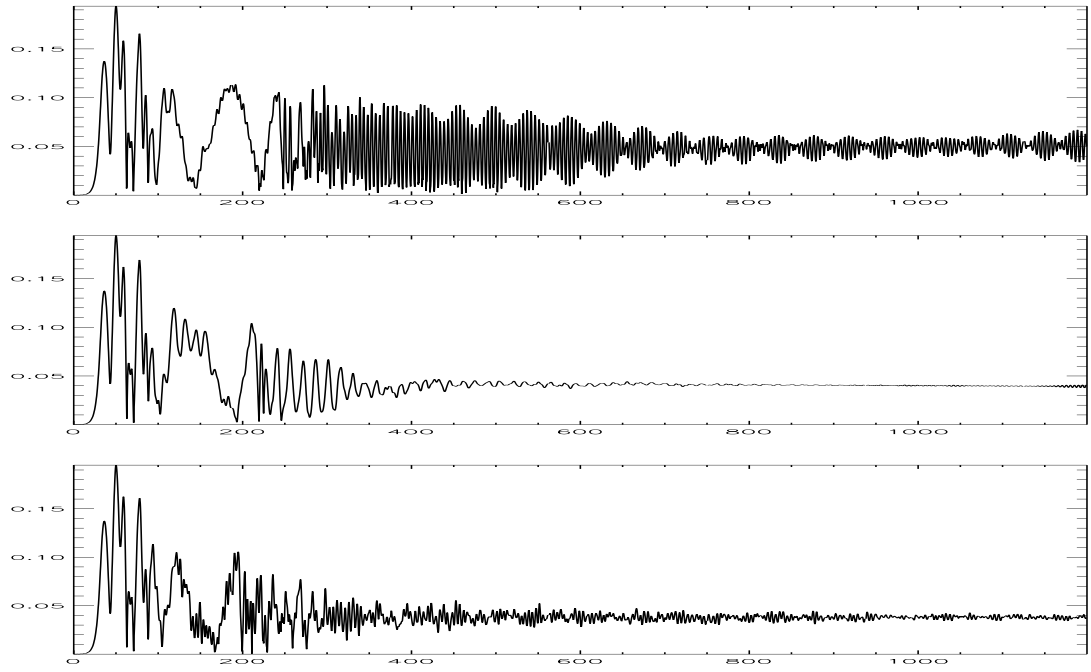

Figure 3.11: The time evolution of $\hat{E}(k = 0.3)$ (most unstable mode) for the VL2, VL3 and SPL schemes (same symbols as Fig. 3.10).

Around $t = 200$, the VL2 invariant and, less pronounced, the VL3 and than SPL invariants, show a transient phase where the invariant tends to become almost constant up to the final two vortex merging where a new decrease is observed. Furthermore, both VL3 and SPL invariants become again constant at nearly the same level, while a slow, but significant asymptotic decrease is observed for VL2. A similar behaviour is shown by the entropy (see second frame of Fig.3.9). At every decreasing jump of the third invariant corresponds an increasing jump of the entropy.

Furthermore there is the same transient stabilization for $t \simeq 200$, most evident for VL2, as in the evolution of I_3. It is then interesting to note that the SPL algorithm assume a strange behaviour for $t < 100$. In fact, the SPL entropy initially decreases while the entropies for VL2 and VL3 runs show monotonic increasing evolution in time. This means that while VL2 and VL3 systems loose informations, stored on small scales of the distribution function through the numerical dissipation, SPL algorithm initially introduces artificial informations in the plasma under the form of small scales fluctuations. Furthermore asymptotically SPL entropy stabilizes on a larger value

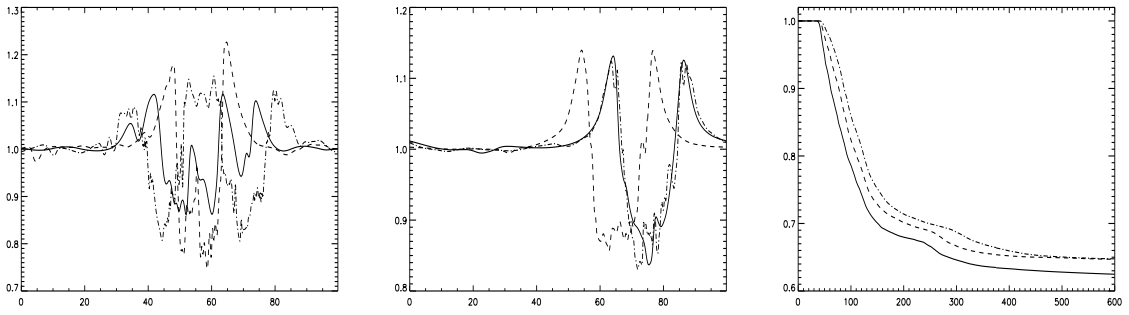

Figure 3.12: The density at $t = 250$ and $t = 600$, first and second frame, run D, E and F (continuous, dashed and dash - dotted line, respectively. Last frame: the time evolution of I_3 for run D, E and F.

respect to VL3 entropy.

The effect of the different amounts of dissipation introduced by the three numerical schemes is clear also looking at the discrete electric field Fourier spectra of the three runs, defined as:

$$\hat{E}(n,t) = \frac{1}{N_x} \sum_{l=1}^{N_x} E(x_l,t)\, \exp\left[-2\pi i\ (l-1)n/N_x\right], \tag{3.2.2}$$

where $n = 0, .., N_x - 1$ is the discrete wave number defined in terms of the wave vector $k_x = 2\pi n/L_x$, $L_x = N_x dx$. From Fig.3.10, first frame, we observe that the three spectra are identical at the end of the linear phase but they evolve in very different ways during the non linear phase (see second frame). This is due to the fact that the merging processes of the three runs are very different. When the systems have reached the new stable state in which only one vortex is present, the spectra of VL3 and SPL runs come back to be very similar while VL2 spectrum remains significantly different. The reason of these behaviours can be searched in the fact that VL3 and SPL produce finally the same kind of phase space vortex while VL2 vortex presents some different characteristics. If then we look in Fig.3.11 at the time evolution of $\hat{E}$ for the most unstable mode, $k = 0.3$, we observe that as soon as the merging process starts, i.e. for $t > 80$, the behaviour of the three schemes curves become significantly different.

However, in the asymptotic limit, while VL3 and SPL curves lead to about the same value, even if SPL run shows small amplitude fluctuations, VL2 curve assumes

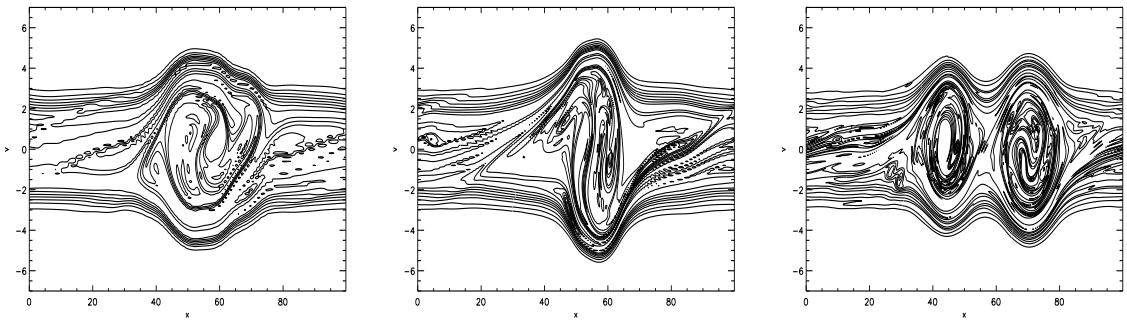

Figure 3.13: The d.f. in the phase space at t=250 for run D, E and F, respectively.

a different asymptotic behaviour. VL2 curve shows high frequency oscillations of relevant amplitude even at large times which are due to numerical instability of the algorithm. To obtain more stable results for VL2 simulations it's necessary to increase the number of grid points of the run. In this way both the asymptotic spectrum and the asymptotic behaviour of the most unstable mode for VL2 run become more similar to the VL3 and SPL ones. However the results in the intermediate regime $80 < t < 400$ remains different both from VL3 and SPL.

The same kind of results has been obtained from the comparison of three runs made with the same algorithm but with different resolutions: $dx = 0.1$ and $dv = 0.1$ (run D), $dx = 0.05$ and $dv = 0.05$ (run E), $dx = 0.025$ and $dv = 0.025$ (run F). The runs are made with the same physical and numerical parameters, and initial conditions, of the previous ones. Here we report the results obtained using the VL3 algorithm.

First we show in Fig.3.12 (third frame) the behaviour of the third invariants I_3. We can observe that the deepness of both the two jumps, the first corresponding to the formation of the five initial vortices and for the second due to the final merging process of two main vortices in the final single one, increases with the decrease of numerical accuracy, hence from run F to D. While the first jump happens at the same time for all runs, the second jump depends on the accuracy: more the run is accurate, later I_3 shows this second decrease. Furthermore, even in this case, and perhaps in a more evident way, I_3 for all runs, tend to stabilize in the time interval $150 < t < 250$, i.e. after the five vortices are formed and before the final two vortex merging process begins.

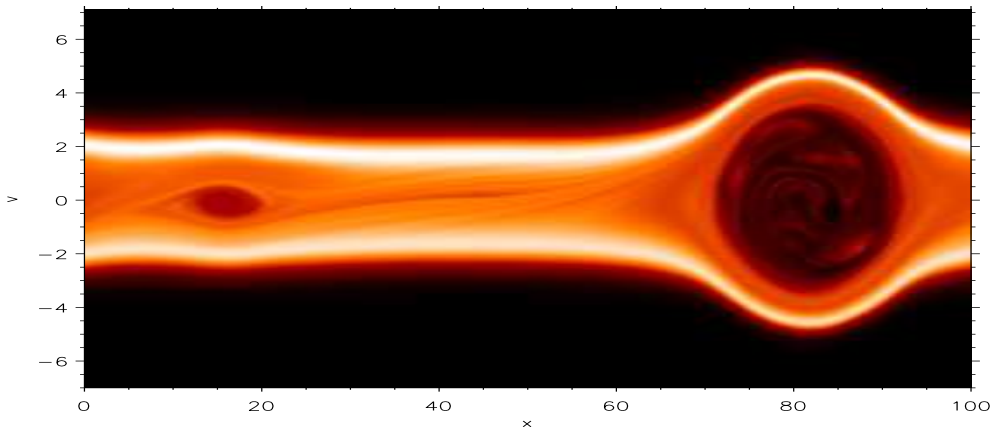

Figure 3.14: The d.f. in the phase space at t=900 for run E.

In Fig.3.13 we report the distribution functions in the phase space of these runs at time $t = 250$, i.e. in correspondence of the merging process of the vortices. From this figure it is clear how the numerical mesh size modifies the evolution of the vortices interaction process. Differences in the evolution of the inverse cascade for the three runs are also very evident if we look, in Fig.3.12, at the density profiles of the systems. We can see that during the merging process (Fig.3.12 first frame), at $t = 250$, density fluctuations differences among the three runs arrive up to $\sim 20\%$. In the asymptotic regime, instead run D and F tend to reach a very similar density profile (Fig.3.12 second frame). However, these final states must be considered as different since the number of trapped particles are different as in the previous case. On the other hand, the electric and density fields for run E remain significantly different also in the asymptotic phase, corresponding to a vortex, located in a different position with respect to runs D and F (see Fig. 3.13, second frame). This is due to the fact that, for run E, as can be seen in Fig.3.14 during the merging process, a little vortex appears in the phase space. This little vortex attracts the main final vortex changing its final position.

Seen the particular result obtained for run E, we performed the three runs also with the SPL algorithm. We obtained that the final vortices of the three runs result displaced in different positions: greater is the accuracy of the run and more the final vortex is shifted towards right. Also in this case, the evolution and final states of the runs depends on the numerical mesh chosen.

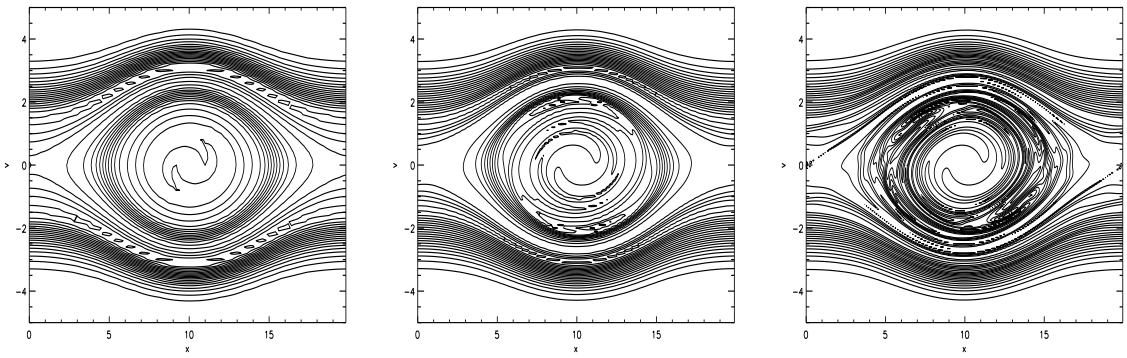

Figure 3.15: The d.f. in the phase space at t=1200 for run G, H and L, respectively.

Finally, in order to clearly distinguish the role of dissipative effects in the process of vortex merging and of vortex formation, we have performed three other runs, namely runs G, H and L, identical to runs D, E, and F, but using a reduced simulation interval, $L_x = 20$, such that only one vortex is generated by the development of the instability.

In this case, as shown in Fig.3.15, all runs generate asymptotically, at $t = 1200$, a phase space vortex centered around $v_0 = 0$ and $x_0 = L_x/2$. However, the distribution and the number of the vortices particles are different. In fact, normalizing to one the total number of trapped particles of run N, $n_L^{vort} = 1$, we obtained: $n_H^{vort} = 0.76$, $n_G^{vort} = 0.72$. Also in this case, differences are present for the third invariants and the entropies both in the trends as in the asymptotic values. Since only one vortex is developed by the system, only one jump appears both in I_3 and in the entropy. In this case this jump happens always first for more dissipative run and then for less dissipative ones (first for run G, then for run H and finally for run L). Furthermore, as in the five vortices case, the deepness of the jump is different:

larger for the more dissipative cases and smaller for the less dissipative ones. Although, for runs G, H and L, the electric and density field evolution is now almost identical also during the non linear regime, from saturation to the stable asymptotic phase, the final states reached by the three runs can be considered different because of the differences in the number of trapped particles and their distribution (as shown before).

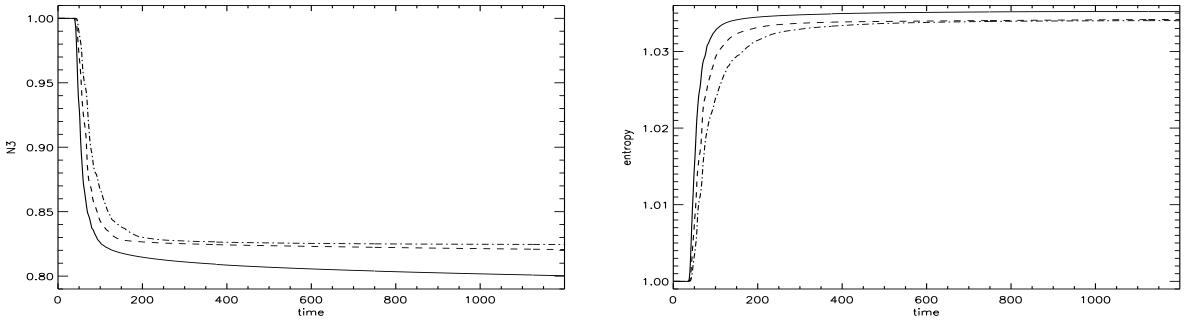

Figure 3.16: Last frame: the time evolution of I_3 and $\mathcal{S}$ for run G, H and L (continuous, dashed and dash - dotted line, respectively).

3.3 The echo benchmark

Until now, we have shown that the numerical dissipation, introduced by the algorithm when the numerical mesh becomes unable to describe the small plasma dynamics, produces significant effects on the macroscopic evolution of the system up to determine different final macroscopic states, even if the dissipation length scale is much smaller than the physical ones. When artificial dissipation comes into play, even if we are formally dealing with a collisionless plasma, the final effect that it will produce on the system will be very similar to inserting in the Vlasov equation a collisional operator. Since the echo phenomenon is one of the most sensitive process to collisions and its non linear analytical solutions for second order echoes are known, we decided to use the echo as a benchmark for the numerical schemes adopted until now. With the help of this test we investigated their dissipative properties, comparing numerical results with those predicted by the theory.

We performed a number of simulations of the echo process using different numerical accuracies by varying the number of grid points and/or the numerical scheme, choosing among the VL2, VL3 and SPL algorithms. The system can be described with the 1D-1V Vlasov - Poisson equations 3.1.1, 3.1.2, for a fixed neutralizing background, with $L_x = 5\pi$ and $-5 < v < 5$ and with periodic boundary conditions. Two distinct sinusoidal perturbations are imposed on an initial Maxwellian distribution function, $f_{_M}(x, v, 0) = \exp(-v^2)/\sqrt{\pi}$, at $t = 0$ and at $t \equiv \tau = 800$, both with amplitude $\epsilon = 10^{-6}$ but with wave vectors $k_1 = 0.4$ and $k_2 = 0.8$:

$$\delta f_1 = \epsilon \ \cos(k_1 x) f_{_M}, \quad \delta f_2 = \epsilon \ \cos(k_2 x) f_{_M} \tag{3.3.1}$$

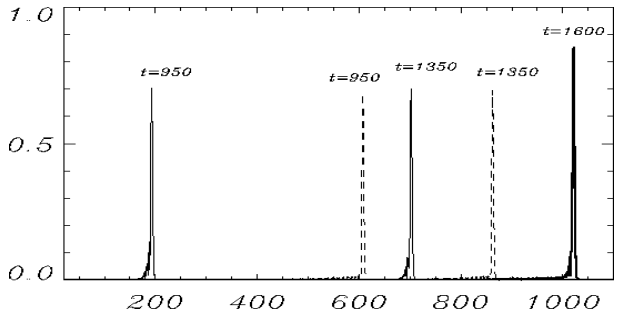

Figure 3.17: Space averaged velocity Fourier transform $\bar{f}(n_v)$ multiplied by 10^7 *vs.* n_v for run B at $t = 950, 1350, 1600$. Continuous, dashed and thick lines correspond to the k_1, k_2 and echo signals.

As a result, an echo with wave vector $k_3 = k_2 - k_1 = 0.4$ is generated at $t_\chi \equiv \tau' = (k_2/k_3)\tau = 1600$. The choice of the time delay, $\tau = 800$, is motivated by the requirement that the second pulse must be excited when the first one has been almost completely Landau damped. We have verified, with a number of test runs, that the echo's amplitude is independent of the spatial grid spacing (at least for $N_x \geq 32$), in agreement with the echo generation process (interference in velocity space of the ballistic terms). All the runs presented in the following have the same initial conditions (including the launch of the second pulse) with $N_x = 32$, but with different number of velocity points, namely $N_v = 1201$, $N_v = 2201$, $N_v = 2401$, $N_v = 3601$, $N_v = 4801$, $N_v = 19201$ corresponding to run A, B, C, D, E, and F, respectively. The ballistic evolution of the two disturbances and the echo formation are well illustrated by considering the discrete Fourier transform of the distribution function,

$$\tilde{f}(x_\alpha, n_v) = \frac{1}{N_v} \sum_\beta f(x_\alpha, v_\beta) \exp\left[-2\pi i n_v \tilde{\beta})/N_v\right] \tag{3.3.2}$$

where $-N_v/2 \leq \beta \leq N_v/2$, $\tilde{\beta} = \beta + N_v/2$, and $n_v = 0, .., N_v$ is the discrete "velocity wave number" defined in terms of the velocity wave vector q [36] by $n_v = qL_v/2\pi$, with $L_v = N_v dv$, $v_\beta = \beta dv$ ($dv \equiv$ velocity mesh size). On the discrete grid the ballistic term $\exp(ikvt)$ reduces to $\exp(ik\beta dvt)$. Therefore, the grid discretization introduces an artificial periodicity in the ballistic component of the distribution function, with a period equal to the recurrence time [37] $T_R = 2\pi/k\,dv$. As a consequence, the ballistic term of a Landau damped plasma wave will produce an artificial ghost

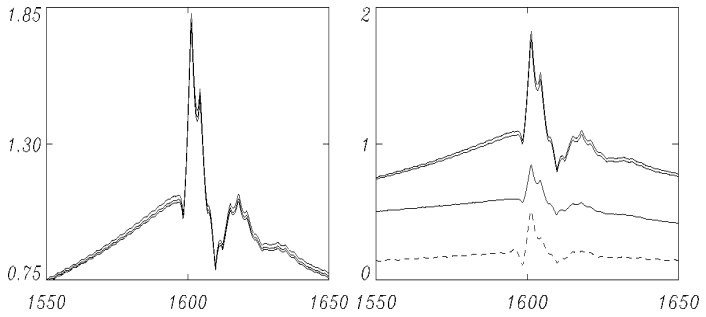

Figure 3.18: Echo's amplitudes multiplied by 10^{10} *vs.* time. Left frame (bottom to top): Runs B, C, D, E, F (curves D, E, F are coincident), VL3 algorithm. Right frame (bottom to top): Run B, VL2 algorithm (dashed line), Run A, B and F, VL3 algorithm (continuous lines).

density perturbation at $t = T_R$. In fact the wave number n_v reaches its maximum value at $n_v^{max} = N_v/2$ allowed by the discrete transform already at $t = T_R/2$. This initiates the numerical (finite grid) reflection that leads to the ghost formation at $t = T_R$ and/or causes strong dissipative or dispersive effects corresponding to the fact that the length scale of the velocity fluctuations is equal to the grid size. On this basis we present only simulations such that $t_\chi < t_{max} < T_R/2$ ($t_{max} \equiv$ final time of the simulation) except for run A.

In Fig. 3.17 we illustrate the formation of the echo by plotting the space average of the absolute value of the discrete Fourier transform in velocity space $\bar{f}(n_v) \equiv \sum_{\alpha=1}^{N_x} |\tilde{f}(x_\alpha, n_v)|/N_x$ *vs.* n_v for run B at $t = 950, 1350, 1600$. We see that the two peaks at $t = 950$, corresponding to the ballistic terms of the two excited waves, move toward increasingly large n_v [36] at $t = 1350$, with $n_{v,1} = (L_v/2\pi)\, k_1\, t$ and $n_{v,2} = (L_v/2\pi)\, k_2\, t$. Since the speed in velocity wave-number space of the second peak is twice that of the first, at $t = 1600$ the second peak reaches the first at $n_v = n_v^\chi$ and the echo is generated. In all presented runs, except for run A, we have $n_v^\chi = 1020$.

In Fig. 3.18 we show the (maximum) echo's amplitude *vs* time for all runs obtained by using the VL3 algorithm (continuous lines) and for run B by using the VL2 algorithm (dashed line, right frame). The curves resulting from the same run made by using the spline algorithm coincides with the VL3 curve. We see that the characteristic time for the occurrence of the echo is, in all cases, in agreement with the theoretical analysis [1] which predicts the occurrence of the echo at $t_\chi \equiv \tau' = (k_2/k_3)\,\tau$. We

consider now the exponential, non oscillating part of the echo time evolution which, for $k_3 = k_1$, is expresses as $exp[\pm\gamma_\pm (t - \tau')]$, as showed in Section 1.3, where the plus and minus sign refer to the growth and damping rate, respectively, i.e. before and after $t = \tau'$. In the analytical theory $\gamma_+ = \gamma_- \equiv \gamma_1$ (where γ_1 is the Landau damping rate of the first pulse). In our calculations $\gamma_1 = 0.0079$. In runs D, E, and F, the observed echo growth and damping rates are in excellent agreement with the collisionless theory, i.e. $\gamma_\pm^{echo} = \pm 0.0079$. On the other hand, in runs C, B and A, the growth and damping rates are different, namely $\gamma_+ = 0.0076, 0.0075, 0.004$ and $\gamma_- = 0.0079, 0.0077, 0.0071$. Apart from the quantitative difference with respect to γ_1, the difference between γ_+ and γ_- for the same run indicates that the numerical collisional operator cannot be considered as velocity independent. The only significant difference with respect to the theoretical analysis is the strong peak of the echo's amplitude at $t \simeq \tau'$ followed by rapid oscillations in the next $20 - 30$ times, after which the time evolution becomes again exponential (now decreasing with time) as in the analytical case. On the other hand, we observe that (at all times) the echo's amplitude plotted in Fig. 3.18 is increasingly reduced for runs C, B and, in particular, for run A. This amplitude reduction is a consequence of numerical diffusive effects which increase as the number of grid points is reduced. Here numerical dissipation comes into play when the typical length scale generated by the ballistic term becomes comparable with the grid length scale, i.e. when the velocity wave number associated to the ballistic peak (see Fig. 3.17) becomes comparable to the grid size wave number, $n_v \sim n_v^{max}$. In the case of runs B and C this happens when approaching the echo generation time since $n_v^\chi \sim n_v^{max}$, while for run A dissipative effects start to be important at the pulse reflection time $t \sim T_R/2$. In runs D, E and F, instead, numerical effects are negligible since $n_v^\chi \ll n_v^{max}$ up to the end of the simulations.

In Fig. 3.18, right frame, we also plot the time evolution of the (maximum) echo amplitude in the case of run B obtained by using the second order accurate VL2 scheme (dashed line). This plot, to be compared with the corresponding curve of run B (second curve from top, same frame) made with the third order accurate VL3 scheme, clearly shows that the less accurate algorithm gives a lower amplitude echo with a different shape in time with $\gamma_+ = 0.0091$ and $\gamma_- = 0.0083$. We stress that the echo process provides a very selective check of the intrinsic numerical diffusion effects since all the other typical checks (energy conservation, the conservation of a finite

subset of Casimir invariants typically up to second or third invariant) give exactly the same results for the three schemes.

We have calculated the (space averaged) phase difference Δ_ϕ between the peaks of the first and second pulse at $t_1 = 900$, slightly after the launch of the second pulse, and at $t_2 = 1400$, slightly before the echo. We observe that the phase error $\Delta_\phi(t_2) - \Delta_\phi(t_1)$ due to the numerical integration remains small, of the order of 0.018π for run F, and than it increases linearly with the decrease in the number of velocity grid points in the other runs. The only exception is run A for which we observe a strong jump in such space averaged phase error. More important, in run A the phase error depends on the specific x_α grid point, while it is space independent in the others.

The results presented in Fig. 3.18 (and others not illustrated here) show that the echo's amplitude increases with increasing N_v and saturates at the level obtained in run D for $N_v \geq 3601$. Therefore, we refer to the echo of runs D, E and F as to the collisionless echo. This is in agreement with the theoretical argument that the effects of a collisional operator (in our case numerical, but still of diffusive type) tends to destroy the echo generation process by causing the decay of the ballistic term. The artificial dissipation of any numerical code could in principle be thought as due to some (a priori unknown) collisional operator which we assumed for our simulations to be of the same form as the velocity space diffusion operator $\approx \partial^2(D_2 f)/\partial v^2$ used by O'Neil in Ref. [15]. If we assume in addition D_2 to be independent of time and of velocity, we can apply O'Neil's result to parametrize the ratio found numerically between the collisionless and collisional echoes as $\exp\left[-D_2 k_1^2(2\tau^3 - (t-\tau')^3)/3\right]$ (with $k_2 = 2k_1$). However, by comparing the amplitudes obtained in the different runs we found that it is not possible to define a unique value for D_2, which implies that the numerical "collisional operators" corresponding to the VL2, VL3 and SPLINE algorithms are characterized by a more complex structure. This is in agreement with the previous analysis concerning the growth and damping rates $\gamma_\pm$ of the echo time evolution indicating that the numerical collisional operator is velocity dependent.

Let us now consider the case of run A for which the maximum allowed wave number $n_v^{max,A} = 600$ is smaller than that at which the echo should be generated, $n_v^\chi \simeq 1020$ (as observed in all the other runs). In Fig. 3.19 we show, in analogy with Fig. 3.17 and using the same style, the space average discrete Fourier transform $\bar{f}(n_v)$ of the two pulses in velocity space at $t = 850$ and $t = 1400$ and their superposition at $n_v \simeq 180$

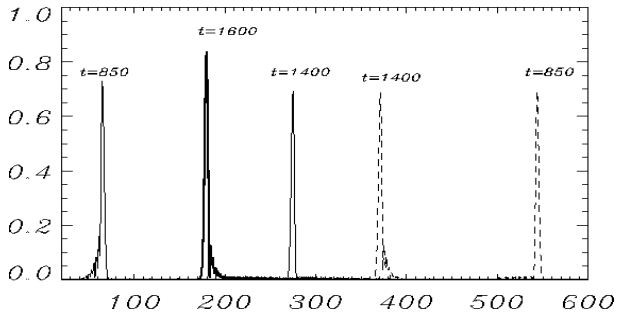

Figure 3.19: Run A: the same as Fig. 3.17 at $t = 850, 1400, 1600$.

at $\tau' = 1600$. We see that both pulses are reflected at $n_v = n_v^{max,A}$ after which they propagate backward towards large scales. Eventually, at $t = \tau'$, an echo is generated (symmetrically with respect to the other runs) at $n_v^{echo,A} \simeq 200 = n_v^{max,A} - \Delta n_v$, where $\Delta n_v = n_v^{\chi} - n_v^{max,A} \simeq 400$. However, a strong amplitude difference between run A and B is observed in the amplitude of the echoes (see Fig. 3.18). This indicates that, during the artificial process of pulse reflection, significant dissipative and/or dispersive effects are introduced. Indeed, after reflection we observe a phase error substantially larger than two times the phase error of run B, i.e. much larger than that expected from the difference in the grid resolution of N_v between run B and A. Finally, we note that after the reflection of the first pulse and before that of the second, the two signal meet at $t = 940$ without showing any interference effect, as expected from the analysis of the ballistic term. Thus, even if for run A we have $t_{max} < T_R$, and even if we do observe the formation of an echo at the right time, although with reduced amplitude, the turning back of the ballistic term towards large velocity scale lengths invalidates the numerical simulation since part of the macroscopic dynamics of the system is artificially altered. Artificial alterations of such a type could be crucial when studying Langmuir turbulence and/or strong non linear effects where part of the energy is injected at larger wavenumbers where the numerical recurrence time is shorter. In order to avoid reflection as well as recurrence effects, we introduced in the code a compact finite differences filter (see Ref. [53], Eq. C.2.2) which dissipates (smoothly) the signal for n_v larger than a threshold value n_v^*, leaving the signal unchanged for $n_v < n_v^*$. The dissipation rate and the threshold value n_v^* of the filter depend on a single free parameter η (the filter efficiency is increased for decreasing values of η). The filter is applied, at each spatial point x_α, to the

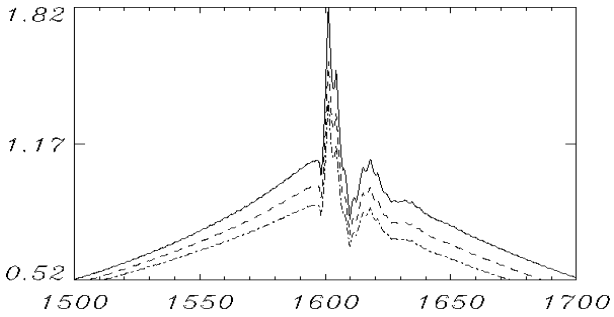

Figure 3.20: Echo amplitudes multiplied by 10^{10} vs time for run D (continues line) and for two identical runs (dashed and dash - dotted line) with a velocity space filter ($\eta = 0.3, 0.1$) applied each $\Delta t = 0.1$.

velocity Fourier transformed distribution function, Eq. 3.3.2. In Fig.3.20 we show the echo's amplitude vs time for the collisionless run D (continuous line, same as in Fig. 3.18) and for the "collisional" runs D* (dashed and dash - dotted line) defined as the same run as run D to which the filter ($\eta = 0.3, 0.1$) is applied every $\Delta t = 0.1$. We see that in runs D* a "collisional" echo is generated at $t = \tau'$ but with a lower amplitude (about 12, 24 % smaller) due to the dissipative effects of the filter on the ballistic oscillations of the distribution function. In the velocity Fourier space, the ballistic pulses of the filtered run are exactly equal to those of the non-filtered run for $n_v < 450, 250$ and then start to decrease. More importantly, due to the presence of the filter, the recurrence effect is no longer observed. In other words, by tuning the filter coefficient, it is possible to eliminate the artificial feedback on the large velocity scale-lengths of the system without introducing diffusive effects on such large scales. Finally, as for the weakly collisional runs B and C, we observe that the growth and damping rate of the echo evolution, namely $\gamma_{\pm}$, differ more and more when the filter efficiency is increased. This is in agreement with the fact that the filter smoothing (i.e. diffusion) is not velocity independent. We underline that identical (qualitatively) results have been obtained when the amplitudes of the two perturbations, see Eq. (3), are different.

3.4 Correlations

Up to now we've seen that, in Vlasov simulations, when the numerical mesh becomes unable to describes the small length scales fluctuations generated by the system, both the evolution and the final macroscopic state of the system are affected. The effect is in some way similar to introduce a (grid and algorithm dependent) collisional operator in the Vlasov-Poisson system of equations. The properties os such operator are important to select the asymptotic final state of the system. We decided to investigate if, in correspondence to the inability of the numerical simulation to properly describe the small scale dynamics, binary correlations between individual particles come into play, even if the plasma under study is formally collisionless.

Here we present the study of particle correlations on the non linear evolution of the two stream instability. Initial conditions and parameters of the simulations are the same as run G described in section 2.2, apart for the velocity grid spacing that here is taken as $dv = 0.05$.

To study the correlations between similar particles, we introduced in the numerical simulations a large number of passive charged tracer particles. These tracers are test particles whose presence is not taken into account neither for the computation of the distribution function used in the Vlasov equation nor for that of the electric field of the system. Their evolution, in time, is set following the motion equations:

$$\frac{dx}{dt} = v \quad \frac{dv}{dt} = -\frac{e}{m}E(x,t) \tag{3.4.1}$$

where, we recall, the electric field $E(x,t)$ represents the self-consistent field calculated evolving the Vlasov-Poisson system of equations. All the simulations are made solving the Vlasov-Poisson equations on a numerical mesh with $dx = 0.1$ and $dv = 0.05$. The initial velocities of all tracers are chosen in the range $-2.5 < v < 2.5$ while the initial positions can be chosen all along the dimension of the space box L_x. In this portion of the phase space, tracers are randomly distributed not on the numerical mesh points but on the continuous (x, v) space (see Fig.3.21, left frame).

If we divide this portion of phase space in cells, the number of tracer particles present in each cell of this portion of the phase space is about the same. Since our numerical simulations are performed using a single processor, the maximum total number of passive particles that we can make evolve by the code is limited (about

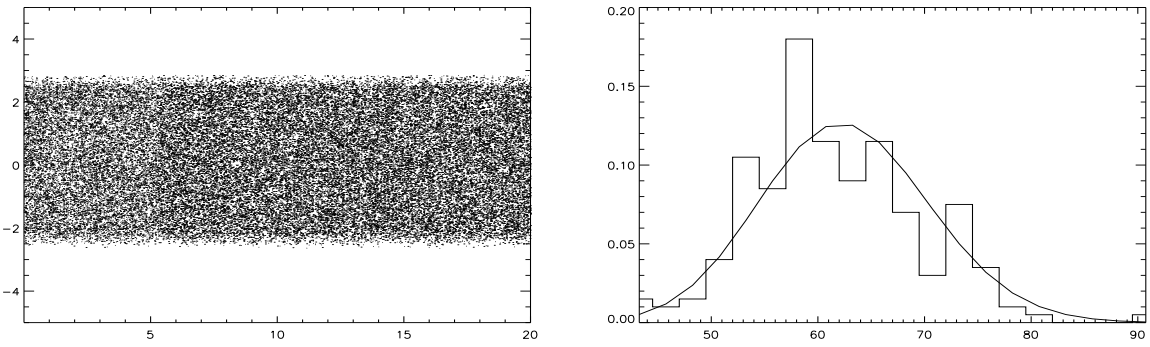

Figure 3.21: Left frame: the initial distribution of tracers in the phase space. Right frame: the histogram of the distribution at $t = 0$ of the number of particles per cell for a total number of 200 cells on which there is superposed the expected Poisson distribution.

an half million). Furthermore, for our study, to obtain statistically significant results the phase space must be divided in very small cells, producing a limited average number of particles per cell. For these reasons it is necessary to search a compromise in the choose of the total number of tracer particles to adopt and the size of the cell: this number must be reasonable to perform a simulation but, at the same time, sufficiently Poissonian to be statistically significant. For this reason, first of all, we made some tests to understand how many cells and particles per cell must be taken into account to obtain that the distribution of the number of particles in the cells could be considered Poissonian.

The Poissonian distribution of reference is:

$$P(\nu) = \frac{\mu^\nu}{\nu!} e^\mu \,. \tag{3.4.2}$$

where μ and ν represent the average number of particles and the number of particles in cells, respectively. First we took 50000 particles and we chose cells of dimension $\Delta x = 0.25\lambda_D$ and $\Delta v = 0.25 v_{th}$, corresponding to an average number of tracers for cell of about 60. It is important to note that for the study of particle correlations, we will always consider cells smaller than the physical characteristic length λ_D that represents the smaller physical scale over which is valid the mean field theory and than v_{th}. By making several cases we found that the minimum number of cells

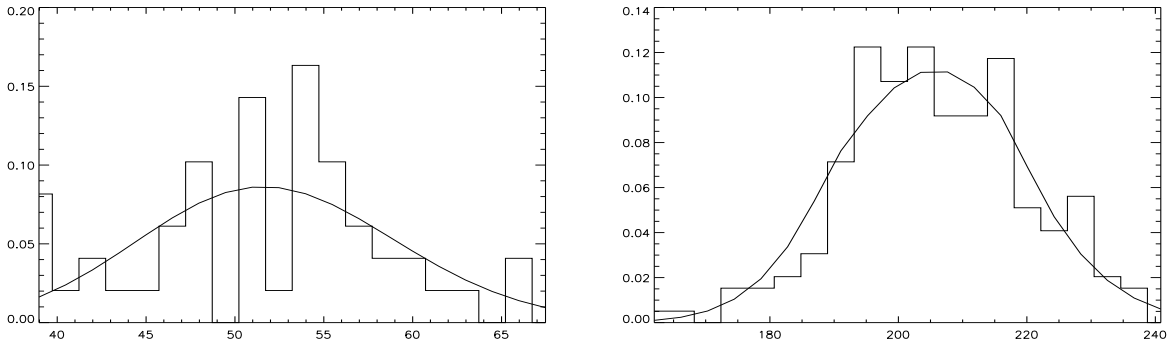

Figure 3.22: The histograms of the distribution, at $t = 0$, of the number of particles per cell respectively, in the left frame, for a total number of 50 cells with about 50 particles per cell, and, in the right frame, for a total number of 200 cells with about 200 particles per cell, with the expected Poisson distribution superposed.

to consider to obtain a Poissonian distribution is 200 (see Fig.3.21, right frame). Then we took 500000 tracers (about the maximum value allowed by single processor simulations) and we decided to examine the distribution of the number of particles in the cells taking a limited number of cells, with respect to the total number in which the portion of phase space containing the particles is divided, equal to the average number of particles per cell. Since the total number of tracers is fixed (500000) different average number of particles in the cells can be obtained by varying the cells' dimensions. Therefore the dimension of the cells will depends on the average number of particles per cell we want to obtain: smaller is the average number of particles, smaller will be the dimension of the cells. We analyzed four cases:

1. 25 particles per cell and 25 cells, corresponding to cells of the dimension $\Delta x = 0.1\lambda_D$ and $\Delta v = 0.05 v_{th}$;

2. 50 particles per cell and 50 cells, corresponding to cells of the dimension $\Delta x = 0.14\lambda_D$ and $\Delta v = 0.07 v_{th}$ (see left frame Fig.3.22);

3. 100 particles per cell and 100 cells, corresponding to cells of the dimension $\Delta x = 0.2\lambda_D$ and $\Delta v = 0.1 v_{th}$;

4. 200 particles per cell and 200 cells, corresponding to cells of the dimension $\Delta x = 0.28\lambda_D$ and $\Delta v = 0.14 v_{th}$ (see right frame Fig.3.22).

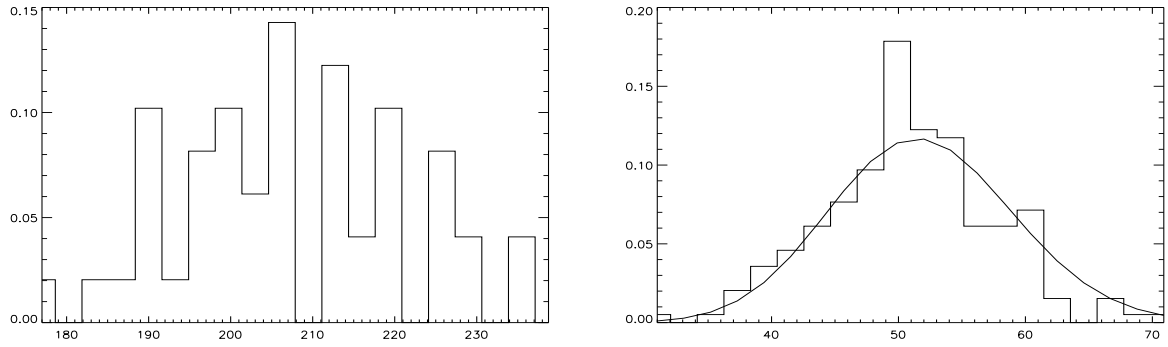

Figure 3.23: The histograms of the distribution, at $t = 0$, of the number of particles per cell respectively, in the left frame, for a total number of 50 cells with about 200 particles per cell, and, in the right frame, for a total number of 200 cells with about 50 particles per cell, with the expected Poisson distribution superposed.

From these tests we observe that only cases 3) and 4) give a distribution similar to a Poissonian.

To understand which quantities between the number of particles per cell and the number of cells is the more significant to generate a good statistics, we made other two tests. The first, represented in the first frame of Fig.3.23, is a case in which are considered 50 cells with an average number of particles per cell of 200; the second test, showed in the second frame of Fig.3.23, is made using 200 cells with an average number of particles per cell of 50. From the comparison of the two tests is clear that the number of cells is the most important quantity.

From these results, we decided to use, for the study of correlations in the two stream instability simulation, 500000 tracers and to divide the phase space, for the investigation of their dynamics, in cells of dimension $\Delta x = 0.1$ and $\Delta v = 0.06$. In these conditions the average number of particles per cell is 30. As shown in 3.24, the distribution of the number of particles in the cells is quite correctly described by a Poissonian if the statistics is made for almost 200 cells of the total 20000 in which is divided the phase space.

Before performing the correlations study, we have checked that the evolution in time of distribution function, even during the non linear regime (for example during and after the formation of a vortex), is accurately reconstructed by the number of particles per cell N_A normalized to the total number of tracer particles of the system.

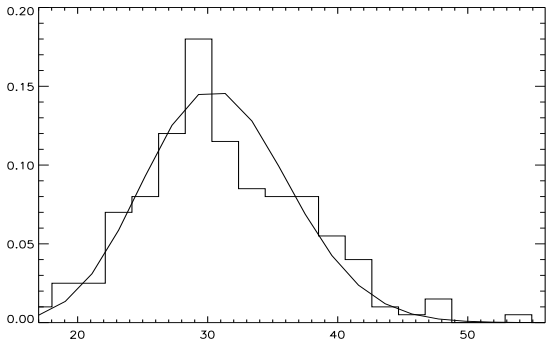

Figure 3.24: The histogram of the distribution, at $t = 0$, of the number of particles per cell for a total number of 200 cells with about 30 particles per cell, with the expected Poisson distribution superposed.

This ensures that the dynamics of the passive tracers follows the evolution of the instability.

We hence studied the correlation between particles introducing a binary correlation function defined as follows. We choose a box of cells in the phase space of hight $\mathcal{L}_v = 1.5 v_{th}$ and of length $\mathcal{L}_x = 2\lambda_D$, containing about 500 cells and, in this box, called box A, we counted the number of particles N_A for each cell. Once chosen the distance at which we want to search correlations, that we will call L_c, we define another box of the same dimension as box A but at a distance L_c from it, called box B. Box B can be taken in an elsewhere position at distance L_c respect to box A. Since there are no privileged directions in the phase space, at least before the formation of the vortex, for simplicity we considered L_c only along the space direction. Also in this box we computed the number of particles N_B present in each cell. For each box A and B the average number of particles contained in a cell, $< N_A >$ and $< N_B >$, has been computed. Then we calculated the product $N_A N_B$ of the number of particles contained in a single cell of the box A and those contained in the corresponding single cell of the box B at distance L_c. At this point we computed the average of all the products $N_A N_B$ between all the corresponding coupled cells as sketched before. We've hence defined our correlation function at a certain instant of time as

$$C_{A,B} =< N_A N_B > - < N_A >< N_B > \ . \tag{3.4.3}$$

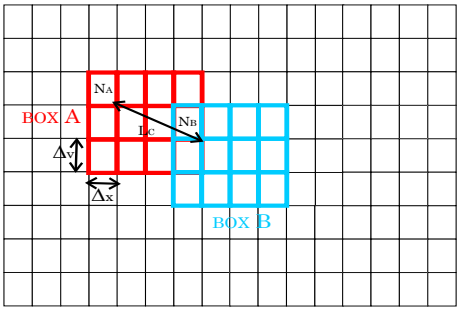

Figure 3.25: An example of a possible displacement of box A and B for the study of correlation at distance L_c

The investigation of correlations has been made by centering box A in different points of the phase space and searching correlations for different distances L_c but with the same criterion. This correlation function is computed at different times.

Here we show the particle correlation results for the two stream instability evolution. First of all, we found that if we put box A in the center of the phase space vortex both short and long distance correlations are not present at all times. Then we put box A on the boundary of the vortex, as shown in Fig.3.26, and we computed the correlation function for the following cases:

1. $L_c = 0.1\lambda_D$;
2. $L_c = 0.5\lambda_D$;
3. $L_c = -0.5\lambda_D$;
4. $L_c = -6.4\lambda_D$ (corresponding to a half vortex distance);
5. $L_c = -12.8\lambda_D$ (corresponding to a vortex distance).

Results are presented in Fig.3.27. On this figure we superpose also the trend of the third invariant I_3 to show the time at which the Vlasov equation is "distorted" by the insertion of numerical effects in the system from the numerical scheme. However, since I_3 decreases when small scales lengths are reached in the system, to make more evident the comparison with the particle correlation functions, we decided to show it overturned and multiplied by a positive constant value to amplify its amplitude. We observe that only for the case 4 (dashed line), i.e. correlations searched at a half

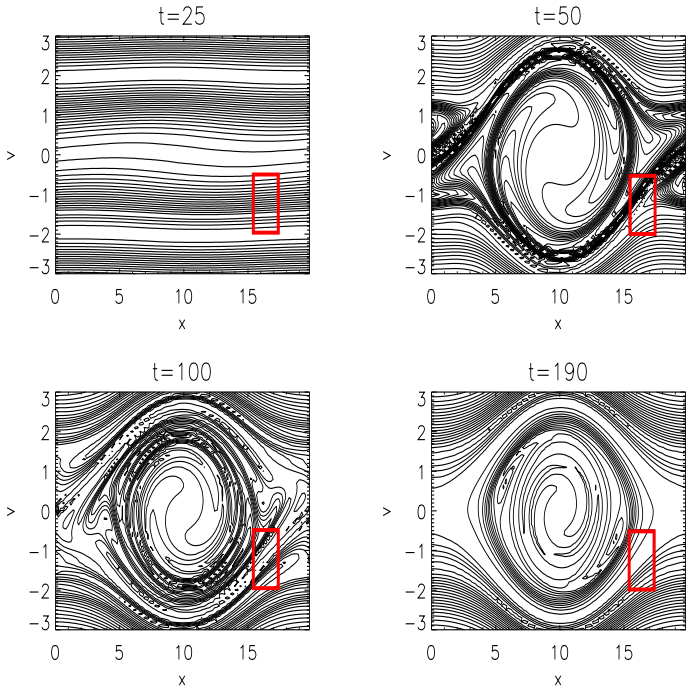

Figure 3.26: The electron distribution function at 4 different times:$t = 25, t = 50, t = 100et = 190$.

vortex distance, the correlation function remains approximately zero at all times. For the other four cases $C_{A,B}$ begins to increase at about the same time when the (upside-down) third invariant increases and, as the third invariant, it tends to be stabilized to a constant value for $t > 150$. From Fig.3.27 we can also observe that correlations are more accentuated from case 1 (dot-dashed line), to case 5 (pointed line), i.e. from shorter correlation distances L_c to longer ones. Furthermore, the saturation values of the correlation functions depends only on the distance L_c and not from the direction. This can be seen comparing case 2 (3-point-dashed line) and 3 (long dashed line), for which the correlation length is the same but in case 2 box B has been put at the right side respect to box A while in case 3 box B is at the left of box A. The conclusion is that correlations are generated only in correspondence of the boundary region of the phase space between trapped and untrapped particles.

From these results it is possible to give an "operative" estimation of the parameter g (the parameter that measures the presence of binary interactions in a plasma, as explained in Section 1.6) of the plasma under exam. Parameter g is defined as:

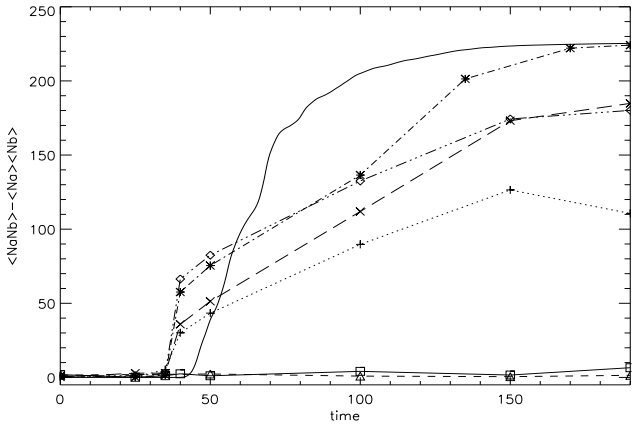

Figure 3.27: Curves of spatial correlations vs time for different lengths of correlation and displacement of box A. Continuous line correspond to the upside-down scaled third invariant, dot-dashed line to case 1), 3-point-dashed line to case 2), long dashed line to case 3), dashed line to case 4) and pointed line to case 5).

$$f_2(x_A, x_B, v_A, v_B) = f_1(x_A, v_A) f_1(x_B, v_B)(1 + g) \tag{3.4.4}$$

where $f_2(x_A, x_B, v_A, v_B)$ represents the two particles distribution function related the probability density of finding simultaneously one particle in the phase space position (x_A, v_A) and another in the point (x_B, v_B), while $f_1(x_A, v_A)$ and $f_1(x_B, v_B)$ are the one particle distribution function related to the probability density to find respectively one particle in the position (x_A, v_A) or (x_B, v_B). Rewriting this equations using the function of the number of particles defined in our study we obtain:

$$\frac{< N_A N_B >}{N_{tot}^2} = \frac{< N_A >}{N_{tot}} \frac{< N_B >}{N_{tot}} (1 + g) \tag{3.4.5}$$

where N_{tot} is the total number of tracers of the simulation. Therefore g can be expressed as:

$$g = \frac{< N_A N_B > - < N_A >< N_B >}{< N_A >< N_B >} = \frac{C_{A,B}}{< N_A >< N_B >} \,. \tag{3.4.6}$$

We measured the values of g at $t = 0$, g_0, and at the final time of the simulation, i.e. where the correlation function reach a constant asymptotic value, $g_{t_{end}}$. The maximum values we found are: $g_{0,max} = 10^{-3}$ and $g_{t_{end},max} = 0.26$. We can note, first of all, that $g_{0,max}$ assume a very large value with respect to those considered by the theory since the number of tracers is too small for describing a real plasma. However, since the $g_{t_{end}}$ is about two order of magnitude larger than at the initial time of the simulation, we can say that correlations and hence interactions among particles have been created in the plasma even if it is formally collisionless. We computed the g_0 and $g_{t_{end}}$ values in other two runs with the same initial conditions and parameters of this already showed, but with a different number of tracers, 50000 and 200000, respectively. We obtained that both the $g_{t_{end}}$ values at different correlation lengths as well as the maximum value $g_{t_{end},max}$ are nearly the same of the 500000 tracers run. Instead the maximum value of g at the initial time, $g_{0,max}$, results different in the three cases: $g_{0,max} = 10^{-3}$ for 500000 tracers, $g_{0,max} = 4.910^{-3}$ for 200000 tracers and $g_{0,max} = 10^{-2}$ for 50000 tracers. Therefore, as expected, more tracers we insert in the simulation, more the initial value of g becomes small and, consequently, we can appreciate a larger difference between the initial and the final g values.

At the same time of the computing of the correlation function, we studied the tracers trajectories in time, calculating for each of them the correspondent maximum Lyapunov exponent both with VL2 and VL3 algorithms. Lyapunov exponents are the average exponential rates of divergence or convergence of nearby orbits in phase space. The spectrum of Lyapunov exponents for a n-dimensional phase space is obtained following the long time evolution of an infinitesimal n-sphere of initial conditions. This sphere becomes in time an n dimensional ellipsoid. The ith one dimensional Lyapunov exponent is then defined in terms of the length of the ellipsoidal axis $p_i(t)$:

$$\lambda_i = \lim_{t\to\infty} \frac{1}{t} \log_2 \frac{p_i(t)}{p_i(0)} \,. \tag{3.4.7}$$

Any system containing at least one positive Lyapunov exponent is defined to be chaotic. For their computation we used the ODE algorithm described in reference [54]. We observed, in agreement with Valentini et al. [55] made in the case of the non linear Landau damping, that the maximum values of Lyapunov exponent appear in the zone around the separatrix between the trapping vortex and the free motion (see

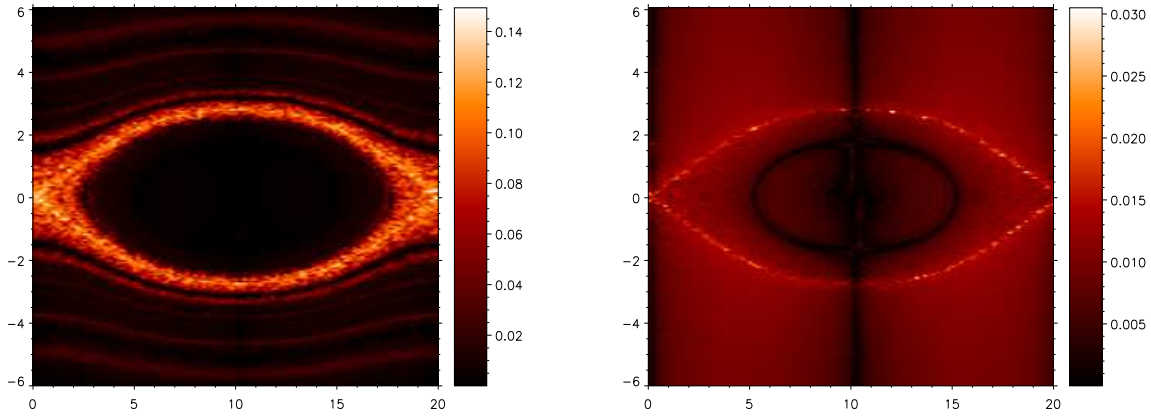

Figure 3.28: Asymptotic Lyapunov exponent distribution in the phase space obtained with VL2 (left frame) and VL3 (right frame) numerical schemes.

Fig.3.28) indicating that particles in this region present chaotic trajectories. These particles have a kinetic energy comparable to the potential energy. Therefore small fluctuations of the electric field can determine trapping or detrapping of the particles from the potential well producing miscellaneous trajectories. This behaviour would not be allowed by Vlasov collisionless theory since each particle is forced to follow an isoline of the distribution function. However when numerical effects come into play, different isolines are reconnected permitting the passage of a particle from a close orbit to a free motion and viceversa. Furthermore, the VL2 run present a larger chaotic region with respect to the VL3 one.

Comparing this result with the one obtained for the correlation function, we observe that the region in which correlations are present corresponds to the region in which particles trajectories are chaotic. The two things are in fact strictly correlated. The reconnection of the isolines of the distribution function, due the inability of the numerical scheme to describe the small dynamics of the system, corresponds to affect the self-consistent electric field with small fluctuations. Therefore two particles with about the same initial conditions, can feel slightly different electric field that, for particles in this critical region, can give origin to really different trajectories. For example, if the two particles are both initially untrapped, since their kinetic energy is comparable to the potential one, two different little fluctuation in the electric field can permit the trapping of one of them but leave the other particle free. The significant

differentiation of the trajectories of the two nearby particles is the same that can be obtained if we consider binary interactions between particles. In other words, two nearby particles which can evolve in a very different ways cannot be considered as statistically independent. Obviously fluctuations affect also particles of the vortices far from the separatrix but, in this case the only change that we can obtain is that a particle goes on another closed orbit. Therefore two particles remain anyhow nearby, as if they continue to feel the same average electric field.

A proof of the fact that correlations are introduced by numerical representation of the continuum Vlasov theory, is given by the result of another kind of simulation. We considered a system where the field produced by the plasma particles is neglected and an external sinusoidal fixed electric field is taken. Although even in this case a vortex is formed in the phase space, we found no correlations at any times and for all distances. In this case in fact the field doesn't fluctuate and so the tracers are forced to remain on their orbits.

3.5 Conclusions

The results presented in this chapter show that, when the non linear long time dynamics of a collisionless plasma is investigated through a Vlasov code, there is a time that depends on the numerical scheme and grid used, for which the Vlasov theory is locally violated. As previously seen, the phase space region where important particles correlations are generated is a very small part with respect to those where numerical problems in describing small scales dynamics come into play. For example in our case all the vortex is affected by small scales grid effects, but only its boundary, i.e. the separatrix, shows important growth of the correlation factor g. Therefore, in all those regions where these numerical effects are present but no correlations between particles are generated, the Vlasov theory can still be considered as valid. However, even if the violation of the Vlasov equation is limited to "small" phase space regions, it may have important consequences on the macroscopic dynamics. Indeed, depending on the kind of numerical effects, i.e. on the numerical algorithm and/or the grid size (that determines the width of the correlations zone), the evolution and the final state of a system can be significantly different. To avoid that final state depends on such numerical effects, a way could be to find the analytical form of an operator

capable of replacing the numerical smoothing and to insert it in the Vlasov equation. The determination of such an operator is, however, very difficult because we don't know the physical grounds on which it should be based in such critical conditions of a plasma which locally can be far from equilibrium (i.e. the distribution function is not a Maxwellian) and particle correlations not negligible. A way to understand something more on the form of this collisional operator can come from the study of the evolution for large times of the two particle distribution function and from a deeper study of correlation processes.

We have seen that the local violation of Vlasov theory produces effects on the evolution and final macroscopic state of a system. But how much such local problems are quantitatively significant? For example, it is well known that in the magnetic reconnection phenomenon the violation of the magnetic freezing condition, even if very localized with respect to the dimension of the system, makes accessible energetic states, otherwise prohibited, producing a significant release of energy in the system. This is an example of how much a local breaking of a constraint of the motion in a collisionless plasma can bring very important global effects in the plasma. A future issue of this work is therefore to understand if the global effects generated in our case by the local reconnection of the distribution function isolines can produce similar global and quantitatively relevant effects on the system.

Appendix A

Bernstein-Greene-Kruskal (BGK) waves

Bernstein-Greene and Kruskal found, in 1957, exact solutions of the problem of a stationary non-linear electrostatic wave in a one dimensional collisionless plasma [7]. These solutions have been derived from the Vlasov-Poisson system of equations and correspond to stationary travelling wave. They demonstrated that it is possible to construct arbitrary wave solutions considering the presence of a certain number of particles trapped in the potential wells. Hence, given an electric potential configuration, it is possible to find the correspondent distribution of trapped particles necessary to generate such stationary wave. In this section we will show the procedure for finding the distribution function of trapped particles corresponding to a single wave of arbitrary amplitude. We consider a collisionless one dimensional plasma were ions are at rest. We search for solutions of Vlasov and Poisson equations in a coordinate system in which the wave is at rest, the so called wave frame. In this frame of reference the solutions of Vlasov and Poisson equations are stationary ($\partial/\partial t' = 0$). Therefore, if the wave moves in the laboratory frame with a constant velocity v_0, the BGK waves and the distribution function will depend from x' and from x' and v' respectively, where $x' = x - v_0 t$, $v' = v - v_0$ and x and v are the coordinate of the laboratory frame. Since Vlasov-Poisson equations are invariant under such Galilean transformation, they can be written as:

$$\left[v' \frac{\partial}{\partial x'} - \frac{e}{m_e} E_0(x') \frac{\partial}{\partial v'} \right] f_0(x', v') = 0; \tag{A.0.1}$$

$$\frac{\partial E_0(x')}{\partial x'} = -4\pi e \left[\int_{-\infty}^{\infty} f_0(x', v')\, dv' - n_0 \right] . \tag{A.0.2}$$

In the case of one wave, the single particle energy is given by:

$$\varepsilon = \frac{m_e v'^2}{2} - e\phi \tag{A.0.3}$$

where ϕ is the electric potential. Since particle energies are exact invariants of the motion, a solution of Vlasov equation in the case of no trapped electrons (i.e. for electrons with energy $\varepsilon > U_{\phi,max}$, where $U_\phi = -e\phi$ is the potential energy) is:

$$f_0 = \theta(v') f_0^{>}(\varepsilon) + \theta(-v') f_0^{<}(\varepsilon) \tag{A.0.4}$$

where θ is the Heavyside function defined as $\theta(v') = 1$ when $v' > 0$ and $\theta(v') = 0$ when $v' < 0$ and $f_0^{>}$ and $f_0^{<}$ are the distribution functions of un-trapped electrons that moves with positive and negative velocities respectively. Equation A.0.4 satisfies Vlasov equation independently of the partition, at a given energy ε, between the two directions of the velocity of particles. If we instead introduce electrons with energy $U_{\phi,min} < \varepsilon < U_{\phi,max}$ (i.e. trapped particles), it is necessary to impose the condition that the particles must be equally distributed between the two directions in velocity, $f_0^{>}(\varepsilon) = f_0^{<}(\varepsilon)$, otherwise the independence of time of the distribution function is not ensured.

Substituting equation A.0.4 in Poisson equation A.0.2 and introducing the energy ε in place of the velocity, we obtain:

$$\frac{\partial^2 \phi(x')}{\partial x'^2} = 4\pi e \left[2 \int_{U_\phi}^{\infty} \frac{f_0^{>}(\varepsilon) + f_0^{<}(\varepsilon)}{[2m_e(\varepsilon + e\phi)]^{1/2}} d\varepsilon - n_0 \right] . \tag{A.0.5}$$

The above equation can be also write as:

$$\frac{\partial^2 \phi(x')}{\partial x'^2} = 4\pi e 2 \int_{U_{\phi,max}}^{\infty} \frac{f_0^{>}(\varepsilon) + f_0^{<}(\varepsilon)}{[2m_e(\varepsilon + e\phi)]^{1/2}} d\varepsilon + 4\pi e 2 \int_{U_\phi}^{U_{\phi,max}} \frac{f_0^{>}(\varepsilon) + f_0^{<}(\varepsilon)}{[2m_e(\varepsilon + e\phi)]^{1/2}} d\varepsilon - 4\pi e n_0 \tag{A.0.6}$$

where the contributions to the potential of trapped (second term of the right-hand side) and un-trapped (first term of the right hand side) electrons have been separated.

Therefore, if the explicit functional form of the potential ϕ and the distribution function of un-trapped particles are given, the correspondent electron distribution function of trapped electrons can be simply determined, solving the integral equation A.0.6. In this way, it is possible to find the appropriate trapped particles distribution function for almost any potential wave-form with the only condition that the second derivative $\partial^2\phi/\partial x'^2$ must be continuous, as explained in reference [7].

When a potential $\phi(x,t)$ with a more complicated dependence of time is considered, determine stationary solutions becomes more difficult. In fact, in these cases the dependence of time cannot be eliminated simply shifting the reference frame as done in the single wave problem. If the field consists in a superposition of two or more waves, the problem could be gone around using a superposition principle. However, since BGK waves are exact solutions of non-linear equations, they do not satisfy a principle of linear superposition, even in the limit of small amplitude. In fact, if we take $(f^{(1)},\phi^{(1)})$ and $(f^{(2)},\phi^{(2)})$ as the distribution functions and potentials of two BGK waves with velocity $v^{(1)}$ and $v^{(2)}$ respectively, and assuming that as the amplitude of the potential as the deviations $h^{(i)} = f^{(i)} - F$ of the distribution function from the Vlasov equilibrium F are of first order in a small parameter σ, the superposition of these states:

$$\begin{aligned} f^{(S)} &= F + h^{(1)} + h^{(1)} \\ \phi^{(S)} &= \phi^{(1)} + \phi^{(2)} \end{aligned} \tag{A.0.7}$$

will satisfy the Poisson equation but not the Vlasov one. Indeed, Vlasov equation computed on the linear superposition BGK state becomes:

$$\left(\frac{\partial}{\partial t} + v\frac{\partial}{\partial x} + \frac{e}{m_e}\frac{\partial\phi^{(S)}}{\partial x}\frac{\partial}{\partial v}\right) f^{(S)} = -\frac{e}{m_e}\left(\frac{\partial\phi^{(1)}}{\partial x}\frac{\partial h^{(2)}}{\partial v} + \frac{\partial\phi^{(2)}}{\partial x}\frac{\partial h^{(1)}}{\partial v}\right). \tag{A.0.8}$$

Although as $h^{(i)}$ as $\phi^{(i)}$ are of the first order in σ, the right-hand side term of equation A.0.8 is not of the second order in σ everywhere. In fact, near the phase velocities of

the waves, as discussed in section 1.2.2, each single wave distribution function develops a plateau, satisfying the condition $\partial f^{(i)}/\partial v|_{v=v^{(i)}} \simeq 0$. Hence near this points, the right side term becomes of the first order in ϵ and it cannot be neglected respect to the left-hand side term. The Vlasov equation is therefore not satisfied.

In this case, the particle energies ε are no longer conserved. Hence a distribution function constructed with such energies will clearly not satisfy Vlasov equation because ε is no more an invariant of motion. In order to determine a solution, it is therefore necessary to find other exact invariants of the motion on which construct the distribution function. In 1993, Bunchanan and Dorning [**?**] found a solution of the two waves problem building the distribution function from approximate invariants of the motion, i.e. invariants valid over restricted region of the phase space. The chosen of an approximate invariant instead of a global one, i.e. one valid over the entire phase space, is due to the fact that in this case , as for many other in which the potential has a nontrivial dependence of time, the Hamiltonian:

$$H(x,p,t) = \frac{m_e v^2}{2} - e\phi_1(x,t) - e\phi_2(x,t) \tag{A.0.9}$$

is not integrable and so it's impossible to find such global invariant quantities. The approximate invariant are obtained by Bunchanan and Dorning via perturbation methods. The pair of first-order invariants chosen for the waves problem are:

$$\bar{\varepsilon}^{(i)} = \varepsilon^{(i)} - \sigma e \frac{v - v_{0i}}{v - v_{0j}} \phi_j(x,t) \quad i,j = 1,2 \; cyclic \tag{A.0.10}$$

that reduce for $\sigma \to 0$ to the free-particle kinetic energy invariant $m_e(v - v_0)^2/2$. Along the time dependent curve

$$v(x,t) = v_{avg} - \frac{2\sigma e}{m_e \delta v}[\phi_1(x,t) - \phi_2(x,t)] \; , \tag{A.0.11}$$

where $v_{avg} = (v_{01} + v_{02})/2$ and $\delta v = v_{01} - v_{02}$, the two approximate invariants A.0.10 reduce through first order in σ to the same value $\bar{\varepsilon}* = m_e(\delta v)^2/8$. Note that even if $\bar{\varepsilon}^{(1)}$ and $\bar{\varepsilon}^{(2)}$ are not global first-order invariant because of their singularity in the phase velocities v_{02} and v_{01} respectively, nevertheless $\bar{\varepsilon}^{(1)}$ well behave in the region

$v \geq v(x,t)$ and $\bar{\varepsilon}^{(2)}$ in the region $v \leq v(x,t)$. Hence the pair of approximate invariants $\bar{\varepsilon}^{(1)}$ and $\bar{\varepsilon}^{(2)}$ provide, taken together, an invariant quantity valid over the entire phase. This pair of invariants can be used to construct the distribution function of the two-waves problem. So, if with $g(\varepsilon)$ we indicated the BGK function for a single wave for which $f(x,v,t) = g(\varepsilon)$, the two-waves state distribution function f^+ can be define as:

$$f^+(x,v,t) = \begin{cases} g^{(1)}(\bar{\varepsilon}^{(1)}), & v \geq v(x,t) \\ g^{(2)}(\bar{\varepsilon}^{(2)}), & v \leq v(x,t) \end{cases} \tag{A.0.12}$$

where the function $g^{(1)}$ of the first wave with the correspondent approximate invariant $\bar{\varepsilon}^{(1)}$ has been used above the v(x,t) curve, while the function $g^{(2)}$ of the second wave with $\bar{\varepsilon}^{(2)}$ has been used below v(x,t). The definition A.0.12 provide distribution functions that, through first order in σ, satisfy the Vlasov equation. In this way Bunchanan and Dorning also found that two small amplitude single BGK states can be combine through a non-linear superposition principle in which the potentials are superimposed linearly while the distribution functions of the single waves are combined through the non linear rule given in equation A.0.12. The condition of validity of this superposition principle depend on the fact that $\bar{\varepsilon}^{(i)}$ are approximate quantities with errors which are at most $\sim O(\sigma^2/(\delta v)^2)$. Hence, if we want $\bar{\varepsilon}^{(i)}$ to be true first-order invariants, it is necessary that the difference between the phase velocities of the two waves is $\delta v = O(\sigma^s)$ with $s < 1/2$. This implies that the potential amplitudes $\bar{\phi}_i$ (all of first order) must satisfy the condition:

$$\bar{\phi}_1, \bar{\phi}_2 \ll m_e(\delta v)^2/e \ . \tag{A.0.13}$$

Physically this condition reflects the fact that two waves interact less strongly larger their relative phase velocity.

Finally, the non linear superposition principle for BGK states can be extended also to the N small amplitude waves case with a simple generalization of equation A.0.12 based on the introduction of N functions $g^{(i)}(\bar{\varepsilon}^{(i)})$ relative to the N single waves, where the approximate invariants $\bar{\varepsilon}^{(i)}$ are defined on an appropriate set of N nonoverlapping regions that cover together the entire phase space.

Appendix B

Analytical detailed computation of an echo

In section 1.3 we've briefly described how to compute analytically the second order potential related to the echo phenomenon. In this appendix we want to report the computation step by step. Here we begin directly reporting the initial Vlasov and Poisson equations of such system, that we've already presented in section 1.3.

$$\frac{\partial f}{\partial t} + v\frac{\partial f}{\partial x} + \frac{e}{m_e}\frac{\partial \phi}{\partial x}\frac{\partial f}{\partial v} = 0 \tag{B.0.1}$$

$$\frac{\partial^2 \phi}{\partial x^2} = \frac{\partial^2 \phi_{ext}}{\partial x^2} + 4\pi e\left(\int f\, dv \; - \; n_0\right). \tag{B.0.2}$$

We take the usual definition of Fourier and Laplace transforms applied to the perturbed distribution function as:

$$f_k = \int f_1 exp(ikx) dx \tag{B.0.3}$$

$$\tilde{f}_k(v,p) = \int_0^\infty f_k(v,t) e^{-pt} dt \tag{B.0.4}$$

$$f_k(v,t) = \frac{1}{2\pi i}\int_{p_0-i\infty}^{p_0+i\infty} \tilde{f}_k(v,p)e^{pt}dp \tag{B.0.5}$$

By taking the Fourier and Laplace transform to Vlasov and Poisson equations, first the Fourier transform in space obtaining:

$$\frac{\partial f_k(v,t)}{\partial t} + ikvf_k(v,t) = -\frac{e}{m_e}ik\phi_k(t)\frac{\partial f_0(v)}{\partial v} - \frac{e}{m_e}\sum_{k'}{}' i(k-k')\phi_{k-k'}(t)\frac{\partial f_{k'}(v,t)}{\partial v} \tag{B.0.6}$$

$$k^2\phi_k = k^2\phi_{k,ext} - 4\pi e\int f_k(v,t)\,dv. \tag{B.0.7}$$

and then the Laplace transform in time:

$$(p+ikv)\tilde{f}_k(v,p) = -ik\frac{e}{m_e}\tilde{\phi}_k(t)\frac{\partial f_0(v)}{\partial v} - \frac{e}{m_e}\sum_{k'}{}'\int_{p_0-i\infty}^{p_0+i\infty}\frac{dp'}{2\pi}i(k-k')\tilde{\phi}_{k-k'}(p-p')\frac{\partial \tilde{f}_{k'}(v,p')}{\partial v} \tag{B.0.8}$$

$$k^2\tilde{\phi}_k = \frac{k_1^2}{2\omega_{pe}}\phi_{k_1}[\delta(k_1-k)+\delta(k_1+k)] + \frac{k_2^2}{2\omega_{pe}}\phi_{k_2}[\delta(k_2-k)+\delta(k_2+k)]e^{-p\tau} - 4\pi e\int \tilde{f}_k(v,p)\,dv. \tag{B.0.9}$$

Substituting equation B.0.8 in B.0.9 we obtain:

$$\epsilon(k,p)\tilde{\phi}_k = \frac{k_1^2}{2k^2\omega_{pe}}\phi_{k_1}[\delta(k_1-k)+\delta(k_1+k)] + \frac{k_2^2}{2k^2\omega_{pe}}\phi_{k_2}[\delta(k_2-k)+\delta(k_2+k)]e^{-p\tau} + -\frac{\omega_{pe}^2}{k^2}\int dv\sum_{k'}{}'\int_{p_0'-i\infty}^{p_0'+i\infty}\frac{dp'}{2\pi i}i(k-k')\tilde{\phi}_{k-k'}(p-p')\frac{\partial\tilde{f}_{k'}(v,p')}{\partial v} \tag{B.0.10}$$

where

$$\epsilon(k,p) = 1 - \frac{\omega_{pe}^2}{k^2}\int_{-\infty}^{\infty} dv\frac{\partial f_0(v)}{\partial v}\frac{ik}{(p+ikv)}. \tag{B.0.11}$$

is the Landau dielectric function.

At this point equation B.0.10 is expanded in terms of the external applied potentials ϕ_{k_1} and ϕ_{k_2}. The first order solution is obtained neglecting the contribution of the non linear term $(k-k')\frac{\partial \tilde{f}_{k'}(v,p')}{\partial v}$ that gives:

$$\tilde{\phi}_k^{(1)} = \frac{\tilde{\phi}_{k,ext}(p)}{\epsilon(k,p)}. \tag{B.0.12}$$

The second order solution can be obtained by substituting the linearized solution of $\tilde{f}_k$:

$$\tilde{f}_k = \frac{e}{m_e}\frac{k\frac{\partial f_0(v)}{\partial v}}{(ikv+p)}\tilde{\phi}_k \tag{B.0.13}$$

and the first order solution of the potential $\tilde{\phi}_k^{(1)}$ in the non linear term of equation B.0.10. Applying the inverse Laplace transform in time and choosing the wave number $k_3 = k_2 - k_1$ (the one associated to the echo) the second order potential results:

$$\phi_{k_3}^{(2)}(t) = \frac{e}{m_e}\frac{\phi_{k_1}\phi_{k_2}k_1k_2}{4k_3^2}\int_{-\infty}^{+\infty}dv\int_{p_0-i\infty}^{p_0+i\infty}\frac{dp}{2\pi i}\int_{p_0'-i\infty}^{p_0'+i\infty}\frac{dp'}{2\pi i}\frac{ik_3}{\epsilon(k_3,p)(p+ik_3v)^2}\frac{\partial f_0(v)}{\partial v}\times$$
$$\times\left[\frac{e^{pt}e^{-p\tau'}}{\epsilon(k_2,p')\epsilon(-k_1,p-p')(p'+ik_2v)}+\frac{e^{p(t-\tau)}e^{-p'\tau}}{\epsilon(k_2,p-p')\epsilon(-k_1,p')(p'-ik_1v)}\right] \tag{B.0.14}$$

where the p_0 and p_0' contours are defined in the way that $0 < p_0' < p_0$ in order to make converge the integrals. The integration in p and p' can be done using the Cauchy residue method, closing the Landau contours on the side which produces vanishingly small exponentials in the numerator. If we, furthermore, take $|\gamma(k_1)\tau|, |\gamma(k_2)\tau|, |\gamma(k_3)\tau| >> 1$ (i.e. the time τ is long compared with the Landau damping time) and the time between the echo and the second pulse $(\tau'-\tau)$ of the same order of τ (i.e. $|k_3/k_1| \cong 1$), then the poles arising from the roots of the dielectric functions can be neglected because they will produce very small residues respect to the other poles. With these hypothesis, the poles on which to compute the residues will be $p' = ik_1v$ and $p = -ik_3v$ and the previous equation becomes:

$$\phi_{k_3}^{(2)}(t) = \frac{e}{m_e}\frac{\phi_{k_1}\phi_{k_2}k_1k_2ik_1\tau}{4k_3^2}\int_{-\infty}^{+\infty} dv\frac{\partial f_0(v)}{\partial v}\left(\frac{e^{iv[k_1\tau - k_3(t-\tau)]}}{\epsilon(-k_1, ik_1v)\epsilon(k_2, ik_2v)\epsilon(k_3, -ik_3v)}\right). \tag{B.0.15}$$

We can evaluate the integral separately for $t < \tau'$ and $t > \tau'$. When $t < \tau'$ we close the Landau contour in the upper half v plane picking up poles from the Landau roots of $\epsilon(-k_1, ik_1v)$. When instead $t > \tau'$ the Landau contour is closed in the lower half v plane where the poles are the roots of $\epsilon(k_3, -ik_3v)$ and $\epsilon(k_2, -ik_2v)$. We can neglect the contribution of the Landau roots of $\epsilon(k_2, -ik_2v)$ respect to that of $\epsilon(k_3, -ik_3v)$ because the assumption $k_1/k_3 \cong 1$, i.e. $k_2 \cong 2k_3$, implies that $|\gamma(k_2)| >> |\gamma(k_3)|$. Taking as the equilibrium distribution function a Maxwellian of mean thermal energy T we obtain the following time asymptotic solution:

$$\begin{aligned}\phi_{k_3}(2)(t) = \phi_{k_1}\frac{\omega_{pe}e\lambda_D}{T}\tau\frac{\phi_{k_2}k_1^4k_2}{Tk_3(k_1+k_3)^2}\times \\ \times\frac{-(k_3/k_1)\gamma(k_1)e^{\gamma(k_1)k_3/k_1(\tau'-t)}cos[\omega(k_1)(k_3/k_1)(\tau'-t)+\delta}{\{[\omega_{pe}^2(k_3-k_1)/(k_3+k_1)]^2+\gamma(k_1)^2\}\{1/2\}}\ for\ \ t<\tau' \\ \times\frac{\gamma(k_3)e^{\gamma(k_3)(t-\tau')}cos[\omega(k_3)(t-\tau')+\delta'}{\{[\omega_{pe}^2(k_3-k_1)/(k_3+k_1)]^2+\gamma(k_3)^2\}\{1/2\}}\ for\ \ t>\tau'\end{aligned} \tag{B.0.16}$$

where

$$\begin{aligned}\tan(\delta) &= \gamma(k_1)(k_3-k_1)/[\omega_{pe}(k_3+k_1)] \\ \tan(\delta') &= \gamma(k_3)(k_1-k_3)/[\omega_{pe}(k_3+k_1)].\end{aligned} \tag{B.0.17}$$

Appendix C

Propagation of waves in a hot uniformly magnetized plasma

The presence of a magnetic field in a collisionless plasma is a the source of complicated particles orbits and generates new modes associated to particles gyration. The kinetic theory provides the normal modes of propagation of small amplitude waves in such a plasma. The approach, as described in reference [25], is the sequent: we take the Vlasov equation in a collisionless 3D plasma uniformly magnetized, with $\vec{B_0} = B_0\widehat{z}$, linearizing it with the assumptions that $f_\alpha = f_{\alpha,0} + f_{\alpha,1}$, $\vec{B} = B_0\widehat{z} + \vec{B_1}$ and $\vec{E} = \vec{E_1}$, where the index 1 refers to first order (perturbed) quantities:

$$\left(\frac{\partial}{\partial t} + \vec{v}\cdot\nabla + \mu_\alpha\frac{(\vec{v}\times\vec{B_0})}{c}\cdot\nabla_{\vec{v}}\right) f_{\alpha,1}(\vec{x},\vec{v},t) = -\mu_\alpha\left(\vec{E_1} + \frac{(\vec{v}\times\vec{B_1})}{c}\right)\cdot\nabla_{\vec{v}} f_{\alpha,0}$$
$$\mu_\alpha = \mp\frac{q_\alpha}{m_\alpha} \quad with \quad \alpha = e,p \tag{C.0.1}$$

The equilibrium distribution is chosen to satisfy :

$$\begin{aligned}
&\left(\vec{v}\cdot\vec{\nabla}_x + \mu_\alpha\frac{(\vec{v}\times\vec{B_0})}{c}\cdot\vec{\nabla}_v\right) f_{\alpha,0} = 0 \\
&\rho_Q = \overline{n}_p\int f_{p,0}d\vec{v} - \overline{n}_e\int f_{e,0}d\vec{v} = 0 \\
&J = \overline{n}_p\int \vec{v} f_{p,0}d\vec{v} - \overline{n}_e\int \vec{v} f_{e,0}d\vec{v} = 0
\end{aligned} \tag{C.0.2}$$

i.e. there is no net charge and current in the plasma at the equilibrium. Choosing as the equilibrium distribution a Maxwellian distribution of the form:

$$f_{\alpha,0} = \frac{m_\alpha}{2\pi\kappa T_\perp}\left(\frac{m_\alpha}{2\pi\kappa T_\parallel}\right)^{1/2} exp\left[\frac{m_\alpha}{2\kappa}\left(\frac{v_\perp^2}{T_\perp}+\frac{v_\parallel^2}{T_\parallel}\right)\right], \tag{C.0.3}$$

where $v_\perp = \sqrt{(}v_x^2 + v_y^2)$, $v_\parallel = v_z$, the Vlasov equation can be solved by integrating the orbits of the particles in the unperturbed fields. In our case the orbits, expressed for simplicity in cylindrical coordinates in velocity space and in cartesian coordinates in space, are:

$$\begin{aligned} x' &= x - \frac{v_\perp}{\omega_c}sin(\phi-\omega_c\tau) + \frac{v_\perp}{\omega_c}sin(\phi) \\ y' &= y + \frac{v_\perp}{\omega_c}cos(\phi-\omega_c\tau) - \frac{v_\perp}{\omega_c}cos(\phi) \\ z' &= z + v_\parallel\tau \end{aligned} \tag{C.0.4}$$

and

$$\begin{aligned} v_x' &= v_\perp cos(\phi-\omega_c\tau) \\ v_y' &= v_\perp sin(\phi-\omega_c\tau) \\ v_z' &= v_\parallel \end{aligned} \tag{C.0.5}$$

and where $v_x = v_\perp cos(\phi)$, $v_y = v_\perp sin(\phi)$ and $v_z = v_\parallel$. Orbits variables are chosen in the way that $\tau \to 0$, $\vec{x}' \to \vec{x}$ and $\vec{v}' \to \vec{v}$ with x and v fixed points in phase space. Along these orbits, the equilibrium distribution function results to be constant because $f_{\alpha,0}$ is constructed out of constants of the motion. The first order distribution function, instead, can be calculated by integrating the right side of equation C.0.1 along the particles orbits C.0.4, C.0.5 from $\tau = -\infty$ and $\tau = 0$ and assuming a solution for the perturbed fields as $\vec{E}_1(\vec{x},t) = \bar{\vec{E}}_{\vec{k}} exp(i\vec{k}\vec{x} - i\omega t)$ and $\vec{B}_1(\vec{x},t) = \bar{\vec{B}}_{\vec{k}} exp(i\vec{k}\vec{x} - i\omega t)$. Assuming, furthermore, that $f_{\alpha,1}(\vec{x}',\vec{v}',t' \to -\infty) = 0$, then the first order distribution function for a given wave number k results:

$$\bar{f}_{\alpha,\vec{k}}(\vec{x},\vec{v},t) = -\mu_\alpha \int_{-\infty}^{0} \left(\bar{\vec{E}}_{\vec{k}} + \frac{(\vec{v} \times \bar{\vec{B}}_{\vec{k}})}{c} \right) \cdot \nabla_{\vec{v}} f_{\alpha,0}(\vec{v}') exp[i(\vec{k}\vec{X} - \omega t)] d\tau \quad \text{(C.0.6)}$$

with $Im(\omega) > 0$, $\vec{X} = \vec{x}' - \vec{x}$ and $\tau = t' - t$. We evaluate now the field $\bar{\vec{B}}_{\vec{k}}$ in term of $\bar{\vec{E}}_{\vec{k}}$ using the Fourier transformed Maxwell equation:

$$i\vec{k} \times \bar{\vec{E}}_{\vec{k}} = i\frac{\omega}{c}\bar{\vec{B}}_{\vec{k}}. \quad \text{(C.0.7)}$$

Substituting this result in equation C.0.6 and taking $\vec{k}_\perp$ along the x axis (see [25]), one obtains:

$$\begin{aligned} \bar{f}_{\alpha,\vec{k}}(\vec{x},\vec{v},t) = \mu_\alpha \sum_{n,l} \left[\frac{2Zv_\parallel J_l(k_\perp v_\perp/\omega c\alpha) + Xv_\perp(J_{l+1} + J_{l-1}) - iYv_\perp(J_{l+1} - J_{l-1})}{i(\omega - \omega_{c\alpha} - k_\parallel v_\parallel)} \right] \cdot \\ \cdot J_n\left(\frac{k_\perp v_\perp}{\omega_{c\alpha}}\right) exp[i(n-l)\phi] \end{aligned} \quad \text{(C.0.8)}$$

where

$$\begin{aligned} X &= E_x \frac{\partial f_{\alpha,0}}{\partial v_\perp^2} + \frac{v_\parallel}{\omega}(k_\parallel E_x - k_\perp E_z)\left(\frac{\partial f_{\alpha,0}}{\partial v_\parallel^2} - \frac{\partial f_{\alpha,0}}{\partial v_\perp^2}\right) \\ Y &= E_y \frac{\partial f_{\alpha,0}}{\partial v_\perp^2} + \frac{v_\parallel}{\omega} k_\parallel E_y \left(\frac{\partial f_{\alpha,0}}{\partial v_\parallel^2} - \frac{\partial f_{\alpha,0}}{\partial v_\perp^2}\right) \\ Z &= E_z \frac{\partial f_{\alpha,0}}{\partial v_\parallel^2} \end{aligned} \quad \text{(C.0.9)}$$

and J_n are the ordinary Bessel's functions of the first kind. Calculating the perturbed current $\bar{\vec{J}}_{\vec{k}}$ using $\bar{f}_{\alpha,k}$ and substituting it and the expression for $\bar{\vec{B}}_{\vec{k}}$, obtained from equation C.0.7, into Maxwell's equations, we get:

$$\vec{k} \times \vec{k} \times \bar{\vec{E}}_{\vec{k}} = \frac{\omega^2}{c^2} \bar{\vec{E}}_{\vec{k}} + i\frac{\omega}{c} 4\pi \sum_{\alpha} \frac{q_\alpha}{|q_e|} \bar{n}_\alpha \int \vec{v} \bar{f}_{\alpha,k} d\vec{v} \tag{C.0.10}$$

Inserting equation C.0.8 in C.0.10 we obtains three linear homogeneous equations for $\bar{\vec{E}}_{\vec{k}}$ that can be written in the form:

$$\begin{aligned} D_{xx}E_x + D_{xy}E_y + D_{xz}E_z &= 0 \\ D_{yx}E_x + D_{yy}E_y + D_{yz}E_z &= 0 \\ D_{zx}E_x + D_{zy}E_y + D_{zz}E_z &= 0 \end{aligned} \tag{C.0.11}$$

or also as $\vec{D} \cdot \vec{E}$ with $det(D) = 0$ as the solution. $\vec{D}$ is called the dispersion tensor. In our case the coefficient of the dispersion tensor results:

$$\begin{aligned} D_{xx} &= 1 - \frac{k_\parallel^2 c^2}{\omega^2} - \frac{2\pi}{\omega} \sum_{\alpha} \left(\frac{\omega_{p\alpha}^2}{\omega_{c\alpha}} \right) \sum_{n} \Upsilon \left[\frac{n^2 \omega_{c\alpha}^3}{k_\perp^2} J_n^2 \chi_\alpha \right] \\ D_{xy} &= -\frac{2\pi i}{\omega} \sum_{\alpha} \sum_{n} \left(\frac{\omega_{p\alpha}^2}{\omega_{c\alpha}} \right) \Upsilon \left[\frac{n\omega_{c\alpha}^2 v_\perp}{k_\perp} J_n \frac{dJ_n}{d(k_\perp v_\perp / \omega_{c\alpha})} \chi_\alpha \right] \\ D_{xz} &= \frac{k_\parallel k_\perp c^2}{\omega^2} - \frac{2\pi}{\omega} \sum_{\alpha} \sum_{n} \left(\frac{\omega_{p\alpha}^2}{\omega_{c\alpha}} \right) \Upsilon \left[\frac{n\omega_{c\alpha}^2 v_\parallel J_n^2}{k_\perp^2} \Lambda_\alpha \right] \end{aligned} \tag{C.0.12}$$

$$
\begin{aligned}
D_{yx} &= -D_{xy} \\
D_{yy} &= 1 - \frac{(k_\parallel^2 + k_\perp^2 c^2}{\omega^2} - \frac{2\pi}{\omega}\sum_\alpha\sum_n\left(\frac{\omega_{p\alpha}^2}{\omega_{c\alpha}}\right)\Upsilon\left[\omega_{c\alpha}\left(\frac{dJ_n}{d(k_\perp v_\perp/\omega_{c\alpha})}\right)^2 v_\perp^2\chi_\alpha\right] \\
D_{yz} &= \frac{2\pi i}{\omega}\sum_\alpha\sum_n\left(\frac{\omega_{p\alpha}^2}{\omega_{c\alpha}}\right)\Upsilon\left[v_\parallel v_\perp\omega_{c\alpha}J_n\frac{dJ_n}{d(k_\perp v_\perp/\omega_{c\alpha})}\Lambda_\alpha\right] \\
D_{zx} &= \frac{k_\parallel k_\perp c^2}{\omega^2} - \frac{2\pi}{\omega}\sum_\alpha\sum_n\left(\frac{\omega_{p\alpha}^2}{\omega_{c\alpha}}\right)\Upsilon\left[\frac{n\omega_{c\alpha}^2 v_\parallel J_n^2}{k_\perp^2}\chi_\alpha\right] \\
D_{zy} &= -\frac{i}{2\omega}\sum_\alpha\sum_n\left(\frac{\omega_{p\alpha}^2}{\omega_{c\alpha}}\right)\Upsilon\left[v_\parallel v_\perp\omega_{c\alpha}J_n\frac{dJ_n}{d(k_\perp v_\perp/\omega_{c\alpha})}\chi_\alpha\right] \\
D_{zz} &= 1 - \frac{k_\perp^2 c^2}{\omega^2} - \frac{2\pi}{\omega}\sum_\alpha\sum_n\left(\frac{\omega_{p\alpha}^2}{\omega_{c\alpha}}\right)\Upsilon\left[\omega_{c\alpha}v_\parallel^2 J_n^2\Lambda_\alpha\right]
\end{aligned}
\tag{C.0.13}
$$

where Υ is an operator defined as:

$$
\Upsilon[F(v)] \equiv \int_{-\infty}^{+\infty} dv_\parallel \int_0^{+\infty} \frac{2v_\perp F(v_\perp, v_\parallel)}{k_\parallel v_\parallel + n\omega_{c\alpha} - \omega} dv_\perp \tag{C.0.14}
$$

and

$$
\begin{aligned}
\chi_\alpha &\equiv \frac{\partial f_{\alpha 0}}{\partial v_\perp^2}\left(1 - \frac{k_\parallel v_\parallel}{\omega}\right) + \frac{k_\parallel v_\parallel}{\omega}\frac{\partial f_{\alpha 0}}{\partial v_\parallel^2} \\
\Lambda_\alpha &\equiv \frac{\partial f_{\alpha 0}}{\partial v_\parallel^2} - \frac{n\omega_{c\alpha}}{\omega}\left(\frac{\partial}{\partial v_\parallel^2} - \frac{\partial}{\partial v_\perp^2}\right) f_{\alpha 0}
\end{aligned}
\tag{C.0.15}
$$

However, in our case, we're interested only in waves that propagate perpendicular to the magnetic field, i.e. we consider the case in which $k_\parallel = 0$ (we recall that we've chosen a collisionless plasma magnetized with an uniform magnetic field along the z-axis and that $k_\perp = k_x\hat{x}$). This assumption allows to obtain a greatly simplified dispersion relation:

$$\begin{bmatrix} D_{xx} & D_{xy} & 0 \\ D_{yx} & D_{yy} & 0 \\ 0 & 0 & D_{zz} \end{bmatrix} \begin{bmatrix} E_x \\ E_y \\ E_z \end{bmatrix} = 0 \tag{C.0.16}$$

It is important to note that in these conditions, there will be no damping for the waves. In fact, as can be seen from equation C.0.14, the resonance, that for the field-free plasmas is at $\omega = \vec{k} \cdot \vec{v}$, for a magnetized plasma occurs at $\omega - n\omega_{c\alpha} = k_{\parallel} v_{\parallel}$. Only those particles that moves along the magnetic field can contribute to the damping, and they can damp only waves that have a component of propagation along the magnetic field. Since here we are interested only in waves that propagate perpendicular to the magnetic field, i.e. with $k_{\parallel} = 0$, we will have no damping effects.

If we also assume that the distribution function is isotropic, i.e. $\partial f_{\alpha 0}/\partial v_{\parallel}^2 = \partial f_{\alpha 0}/\partial v_{\perp}^2$, one solution of equation C.0.16 becomes:

$$D_{zz} = 1 - \frac{k_{\perp}^2 c^2}{\omega^2} - \frac{2\pi}{\omega} \sum_{\alpha} \sum_{n} \omega_{p\alpha}^2 \int_{-\infty}^{+\infty} dv_{\parallel} \int_{0}^{+\infty} \frac{J_n^2 v_{\perp} f_{\alpha 0}}{\omega - n\omega_{c\alpha}} dv_{\perp} = 0. \tag{C.0.17}$$

This solution represent an electromagnetic wave that propagate in the x direction and with the electric field parallel to the plasma magnetic field $\vec{B_0}$, i.e. along the z-axis. This wave is called an ordinary wave. In the case in which only the term $n = 0$ of the $\sum_n$ contributes to the solution, as for long-wavelengths modes or for high frequency modes, the solutions of this equation can be easily computed setting $J(\frac{k_{\perp} v_{\perp}}{\omega_{c\alpha}}) = 1$ obtaining the following dispersion relation:

$$\omega^2 \approx k_{\perp}^2 c^2 + \omega_{p\alpha}. \tag{C.0.18}$$

In addition, for frequencies near the cyclotron harmonics, the solutions are the form:

$$\omega = n\omega_{c\alpha} \left\{ 1 + O\left[\frac{\omega_{p\alpha}^2}{k_{\perp}^2 c^2} \left(\frac{k_{\perp} v_{\perp}}{\omega_{c\alpha}} \right)^{2n} \right] \right\}, \tag{C.0.19}$$

where $n = 1, 2, 3...$ and $k_\perp v_\perp \omega_{c\alpha} < 1$.

The other eigenmodes of equation C.0.16 can be obtained setting to zero the determinant of the matrix:

$$\begin{pmatrix} D_{xx} & D_{xy} \\ D_{yx} & D_{yy} \end{pmatrix}. \tag{C.0.20}$$

These modes will be waves with the electric field perpendicular to the plasma magnetic field $\vec{B_0}$. In the limit of $k^2c^2 >> \omega_{p\alpha}$, D_{xy} can be neglected and, therefore, the two approximate solutions for the two eigenmodes can be found by setting either D_{xx} or D_{yy} equal to zero. Setting $D_{xx} = 0$ one obtains a mode with k nearly perpendicular to the electric field, the extraordinary wave, which has a dispersion relation as:

$$k^2c^2 - \omega^2 + 2\pi\omega \sum_\alpha \sum_n \omega_{p\alpha}^2 \int_{-\infty}^{+\infty} dv_\parallel \int_0^{+\infty} \frac{(J_n')^2 v_\perp^2}{\omega - n\omega_{c\alpha}} \frac{\partial f_{\alpha 0}}{\partial v_\perp^2} dv_\perp = 0. \tag{C.0.21}$$

As the ordinary wave, even this wave is almost a pure electromagnetic wave. In the limit $B_0 \to 0$ as the ordinary wave as the extraordinary wave become pure electromagnetic waves.

The last mode can be derived from setting $D_{yy} = 0$. Its dispersion relation hence results:

$$k^2 + \sum_\alpha \sum_{n=1}^{+\infty} \frac{\omega_{p\alpha}^2 n^2 4\pi\omega_{c\alpha}^2}{\omega - n\omega_{c\alpha}} \int J_n^2 \frac{\partial f_{\alpha 0}}{\partial v_\perp^2} d\vec{v} = 0. \tag{C.0.22}$$

This mode is called the Bernstein mode [44] and corresponds to an almost pure longitudinal wave. In the limit $B_0 \to 0$ the Bernstein wave reduces to a Langmuir wave at high frequency and to a ion-sound wave at low frequency. The Bernstein modes can propagate only in frequency ranges that lie between the harmonics of the cyclotron frequency with the lowest frequency range of propagation, between ω_{ce} and $2\omega_{ce}$. These modes exist also between the harmonics of ω_{ci}. Let's now look at some cases in which the solution of the dispersion relation is easier to obtain. The first

case is that in which the plasma temperature is low or the waves under study has small k (i.e. long wave length). In this case, for a maxwellian equilibrium distribution function, the solutions are:

$$\begin{aligned} \omega_1 = \omega_H = \sqrt{\omega_{ce}^2 + \omega_{pe}^2} \\ \omega_n \approx n\omega_{ce}, \quad with, \quad n \geq 2 \end{aligned} \tag{C.0.23}$$

where ω_H is called the upper hybrid frequency. Another simple solution is obtained when the plasma density is large and the field strength is small (i.e. in the limit $\omega_{pe}^2 > \omega_{ce}^2$). In this case the lowest Bernstein mode is just below the second harmonic of the cyclotron frequency:

$$\begin{aligned} \omega_1 = 2\omega_{ce}\left(1 - \frac{\omega_{pe}^2 3k^2\pi\kappa T_e}{(\omega_{pe}^2 - 3\omega_{ce}^2)\omega_{ce}^2 8m_e}\right) \\ 3\omega_{ce}^2 < \omega_{pe}^2 \\ k^2 a_{ce}^2 << 1 \end{aligned} \tag{C.0.24}$$

where $a_{ce}^2 = \kappa T_e/m_e\omega_{ce}^2$. Higher harmonics will be just below or just above the harmonics of the cyclotron frequencies depending from the density. If $\omega_{pe}^2 > (n^2-1)\omega_{ce}^2$ then $\omega_n = n\omega_{ce}[1 - O(k^2 a_{ce}^2)^n]$, otherwise $\omega_n = n\omega_{ce}[1 + O(k^2 a_{ce}^2)^n]$. Similar modes are present also near the harmonics of ion cyclotron frequency.

Until now, we've shown the propagation of waves perpendicular to an equilibrium magnetic field in a hot plasma. Now we discuss what happens to the dispersion relations in the case of a cold plasma. This can be easily done using the hot dispersion relations and taking the limit $T_\alpha \to 0$. The results obtained in this way are identical to those derived from the fluid theory. In fact equations C.0.11, C.0.12 and C.0.13 become:

$$\begin{bmatrix} 1 - \frac{\epsilon_1\omega^2}{c^2k^2} & -i\frac{\epsilon_2\omega^2}{c^2k^2} & 0 \\ i\frac{\epsilon_2\omega^2}{c^2k^2} & -\frac{\epsilon_1\omega^2}{c^2k^2} & 0 \\ 0 & 0 & 1 - \frac{\epsilon_3\omega^2}{c^2k^2} \end{bmatrix} \begin{bmatrix} E_x \\ E_y \\ E_z \end{bmatrix} = 0 \tag{C.0.25}$$

where

$$\begin{aligned}\epsilon_1 &= 1 + \frac{\omega_{pe}^2}{\omega_{ce}^2 - \omega^2} + \frac{\omega_{pi}^2}{\omega_{ci}^2 - \omega^2} \\ \epsilon_2 &= \frac{\omega_{ce}}{\omega}\frac{\omega_{pe}^2}{\omega_{ce}^2 - \omega^2} - \frac{\omega_{ci}}{\omega}\frac{\omega_{pi}^2}{\omega_{ci}^2 - \omega^2} \\ \epsilon_3 &= 1 - \frac{\omega_{pe}^2}{\omega} - \frac{\omega_{pi}^2}{\omega}\ .\end{aligned} \tag{C.0.26}$$

Therefore, for high frequencies, we obtain: for waves with electric field only along the z axis, an ordinary wave:

$$k_o = \pm\frac{\omega}{c}\left(1 - \frac{\omega_{pe}^2}{\omega^2}\right)^{1/2} \quad [\vec{E}\|\vec{B}_0] \tag{C.0.27}$$

while for waves with electric field perpendicular to the z axis an extraordinary mode:

$$k_E = \pm\frac{1}{c}\left[\frac{(\omega^2 - \omega_1^2)(\omega^2 - \omega_2^2)}{\omega^2 - \omega_H^2}\right]^{1/2} \quad [\vec{E} \perp \vec{B}_0] \tag{C.0.28}$$

where

$$\begin{aligned}\omega_1 &= \frac{\omega_{ce}}{2}\left[-1 + \left(1 + \frac{4\omega_{pe}^2}{\omega_{ce}^2}\right)^{1/2}\right] \\ \omega_2 &= \frac{\omega_{ce}}{2}\left[1 + \left(1 + \frac{4\omega_{pe}^2}{\omega_{ce}^2}\right)^{1/2}\right]\ .\end{aligned} \tag{C.0.29}$$

The extraordinary mode has two distinct frequency ranges, with characteristic index of refraction:

- $\omega \gg \omega_H$: electromagnetic wave; $n^2 = \left(\frac{kc}{\omega}\right)^2 = 1$
- $\omega \ll \omega_H$: upper hybrid resonance; $n^2 \gg 1$,

and there are two bands $\omega_H < \omega < \omega_2$ and $\omega < \omega_1$ in which the wave doesn't propagate that are a characteristic of the cold plasma regime. Note also that in this fluid regime, no Bernstein modes exist. Furthermore the extraordinary wave is not a pure transverse wave except at limiting frequencies.

At lower frequencies, $\omega \ll \omega_{ce}$, when ion motion becomes important, the extraordinary wave appears again at a frequency $\omega_{LH} = \sqrt{\omega_{ci}\omega_{ce}}$, called the lower hybrid frequency, with dispersion relation given by:

$$k^2 = -\frac{\omega^2}{c^2}\frac{\omega_{ce}^2(\omega_{ci}^2) - \omega^2)(\epsilon_1 - \epsilon_2)}{\omega_H^2\left(\omega^2 - \omega_{ce}\omega_{ci}\frac{\omega_{pe}^2+\omega_{ce}\omega_{ci}}{\omega_{pe}^2+\omega_{ce}^2}\right)} \tag{C.0.30}$$

where ϵ_1 and ϵ_2 are given in equation C.0.26. In the low frequency limit, $\omega \ll \omega_{ci}$, the dispersion relation becomes:

$$\frac{k^2c^2}{\omega^2} = 1 + \frac{\omega_{pi}^2}{\omega_{ci}^2}\,. \tag{C.0.31}$$

This wave, since we are in the limit $k \to k_\perp$, is called the magnetosonic wave and can be written as:

$$\omega = \frac{k^2V_A^2}{1 + V_A^2/c^2} \tag{C.0.32}$$

where $V_A = B/\sqrt{4\pi n m_i}$ is the Alfven speed.

C.1 Harris pinch

A strong difficulty when one is dealing with a magnetized inhomogeneous plasma, is to find a non trivial equilibrium state, solution of the Vlasov-Maxwell equations. One of this Vlasov equilibria has been found by Harris [45] in 1961. He found an exact solution of the Vlasov-Maxwell system of equations which describes a collisionless plasma confined between two regions of oppositely directed magnetic fields. In this section we will describe the procedure and the result achieved by Harris.

First of all Harris considered a continuous distribution of velocities that assumes a Maxwellian form at the plane where the magnetic field vanishes. To compute the

equilibrium solution, for which $\partial/\partial t' = 0$, is necessary to solve the following the two stationary Vlasov equations for electrons and ions, the Ampere equation and the Poisson one:

$$v\frac{\delta f_e}{\delta x} - \frac{e}{m_e}(E + v \times B)\frac{\delta f_e}{\delta v} = 0 \tag{C.1.1}$$

$$v\frac{\delta f_i}{\delta x} + \frac{e}{m_i}(E + v \times B)\frac{\delta f_i}{\delta v} = 0 \tag{C.1.2}$$

$$\nabla \times B = \frac{4\pi e}{c}\left(\int_{-\infty}^{+\infty} f_i v d^3v - \int_{-\infty}^{+\infty} f_e v d^3v\right) \tag{C.1.3}$$

$$\frac{\delta E}{\delta x} = 4\pi e\left(\int_{-\infty}^{+\infty} f_i d^3v - \int_{-\infty}^{+\infty} f_e d^3v\right) \ . \tag{C.1.4}$$

Solutions of equations C.1.1 or C.1.2 will be given by any function of particles constant of the motion. Assuming that as the fields ,E and B, as the distribution functions depend only from the x coordinate, then we can take as the constants of the motion the energy and the momenta conjugate to y and z:

$$\begin{aligned} \varepsilon_{i,e} &= \frac{1}{2}m_{i,e}\left(v_x^2 + v_y^2 + v_z^2\right) \pm e\phi(x) \\ p_{y_{i,e}} &= m_{i,e}v_y \pm \frac{e}{c}A_y(x) \\ p_{z_{i,e}} &= m_{i,e}v_z \pm \frac{e}{c}A_z(x) \end{aligned} \tag{C.1.5}$$

where ϕ is the electric potential and $\vec{A}(x)$ is the potential vector. Furthermore, we assume that the electric field $\vec{E}$ has only the x component and the magnetic field $\vec{B}$ has only the z component, and we can take the potential vector to have only the y component. Hence, using these assumption and rearranging the three equations C.1.5, we obtain three constants of the motion of the form:

$$\alpha_{1_{i,e}}^2 = \frac{2\varepsilon_{i,e}}{m_{i,e}} - \frac{\left(p_{y_{i,e}}^2 + p_{z_{i,e}}^2\right)}{m_{i,e}^2} = v_x^2 \mp \frac{2e}{m_{i,e}c} v_y A_y - \frac{e^2}{m_{i,e}^2 c^2} A_y^2 \pm \frac{2e}{m_{i,e}} \phi(x)$$

$$\alpha_{2_{i,e}} = \frac{p_{y_{i,e}}}{m_{i,e}} = v_y \pm \frac{e}{m_{i,e}c} A_y(x) \qquad \text{(C.1.6)}$$

$$\alpha_{3_{i,e}} = \frac{p_{z_{i,e}}}{m_{i,e}} = v_z$$

To satisfy the Vlasov equations, the distribution functions for ions and electrons can be constructed on the set $(\alpha_{1_i}, \alpha_{2_i}, \alpha_{3_i})$ and $(\alpha_{1_e}, \alpha_{2_e}, \alpha_{3_e})$ respectively, obtaining:

$$f_i = \left(\frac{m_i}{2\pi\kappa T}\right)^{\frac{3}{2}} N exp[-\frac{m_i}{2\kappa T}(\alpha_{1_i}^2 + (\alpha_{2_i} - V_i)^2 + \alpha_{3_i}^2)] \qquad \text{(C.1.7)}$$

$$f_e = \left(\frac{m_e}{2\pi\kappa T}\right)^{\frac{3}{2}} N exp[-\frac{m_e}{2\kappa T}(\alpha_{1_e}^2 + (\alpha_{2_e} - V_e)^2 + \alpha_{3_e}^2)] \qquad \text{(C.1.8)}$$

where V_i and V_e are the mean velocities of ions and electrons respectively. Assuming that $V_e = -V_i = -V$ and substituting equations C.1.7 and C.1.8 in C.1.3 and C.1.4, one obtains:

$$\frac{d^2\phi}{dx^2} = -4\pi N e exp\left(\frac{e}{c\kappa T} V A_y\right)\left[exp\left(-\frac{e}{\kappa T}\phi\right) - exp\left(+\frac{e}{\kappa T}\phi\right)\right] \qquad \text{(C.1.9)}$$

$$\frac{d^2 A_y}{dx^2} = -4\pi N e exp\left(\frac{e}{c\kappa T} V A_y\right)\left[exp\left(-\frac{e}{\kappa T}\phi\right) + exp\left(+\frac{e}{\kappa T}\phi\right)\right] . \qquad \text{(C.1.10)}$$

If we choose the electric potential $\phi = 0$, then equation C.1.9 is satisfied and equation C.1.10 becomes:

$$\frac{d^2 A_y}{dx^2} = -\frac{8\pi N e V}{c} exp\left(\frac{e}{c\kappa T} V A_y\right) . \qquad \text{(C.1.11)}$$

To solve this non linear equation, at $x = 0$ we impose the boundary conditions:

$$A_y = 0 \tag{C.1.12}$$

and

$$B = \frac{dA_y}{dx} = 0 \tag{C.1.13}$$

then the solution of equation C.1.11 is:

$$A_y = -\frac{2\kappa T c}{eV} \log \cosh \left(\frac{xV}{e\lambda_D} \right) \tag{C.1.14}$$

where λ_D is the Debye length. Therefore for the magnetic field we obtain:

$$B = -\sqrt{16\pi\kappa T N} \tanh \left(\frac{xV}{e\lambda_D} \right) . \tag{C.1.15}$$

The equilibrium state already described is called the Harris pinch.

Appendix D

Numerical electromagnetic results

Self-consistent electromagnetic fields in spatially non-uniform plasmas represent one of the fundamental aspects of plasma physics with several implications both in microwave and laser based experiments. The problem is relevant for magnetized plasmas, as well, when Bernstein waves are excited as a consequence of mode conversion close to the hybrid plasma resonances. Recently, a renewed interest for electron Bernstein wave physics has appeared due to the possibility of implementing an attractive radiation emission diagnostic in fusion plasmas [56, 57, 58]. Then it is interesting to investigate the kinetic aspects of the propagation of electromagnetic as well as electrostatic fields in a non uniform plasma with arbitrary density and magnetic field scales, and electric field amplitudes. Here, we present, using a 1D2V Vlasov-Ampere VL3 code with open boundary conditions, for first the investigation of the propagation of spatially localized finite amplitude electromagnetic perturbations in a homogeneous magnetized collisionless plasma and then the study of electromagnetic fields propagating in a given equilibrium plasma configuration where both plasma density and magnetic field are inhomogeneous.

D.1 Propagation of finite amplitude electromagnetic perturbations in a homogeneous magnetized collisionless plasma

For this first investigation, we considered a one dimensional magnetized plasma, localized in the region $0 < x < L$, homogeneous in the plane (y, z), with unperturbed density $n_0 = n_{e0} = Zn_{i0}$, and magnetic field $B_0 = B_0\hat{e}_z$. The relevant dimensionless non relativistic normalized Vlasov equations take the form

$$\frac{\partial f_a}{\partial t} + v_x\frac{\partial f_a}{\partial x} - \mu_a[E_x + v_y(B_z + B_0)]\frac{\partial f_a}{\partial v_x} - \mu_a[E_y - v_x(B_z + B_0)]\frac{\partial f_a}{\partial v_y} = 0 \quad \text{(D.1.1)}$$

where $a = e, i$, $\mu_e = 1$ and $\mu_i = -Z\frac{m_e}{m_i}$. The normalization variables are defined as follows: $t \to t\omega_{pe}$, $x \to x/d_e$ (where d_e is the electron skin depth defined as $d_e = c/\omega_{pe}$), $v \to v/c$, $E(B) \to eE(B)/m_e c\omega_{pe}$. As a result, in our units, the normalized length scale is the electron skin depth $d_e = 1$, while the (dimensionless) electrostatic length scale, the Debye length, is equal to the normalized thermal velocity, $\lambda_D = v_{th,e}/c$. In Eq.D.1.1 B_0 is a constant background magnetic field, while $B_z(x,t)$ and $E_{x,y}(x,t)$ are the self-consistent fields that satisfy the Maxwell equations:

$$\frac{\partial E_x}{\partial t} = -j_x\ , \quad \frac{\partial E_y}{\partial y} = -\frac{\partial B_z}{\partial x} - j_y\,, \quad \text{(D.1.2)}$$

where the two relevant components of the current density are $j_x = Zn_iV_{ix} - n_eV_{ex}$ and $j_y = Zn_iV_{iy} - n_eV_{ey}$. The Poisson equation (used as a check in the code) takes the form

$$\frac{\partial E_x}{\partial x} = \rho\,, \quad \text{(D.1.3)}$$

where the charge density is $\rho = Zn_i - n_e$. The system is perturbed at the left boundary with driving electric field modelled as

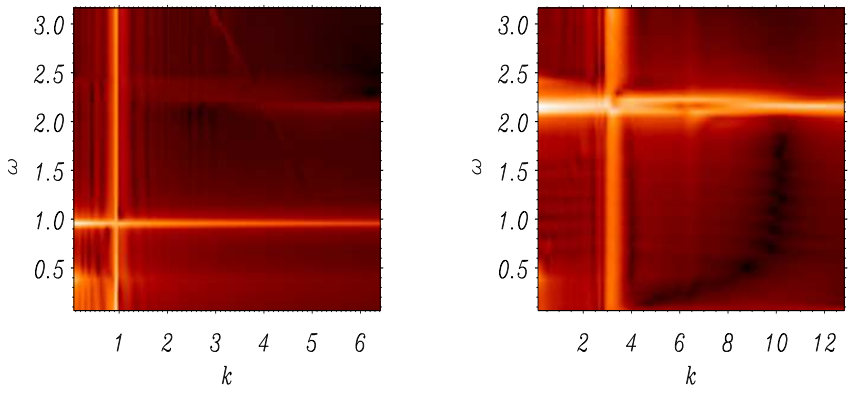

Figure D.1: The k-spectra of the electric field for $\omega = 0.95$, left frame (a), and $\omega = 2.1$, right frame (b).

$$E_x^{dr}(x=0,t) = \epsilon_1 \mathcal{A};\;\; E_y^{dr}(x=0,t) = \epsilon_2 \mathcal{A};\;\; B_z^{dr}(x=0,t) = \epsilon_2 \mathcal{A};\;\; \mathcal{A} = e^{t^2/\tau^2} \sin \omega t \tag{D.1.4}$$

where $\epsilon_{1,2}$ are constant amplitudes and ω is the pump frequency. This model allows one to perturb the system at one boundary of the range $[0, L]$ either by an electromagnetic ($\epsilon_1 = 0$ o $\epsilon_2 \neq 0$) or by an electrostatic ($\epsilon_1 \neq 0$ o $\epsilon_2 = 0$) disturbance. The consistent polarization and wave vector are then defined by the kinetic plasma response, which comprises the nonlinear coupling between particle motion and fields contained in the Vlasov Eq.D.1.1.

Tests aimed at reproducing the wave-plasma interaction in the low-amplitude (linear) regime have been performed by injecting a "pure" electromagnetic wave (i.e. $E_x^{dr} = 0$) at the left boundary, $x = 0$, with $\epsilon_2 = 0.005$, or by exciting an electrostatic perturbation (i.e. $E_y^{dr} = B_Z^{dr} = 0$) nearby the left boundary, $x \neq 0$, using a normalized amplitude $\epsilon_1 = 001$. In all cases $v_{th,e}/c = 0.1$. In dimensionless units the magnetic field is equal to the electron cyclotron frequency and the value $B = \omega_{ce} = 2$ has been chosen in all simulations. Two values of the pump frequency have been considered: $\omega = 0.95$ (a) and $\omega = 2.1$ (b). Note that the upper hybrid frequency is $\omega_H = \sqrt{1 + B^2} = 2.24$ and the cutoff is $\omega_{co} = B/2 + \sqrt{1 + B^2/4} = 2.41$. According to the linear theory of cyclotron waves [15] the cold branches of the dispersion relation

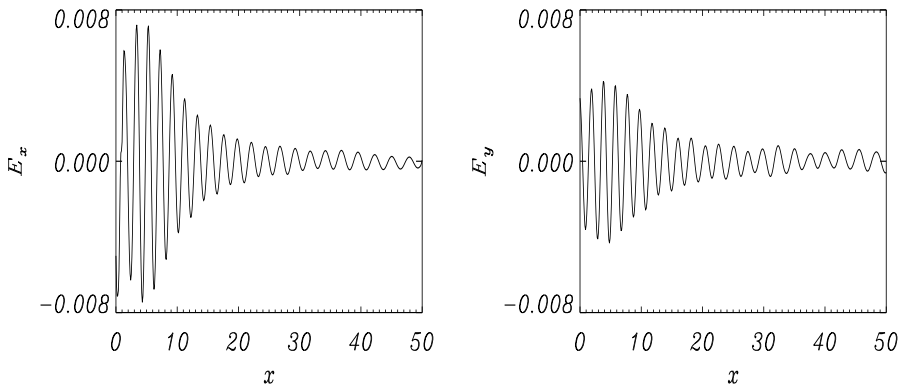

Figure D.2: The longitudinal, E_x, and transversal, E_y components of the electric field for $\omega = 2.1$.

of an extraordinary mode propagating perpendicularly to the magnetic field have a dimensionless wave vector $k \approx 3.2$ and $k \approx 0.94$ for two chosen frequencies, 2.1 and 0.95, respectively.

As it is seen in Fig.D.1 the k-spectra of the electric field manifest a sharp maximum around the corresponding wave vectors, together with other features at higher k's, independently of the method of excitation (electrostatic or electromagnetic). Moreover, since we are dealing with a hot plasma, we should expect also a component at higher k, due to the conversion of the incoming electromagnetic energy into electrostatic electron Bernstein waves. In this respect the most interesting spectrum is that of case (b), since the $\omega_{ce} < \omega < \omega_H$, where modes with $k \approx 10.8$ should be excited. However, in this preliminary work where we deal with small amplitude external pumps and relatively short time of propagation, this effect is not seen. In Fig.D.2 we plot the longitudinal and transversal components of the electric field, first and second frame, respectively, in the case of an electromagnetic external driver of amplitude $\epsilon_2 = 0.005$ and frequency $\omega = 2.1$. We see that near the left boundary the energy is transferred to the electrostatic counterpart and then, after propagating to the right a few d_e at $x \simeq 20$, the amplitudes become nearly constant with $E_x \simeq E_y$. We think that this is due to the warm plasma response.

In Fig. D.3 we draw the isolines of the electron distribution function at $t = 100$ in the (v, x) phase space at fixed v_y velocity, namely $v_y = -0.038$, first frame, and

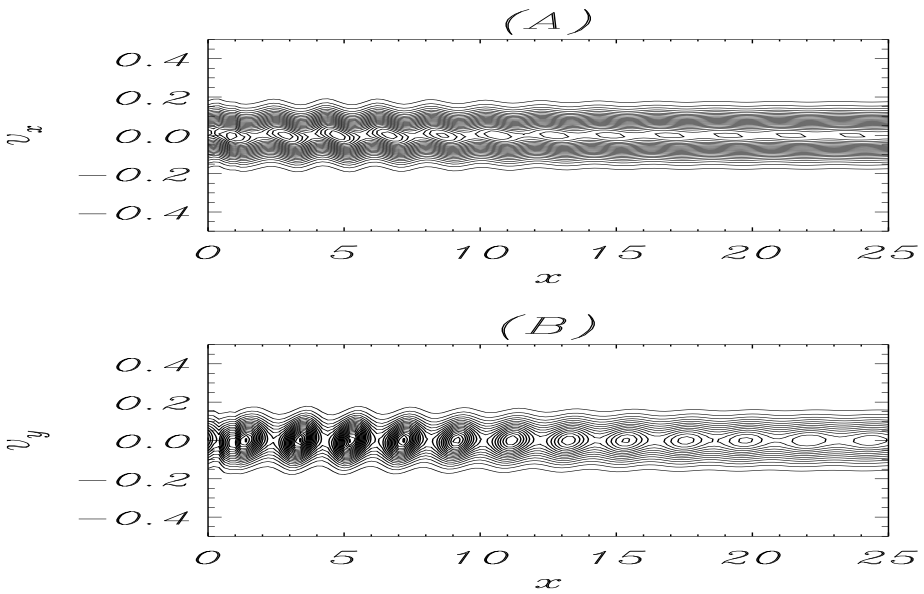

Figure D.3: The electron distribution function at $t = 100$ in the (x, vx) phase space with $v_y = -0.038$, frame (A), and $v_x = -0.19$, frame (B) for $\omega = 2.1$.

$v_y = -0.19$, second frame. This figure shows the rotation of the particles around the magnetic field corresponding vortex like structures of typical size of the order of the selected v_y value. In the present analysis the value $v_{th,e}/c = 0.1$ has been chosen, which corresponds to an electron temperature of $T_e \approx 10keV$. However, the propagation of cyclotron waves is well described already by the non relativistic theory. Moreover, for the frequency values which have been considered, that is $\omega = 0.95$ and $\omega = 2.1$ even in the relativistic case, no appreciable collisionless damping is expected.

D.2 Propagation of finite amplitude electromagnetic perturbations in a inhomogeneous magnetized collisionless plasma

In this last section we will show numerical simulations of the evolution of electromagnetic waves injected from the boundary in a inhomogeneous magnetized collisionless

plasma by means of the 1D2V Ampere-Vlasov VL3 numerical code. We took system for which the unperturbed equilibrium configuration is that of the Harris pinch [4]. It is the result of the one-dimensional equilibrium (in x) between a localized plasma layer and a transverse (with respect to the direction of the plasma gradients, for example in z) non uniform magnetic field, which changes sign in correspondence of the maximum plasma density ($x = 0$). All physical quantities are uniform in the plane y, z. This equilibrium geometry represents a useful model to investigate wave propagation in a non uniform magnetized plasma, since cut-off and resonance are met from a wave excited far from plasma layer (that is at $x = -\infty$). The numerical scheme solves the 1D - 2V normalized Vlasov equation

$$\frac{\delta f_\alpha}{\delta t} + v_\alpha \frac{\delta f_\alpha}{\delta x} - \mu_a (E + v \times B) \frac{\delta f_\alpha}{\delta v} = 0 \quad with \quad \alpha = e, p \tag{D.2.1}$$

with open boundary conditions, where $a = e, i$, $\mu_e = 1$, $\mu_i = -\frac{m_e}{m_i}$ and the normalization variables are defined as in the previous section. The equilibrium Harris configuration at t = 0 for a neutral plasma layer (electrostatic potential $\Phi(t = 0) = 0$), composed by Maxwellian electrons and ions, is described by the distribution functions

$$f_e = (\frac{\beta_e}{2\pi}) N_1 exp[-\beta_e (v_x^2 + (v_y - V_e)^2 + 2V_e A_y)] + N_0 exp[-\beta_e (v_x^2 + v_y^2)] \tag{D.2.2}$$

$$f_i = (\frac{\beta_i}{2\pi}) N exp[-\beta_i (v_x^2 + (v_y - V_i)^2 - 2V_i A_y)]; \;\; \beta_{ei} = N\,(\beta_i + \beta_e)/\beta_i\,. \tag{D.2.3}$$

The static magnetic field and the vector potential are given by:

$$B_z = -\sqrt{\beta_{ei}/\beta_e}\;\tanh(xV\sqrt{\beta_e \beta_{ei}})\,;\; A_y = -(1/\beta_e)V\,\log[\cosh(xV\sqrt{\beta_e \beta_{ei}})]\,. \tag{D.2.4}$$

The other parameters of the system are $N_1 = 0.9$, $N_0 = 0.1$, $v_{th,e} = 0.1$, $v_{th,i} = 0.00023$, $V_e = -0.05$, $V_i = 0.0005$, $\beta_e = 100$, $R_T = T_i/T_e = 0.01$, $R_m = m_i/m_e = 1836$, $\beta_i = \beta_e R_m / R_T$.

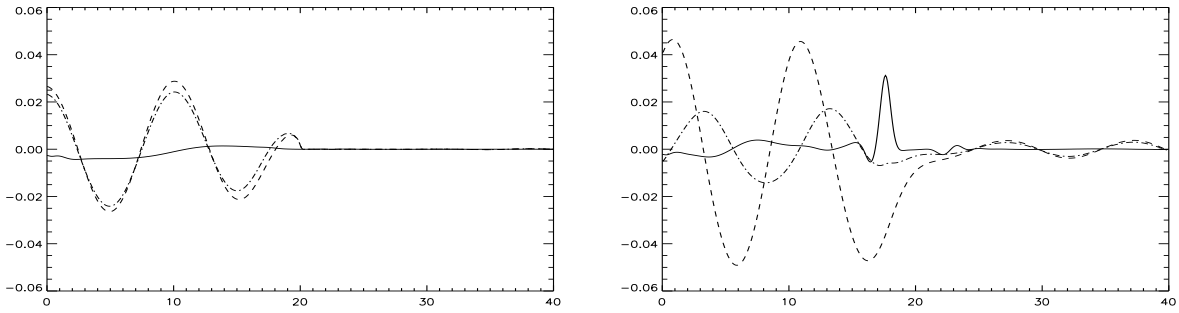

Figure D.4: Left frame: the longitudinal components of the electric field E_x (continuous line), E_y (dashed line) and B_z (dot-dashed line) at t=20. Right frame: the longitudinal components of the electric field E_x (continuous line), E_y (dashed line) and B_z (dot-dashed line) at t=75.

We have studied the propagation of an extraordinary-mode excited (a transverse wave with the electric field E_y^{dr} and the magnetic field B_z^{dr}) from the left boundary of the system, at two frequencies, $\omega_0 = 0.7$ and $\omega_0 = 0.35$. In the former case the excited wave propagates initially in a transparent magnetized plasma, which becomes inaccessible at $x = 17.4$, the position of the linear cut-off. Very close to the cut-off, there is the upper-hybrid cold resonance. The case at $\omega_0 = 0.35$ refers to the excitation of an electromagnetic disturbance at the boundary of an overdense plasma, which becomes more and more overdense approaching $x = 20$, where the magnetic field vanishes. The plasma response has also been sampled at two different driver amplitudes, $E_y^{dr} = 0.01$ and 0.05.

Lets consider first the underdense plasma case ($\omega_0 = 0.7$) for the lower amplitude value $E_y^{dr} = 0.01$. In this case an extraordinary wave propagates as predicted by fluid theory. In the region before the first resonance, the extraordinary wave propagates with a wave number $k_E = 0.63$. When the wave cross the cutoff, its amplitude is smoothed. Furthermore, the propagation of the wave over the resonance produces also an electrostatic wave after that propagates between the two resonances as a plasma wave. Its amplitude grows in time but the maximum remains always lower with respect to the extraordinary wave amplitude. Things becomes more complicated in the case of the higher amplitude value $E_y^{dr} = 0.05$.

In Fig.D.4 the longitudinal component of the electric field E_x (continuous line), the transverse components of the electric field E_y (dashed lines) and of the magnetic

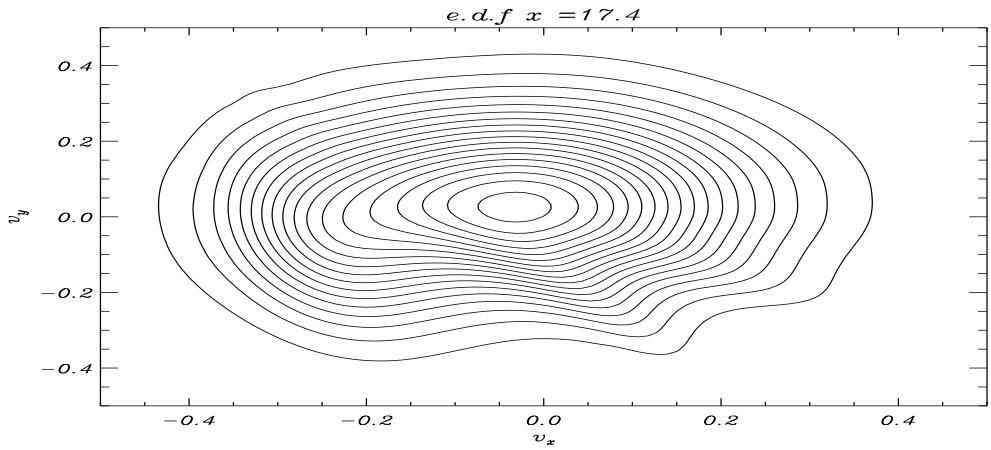

Figure D.5: The electron distribution isocontour ($t = 50$) at $x = 17.4$ for the case $\omega_0 = 0.7$ higher amplitude.

field B_z (dot-dashed lines) are plotted as functions of x at $t = 20$ (a) and at $t = 75$ (b). In Fig.D.4, left frame, it is seen that E_y and B_z are in phase and the corresponding wave-vector $k_x = 0.63$ satisfies the linear dispersion, as expected. With elapsing time, the front of the perturbation reaches the plasma layer, and several effects take place. The electromagnetic part of the disturbance is reflected at the cut-off, while the electrostatic part is enhanced at the upper-hybrid resonance. A small portion of the electromagnetic energy tunnels across the overdense plasma and appears at the side $x > 20$, as a pure extraordinary mode. In Fig.D.4, right frame, the same quantities as in Fig.D.4, left frame, are plotted at a later time. It is seen that the superposition of the incoming and reflected electromagnetic waves has suffered a half-π dephasing between the E_y and B_z, the E_x is strongly peaked at the resonance, and the tunneled electromagnetic wave shows fully phased E_y and B_z, propagating towards the right boundary of the simulation interval. In Fig.D.5, left frame, the contour plot of the electron distribution function at $x = 17.4$ (close to the plasma resonance) in the $v_x; v_y$ plane is shown at $t = 50$. The main distortion of the initial Maxwellian are observed for $v_x > 0$ and $v_y < 0$.

Let's now consider the lower frequency case ($\omega_0 = 0.35$), which corresponds to the excitation of an electromagnetic disturbance which is in cut-off. In Fig.D.6, left frame, E_x (continuous line), E_y (dashed lines), and B_z (dot-dashed lines) are plotted as functions of x for $E_y^{dr} = 0.01$ at $t = 68$ (left frame) and for $E_y^{dr} = 0.05$ at $t = 198$

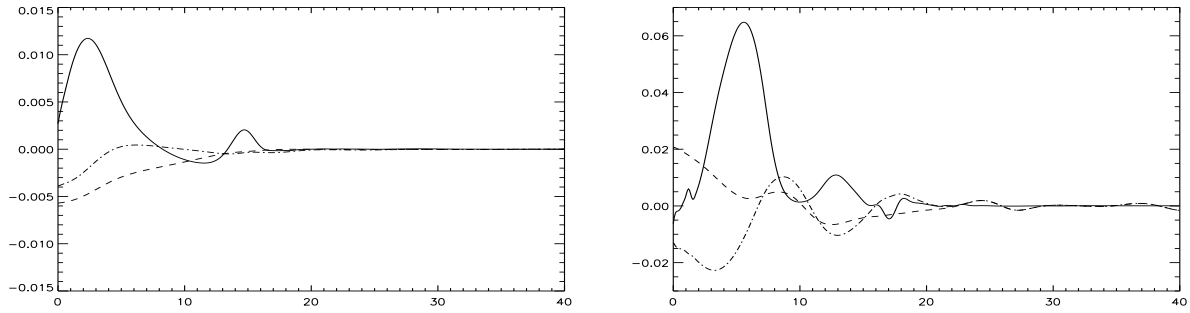

Figure D.6: E_x, E_y and B_z (continuous, dashed and dot-dashed line) vs. x for the lower amplitude run with $\omega_0 = 0.35$ at $t = 68$, and for the higher amplitude case with $\omega_0 = 0.35$ and $t = 198$, left and right frame, respectively.

(right frame). For both excitation amplitudes it is seen that the electromagnetic field is evanescent over approximately $200\lambda_D$. Moreover quite strong electrostatic field fluctuations for $0 < x < 10$ take place. In this case, the electron distribution function is heavily distorted from the initial Maxwellian, as it can be seen in Fig.D.7 , right frame, which shows the isocontours in the plane $v_x; v_y$, at $x = 14.4$ and for $t = 90$.

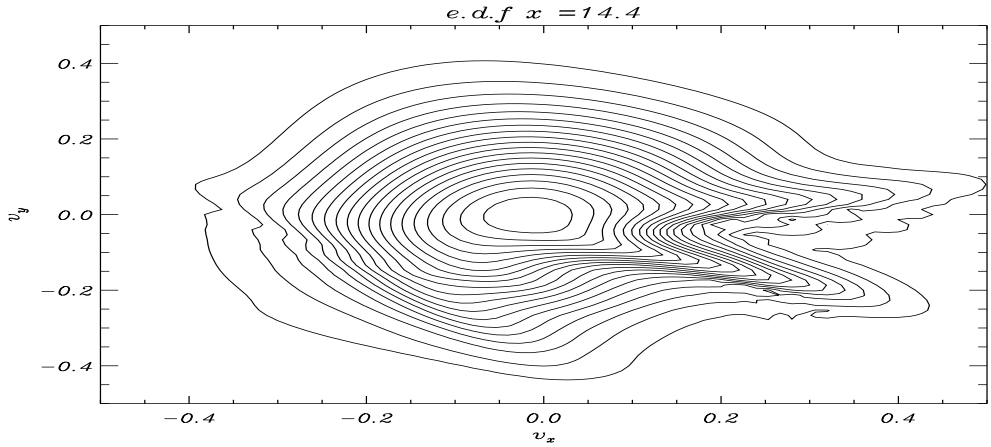

Figure D.7: The electron distribution isocontour ($t = 90$) at $x = 14.4$ for the case $\omega_0 = 0.35$ higher amplitude..

I wish to thank my thesis advisor Dr.Francesco Califano for his help and his patience during these three years of research and in the writing of this thesis and Prof. Francesco Pegoraro for the constructive discussions and the contribution of ideas which have been of fundamental importance for the proceeding of my PhD work. I want also to acknowledge Prof.Mangeney and Prof.Lontano for their precious collaborations in the study of correlations and mode conversion respectively. I also want to thanks all those persons that have supported me during these three years.

Bibliography

[1] R.W. Gould, T.M. O'Neil, J.H. Malmberg, Phys. Rev. Lett. **19**, 219 (1967).

[2] J.H.Malmberg, C.B. Wharton, R.W. Gould et T.M. O'Neil, Phys. Fluids **11**, 1147 (1968).

[3] L.D. Landau, J. Phys. **10**, 25 (1946).

[4] T. O'Neil, Phys. Fluids **8**, 2255 (1965).

[5] C. Lancellotti, J.J. Dorning, Phys. Rev. Lett. **81**, 5137 (1998); J. Math. Phys. **40**, 3895 (1999); Phys. Rev. E **68**, 026406 (2003).

[6] L. Galeotti, F. Califano, Phys. Rev. Lett. **95**, 015002 (2005).

[7] M. Bernstein, J.M. Greene, M.D. Kruskal, Phys. Rev. **108**, 546 (1957).

[8] K.V.Roberts and H.L.Berk, Phys. Rev. Lett., **19**, 297 (1967).

[9] R.E.Ergun et al., Geophys.Res.Lett. **25**, 1 (1998).

[10] J.R.Franz,P.M.Kintner and J.S.Pickett, Geophys.Res.Lett. **25**, 1277 (1998).

[11] H.Matsumoto et al., Geophys.Res.Lett., **21**, 2915 (1994).

[12] S.D.Bale et al., Geopyhs.Res.Lett, **25**, 2929 (1998).

[13] A. Ghizzo, B. Izrar, P. Bertrand, E. Fijalkow, M.R. Feix, M. Shoucri, Phys. Fluids **31**, 72, (1998).

[14] A. Ghizzo, B. Izrar, P. Bertrand, E. Fijalkow, M.R. Feix, M. Shoucri, Phys. Lett. A **120**, 191, (1987).

[15] T.M. O'Neil, Phys. Fluids **11**, 2420 (1968).

[16] L. Galeotti, F. Califano, F. Pegoraro, Phys. Rev. Lett., submitted

[17] P.J. Morrison, Phys. Plasmas, **12**, 058102 (2005).

[18] P.L. Andrews, Phys. Rev. Lett., **54**, 2022 (1985).

[19] S. Nakajima and H.Abe, Phys. Rev. A, **38**, 4373 (1988).

[20] T.H. Stix, Phys. Rev. Lett., **15**, 878 (1965).

[21] A. Weitzner and D.B. Batchelor, Phys. Fluids, **22**, 1355 (1978).

[22] P.C. Efthimion, J.C.Hosea, R. Kaita amd G.Taylor, Rev. Scientific Instruments, **70**, 1018 (1999).

[23] R.A. Cairns and C.N. Lashmore-Davies, Phys. Plasmas, **7**, 4126 (2000).

[24] J. Preinhaelter et al., Rev. Scientific Instruments, **74**, 1437 (2003).

[25] N.A. Krall A.W. Travelpiece, *"Principles of plasma physics"*(San Francisco Press, 1986).

[26] J. Mathews and R.L. Walker, *"Mathematical Methods of Physics"* (W.A. Benjamin, New York, 1970).

[27] M. Buchanan, J.J. Dorning, Phys. Rev. Lett. **70**, 3732 (1993); Phys. Rev. E **50**, 1465 (1994); *ibid* **52**, 3015 (1995).

[28] M. Brunetti, F. Califano, F. Pegoraro, Phys. Rev. E **62**, 4109 (2000).

[29] W.B. Thompson, *"Introduction to plasma physics"* (Pergamon Press, Inc, New York, 1962), p.169.

[30] W.E. Drummond and D. Pines, Nucl. Fusion Suppl. Pt. **3**, 1049 (1962).

[31] T. Dupree, Phys. Fluids **9**, 1773 (1966).

[32] V.I. Karpman, Zh. Eksp. Teor. Fiz. 51, 907 (1996).

[33] C.H. Su, C. Oberman, Phys. Rev. Lett. **20**, 427 (1968).

[34] A.J. Wong, Phys. Fluids **12**, 866 (1969).

[35] A.J. Wong, F. Skiff and M. Ono, Phys. Fluids **26**, 2772 (1983).

[36] Z. Sedlacek, Transp Th. Stat. Phys., in press.

[37] J. Canosa et al., J. Comp. Physics **15**, 495 (1974)

[38] Z. Sedlacek and L. Nocera, Phys. Fluids **48**, 367 (1992).

[39] L. Nocera and A. Mangeney, Phys. Plasmas **6**, 4559 (1999).

[40] V.N. Pavlenko, Sov. Phys. Usp. **26**, 931 (1993).

[41] F. Mottez, Astrophysics and Space Science **277**, 59 (2001).

[42] H. Schamel, Phys. Scripta **T2/1**, 228 (1982).

[43] H.L. Berk, C.E. Nielsen and K.V.Roberts, Phys. Fluids **13**, 980 (1970).

[44] I.B. Bernstein, Phys. Rev. Lett. **109**, 10 (1958).

[45] E.G. Harris, Il Nuovo Cimento **XXIII**, 115 (1962).

[46] J.E. Mayer and M.G. Mayer, *"Statistical Mechanics of Fluids"*, (Wiley, New York, 1940); H.S. Green, Nucl. Fusion., **1**, 69 (1961).

[47] C.Z.Cheng and G.Knorr, J. Comput. Phys. **22**, 330 (1976).

[48] B. Van Leer, J. Comput. Phys. **23**, 276 (1976).

[49] M.R. Feix, P. Bertrand and A. Ghizzo, "Eulerian codes for the Vlasov equation", in *"Advances in kinetic theory and computing"*, (Ed. Perthame, World Scinetific, 1993), p.45.

[50] A.Mangeney, F.Califano, C.Cavazzoni and P.Travnicek, J. Comput. Phys. **179**, 495 (2002).

[51] M.M.Shoucri and R.R.Gagn, J. Comput. Phys. **24**, 445 (1977);

[52] V. Gurevich, Soviet Physics JETP, **26**, 575 (1968)

[53] S.K. Lele, J. Comput. Phys. **103**, 16 (1992)

[54] A. Wolf et al., Physica D **16**, 285 (1985)

[55] F. Valentini et al., Phys. Rev. E, **71**, 017402 (2005)

[56] P.C.Efthimion et al., Phys. Plasmas, **9**, 752 (2002)

[57] P.K. Chattopadhyay, et al., Appl. Phys. Lett. **78**, 595 (2001)

[58] J. Preinhaelter, et al., Rev. Sci. Instr., **74**, 1437 (2003)